DEPARTMENT OF INFORMATION SCIENCE AND TECHNOLOGY

MONTE-CARLO SIMULATION OF AN OPTICAL DIFFERENTIAL PHASE-SHIFT KEYING COMMUNICATION SYSTEM WITH DIRECT DETECTION IMPAIRED BY IN-BAND CROSSTALK

Dissertation presented in partial fulfillment of the Requirements for the Masters Degree on Telecommunications and Information Science

By

Genádio João Faria Martins

Supervisors:

Dr. Luís Cancela, Assistant Professor,

ISCTE-IUL

Dr. João Rebola, Assistant Professor,

ISCTE-IUL

June 2012

DEPARTMENT OF INFORMATION SCIENCE AND TECHNOLOGY

MONTE-CARLO SIMULATION OF AN OPTICAL DIFFERENTIAL PHASE-SHIFT KEYING COMMUNICATION SYSTEM WITH DIRECT DETECTION IMPAIRED BY IN-BAND CROSSTALK

Dissertation presented in partial fulfillment of the Requirements for the Masters Degree on Telecommunications and Information Science

By

Genádio João Faria Martins

Supervisors:

Dr. Luís Cancela, Assistant Professor,

ISCTE-IUL

Dr. João Rebola, Assistant Professor,

ISCTE-IUL

June 2012

Acknowledgments

First of all, I would like to thank my supervisors Prof. João Rebola and Prof. Luís Cancela for all their support throughout this work and their availability and patience in all my doubts and questions. I would like to thank Instituto de Telecomunicações (IT) for providing me material, access to their installations and for the monthly scholarship.

I would like to thank also my family for their support, love and encouragement, which was fundamental for the realization of this dissertation, particularly to my cousin Tonita. A special thanks to my girlfriend Sara Rocha for all her patience and support.

Finally, I would like to thank all my friends, particularly Rui Batalha, João Conduto and Catarina Cruz for all their support and help mainly during the computer simulations.

Thank you all!

Lisbon, 2012

Genádio Martins

Resumo

O renovado interesse nas comunicações ópticas com modulação de fase diferencial DPSK (differential phase-shift keying) provém do facto de esta superar o formato convencional de modulação de intensidade, OOK (on-off keying) em certos aspectos, tais como, sensibilidade do receptor, robustez às limitações da transmissão e tolerância às flutuações da potência do sinal. O crescimento exponencial do tráfego de dados e as vantagens do DPSK levam à necessidade da sua utilização no contexto das redes ópticas, sendo uma das principais limitações físicas das redes ópticas, o crosstalk.

O crosstalk homódino incoerente, devido ao isolamento imperfeito dos componentes ópticos utilizados nos nós da rede óptica, tem sido identificado como uma das maiores limitações existentes no nível físico das redes ópticas.

Esta dissertação apresenta um estudo do impacto do ruído de emissão espontânea amplificada, gerado pela amplificação óptica do sinal, e do crosstalk no desempenho de um sistema de comunicação óptico DPSK com detecção directa e assumindo um receptor balanceado.

O desempenho do sistema é avaliado usando uma simulação estocástica baseada no método de Monte Carlo e comparado com o desempenho obtido a partir de formulações analíticas. Diferentes combinações de filtros ópticos e eléctricos são considerados no receptor óptico DPSK. A influência de imperfeições do receptor óptico DPSK no desempenho é também estudada. Investiga-se também a influência do nível de potência do sinal de crosstalk, o atraso entre o sinal original e o sinal de crosstalk e diferentes sequências de bits no sinal de crosstalk DPSK no desempenho do sistema de comunicação óptico.

Palavras-chave: Sistemas de comunicação óptica, simulação de Monte Carlo, modulação de fase diferencial, crosstalk homódino incoerente e ruído de emissão espontânea amplificada.

Abstract

The renewed interest in optical communications on the differential phase-shift keying (DPSK) modulation format comes from the fact that it outperforms the conventional format on-off keying (OOK), in such aspects, such as receiver sensitivity, robustness to transmission impairments and tolerance to signal power fluctuations. The exponential growth of data traffic and the DPSK advantages over OOK lead to its use on the optical networks environment, where physical limitations, such as crosstalk, may impair significantly the network performance.

In-band crosstalk, due to the imperfect isolation of optical components used in the optical network nodes, has been identified as one of the most severe physical layer limitation in optical transparent network.

This dissertation proposes to study the impact of amplified spontaneous emission noise, generated by the signal optical amplification, and of in-band crosstalk in the performance of an optical DPSK communication system with direct detection using a balanced receiver.

A stochastic simulation based on the Monte Carlo method is used to evaluate the system performance and comparisons with the results obtained using theoretical works are also performed. Different combinations of optical and electrical filters at the optical DPSK receiver are considered. The influence of DPSK receiver imperfections on the system performance is also studied. The influence of the crosstalk level, the delay between the original and the crosstalk signal and different bits sequence on the DPSK crosstalk signal on the system performance is also investigated.

Keywords: Optical communication system, Monte Carlo simulation, differential phase-shift keying, in-band crosstalk and amplified spontaneous emission noise.

Index

1. Introduction 1

1.1. Motivations 1

1.2. Objectives and dissertation organization 2

2. Theoretical concepts 5

2.1. Introduction 5

2.2. Transmitter description 6

2.3. Receiver description 9

2.3.1. Optical amplifier, polarizer and optical filter 9

2.3.2. MZDI and dual photodetector 10

2.3.3. Electrical filter and decision circuit 13

2.4. Implementation of the Monte Carlo simulator 14

2.4.1. Signals simulation 14

2.4.2. Monte Carlo simulation 16

2.4.3. The Monte Carlo simulation flowchart 17

3. Optical DPSK communication system impaired by ASE noise 21

3.1. Introduction 21

3.2. Filters characterization 22

3.2.1. Ideal filter 22

3.2.2. Gaussian filter 22

3.2.3. Lorentzian filter 23

3.2.4. Integrator filter 23

3.2.5. RC filter 24

3.3. Validation of the Monte Carlo simulation 26

3.4. Performance evaluation for different optical and electrical filters combinations 32

3.4.1. Ideal optical filter and integrator electrical filter 32

3.4.2. Gaussian optical filter and integrator electrical filter 33
3.4.3. Lorentzian optical filter and integrator electrical filter 35
3.4.4. Gaussian optical filter and Gaussian electrical filter 36
3.4.5. Gaussian optical filter and RC electrical filter 37
3.4.6. Comparison of the different filters combinations 39
3.5. Impact of the DPSK receiver imperfections 40
3.5.1. Validation of the MC simulation 41
3.5.2. Performance evaluation for different optical and electrical filter combinations 42
3.6. Conclusions 48
4. Optical DPSK communication system impaired by in-band crosstalk 51
4.1. Introduction 51
4.2. In-band crosstalk model 52
4.3. Implementation of the random phase noise 54
4.4. Validation of the Monte Carlo simulation 57
4.5. Performance evaluation 61
4.5.1. Delay between the original signal and the crosstalk signal 62
4.5.2. Different bits sequences on the DPSK crosstalk signal 64
4.5.3. Receiver imperfections 67
4.6. Conclusions 69
5. Conclusions and future work 71
5.1. Future work 73
6. References 75

List of Figures

Figure 2.1 - Schematic block diagram of an optical DPSK communication system. 5
Figure 2.2 - Principle of phase modulation using a MZM (adapted from Fig. 3 of [6]). 6
Figure 2.3 –NRZ signal and the phase of the DPSK signal. 7
Figure 2.4 – PSDs of NRZ (left) and DPSK (right) signals. 8
Figure 2.5 – PSDs of signals $\vec{E}_2(t)$ at constructive port (left) and $\vec{E}_1(t)$ at destructive port (right). 11
Figure 2.6 – Photocurrents, $i_1(t)$, $i_2(t)$ and $i(t)$. 13
Figure 2.7 – Signal at the decision circuit output. 14
Figure 2.8 – Simulated time vector. 15
Figure 2.9 – Simulated frequency vector. 15
Figure 2.10 – Block diagram of the Monte Carlo simulation. 16
Figure 2.11 – Flowchart of the MC simulation for a back-to-back configuration. 18
Figure 3.1 – Ideal filter transfer function for $B_oT_b = 100$. 22
Figure 3.2 – Electrical integrator filter transfer function for $B_eT_b = 1$. 24
Figure 3.3 – Amplitude response of the Gaussian and Lorentzian optical filters. 24
Figure 3.4 – Amplitude response of the Gaussian and RC electrical filters. 25
Figure 3.5 – Group delay of the RC filter for different electrical filter –3 bandwidths. 26
Figure 3.6 – BEP as a function of the optical signal power, for the ideal OF and the integrator EF combination, considering $B_oT_b = 1$, 10 and 100. 27
Figure 3.7 – BEP as a function of the optical signal power, for the ideal OF and the integrator EF combination considering smaller normalized optical filter bandwidths. 28
Figure 3.8 – PDF of the decision variable, for the ideal OF and the integrator EF combination, considering an optical signal power with –47 dBm and $B_oT_b = 1$, 5 and 10. 28
Figure 3.9 – Eye diagram at the decision circuit input for the ideal OF and the integrator EF combination, considering B_oT_b equal to 1 (left), 5 (middle) and 10 (right). 29
Figure 3.10 – BEP as a function of B_oT_b, considering the ideal OF and the integrator EF combination tested for different number of bits. 30
Figure 3.11 – BEP as a function of B_oT_b, for the ideal OF and the integrator EF combination, considering different optical signal powers. 32

Figure 3.12 – PDF of the decision variable, for an ideal OF and an integrator EF combination, considering an optical signal power with –47 dBm for B_oT_b = 1, 1.1, 1.2, 1.3, 1.4 and 1.5. ... 33
Figure 3.13 – BEP as a function of B_oT_b, for the Gaussian OF and the integrator EF combination, considering different optical signal powers. 34
Figure 3.14 – Eye diagram at the decision circuit input for the Gaussian OF and the integrator EF combination, considering B_oT_b equal to 1 (left), 2 (middle) and 10 (right). 35
Figure 3.15 – BEP as a function of B_oT_b, for the Lorentzian OF and the integrator EF combination, considering different optical signal powers. 35
Figure 3.16 – PDF of the decision variable, for the Lorentzian OF and the integrator EF combination, considering an optical power with –47dBm for B_oT_b = 1, 2, 5 and 10. 36
Figure 3.17 – BEP as a function of B_oT_b, for the Gaussian OF and the Gaussian EF combination, considering different optical signal powers. 37
Figure 3.18 – BEP as a function of B_oT_b, for a Gaussian OF and a RC EF combination, considering different optical signal powers. 38
Figure 3.19 – Eye diagram at the decision circuit input, considering a Gaussian OF and a RC EF combination, an optical signal power equal to –47 dBm, for B_oT_b = 2 (left) and B_oT_b = 10 (right). 38
Figure 3.20 – BEP estimates as a function of B_oT_b, for a Gaussian OF and a RC EF combination, considering different signal optical powers and for a sampling time equal to half bit period. 39
Figure 3.21 – BEP as function of the optical signal power for B_oT_b = 5, considering different filters combinations. 40
Figure 3.22 – BEP as a function of the responsivity imbalance for a matched optical filter and absence of electrical filter, considering different values of the interferometer detuning. 42
Figure 3.23 – Power penalty as a function of the responsivity imbalance for an ideal OF and integrator EF combination, considering different values of B_oT_b. 43
Figure 3.24 – Eye diagram at the decision circuit input for an ideal OF and integrator EF, considering K = 0 dB (left), K = 5 dB (middle) and K = 10 dB (right). 44
Figure 3.25 – PDFs of the decision variable, for an ideal OF and integrator EF, considering K = 0 dB (red), K = 5 dB (blue) and K = 10 dB (green). 44
Figure 3.26 – Power penalty as a function of the responsivity imbalance for different values of B_oT_b, considering a Lorentzian OF and integrator EF combination (left) and a Gaussian OF and a Gaussian EF combination (right). 45

Figure 3.27 – Power penalty as a function of the normalized interferometer detuning for an ideal OF and integrator EF combination, considering different values of B_oT_b. 46
Figure 3.28 – Eye diagram at the decision circuit input for an ideal OF and integrator EF, considering $\Delta f\, T_b = 0$ (left), $\Delta f\, T_b = 0.04$ (middle) and $\Delta f\, T_b = 0.08$ (right). 47
Figure 3.29 – Power penalty as a function of the normalized interferometer detuning considering different values of B_oT_b, for a Lorentzian OF and integrator EF combination (left) and for a Gaussian OF and a Gaussian EF combination (right). 48
Figure 4.1 – Schematic block diagram of an optical DPSK balanced receiver impaired by in-band crosstalk. 53
Figure 4.2 – Temporal evolution of the Brownian motion random phase noise, for two independent sample functions. 55
Figure 4.3 – PDF of random phase considering different temporal instants. 56
Figure 4.4 – PDF of the random phase noise difference. 57
Figure 4.5 – BEP as a function of the optical signal power, for an ideal OF and an integrator EF, considering B_oT_b = 1, 10 and 100 and the crosstalk level equal to –12 dB. 58
Figure 4.6 – BEP as a function of the crosstalk level, considering the ideal OF and the integrator EF combination (left) and the Gaussian OF and the RC EF combination (right), for different normalized optical filter bandwidths. 59
Figure 4.7 – Eye diagrams at the decision circuit input for the ideal OF and the integrator EF, for an optical signal power of –45 dBm, B_oT_b = 10 and considering a crosstalk level equal to –30 dB (left), –20 dB (middle) and –12 dB (right). 60
Figure 4.8 – Power penalty as a function of the responsivity imbalance with different interferometer detunings, for the Gaussian OF and the Gaussian EF with a crosstalk level of –15 dB, considering a normalized optical filter bandwidth equal to 5. 61
Figure 4.9 – BEP as a function of the optical signal power, for an ideal OF and an integrator EF combination, a crosstalk level of –12 dB and a normalized optical filter bandwidth equal to 10 (left) and 100 (right), considering different crosstalk signal delays. 62
Figure 4.10 – BEP as a function of the delay between the crosstalk and the original signals, considering a Gaussian OF and a RC EF combination (left) and an ideal OF and an integrator EF combination (right), both for a crosstalk level of –12 dB and B_oT_b = 2. 63
Figure 4.11 – Eye diagram at the decision circuit input considering an ideal OF and an integrator EF combination, for three crosstalk signals delays equal to 0 (left), $T_b/2$ (middle) and T_b (right). 63

Figure 4.12 – BEP as a function of the crosstalk level, considering an ideal OF and an integrator EF combination with an optical signal power of –46 dBm (left) and a Gaussian OF and a RC EF combination with an optical signal power of –45 dBm (right), for different sequence of bits on the DPSK crosstalk signal, considering a normalized optical filter bandwidth equal to 2 and 10. 64
Figure 4.13 – Eye diagrams at the decision circuit input considering a Gaussian OF and a RC combination, for a random bits sequence on the DPSK crosstalk signal (left), an equal bits sequence (middle) and a negated bits sequence (right). 65
Figure 4.14 – PDFs of the decision variable, considering a Gaussian OF and a RC EF, for a random bits sequence on the DPSK crosstalk signal (blue), an equal bits sequence (red) and a negated bit sequence (green). 66
Figure 4.15 – BEP as a function of the responsivity imbalance (left) and of the interferometer detuning (right), for different crosstalk levels, considering a Gaussian OF and a Gaussian EF combination, a normalized optical filter bandwidth equal to 5 and an optical signal power of –45 dBm. 67
Figure 4.16 – PDF of the decision variable, considering responsivity imbalance (left) and of the interferometer detuning (right), for a crosstalk level of –12 dB, considering a Gaussian OF and a Gaussian EF combination, B_oT_b = 5 and an optical signal power of –40 dBm. 68

List of Tables

Table 3.1. Parameters of the simulated optical DPSK communication system impaired by ASE noise. 21
Table 3.2. The evolution of the BEP estimates and the simulation time with the increase of the number of errors, N_e, of the MC simulation. 31
Table 4.1. Parameters of the simulated optical DPSK communication system impaired by in-band crosstalk. 51

List of Acronyms

ASE	Amplified Spontaneous Emission
AWGN	Additive White Gaussian Noise
BEP	Bit-Error Probability
CW	Continuous Wave
DFT	Discrete Fourier Transform
DPSK	Differential Phase-Shift Keying
DQPSK	Differential Quadrature Phase-Shift Keying
EDFA	Erbium Doped Fiber Amplifier
EF	Electrical Filter
FFT	Fourier Fast Transform
IFFT	Inverse Fourier Fast Transform
ISI	Inter-Symbol Interference
MC	Monte Carlo
MZDI	Mach-Zehnder Delay Interferometer
MZM	Mach-Zehnder Modulator
NRZ	Non-Return-to-Zero
OA	Optical Amplifier
OF	Optical Filter
OOK	On-Off Keying
OSNR	Optical Signal-to-Noise Ratio
PDF	Probability Density Function
PIN	Positive Intrinsic Negative
PM	Phase Modulator
PSD	Power Spectral Density
PSK	Phase-Shift-Keying
SOA	Semicondutor Optical Amplifier
WDM	Wavelength Division Multiplexing

1. Introduction

1.1. Motivations

In the last few years, the data traffic in the communication networks had an exponential growth. Communication networks are undergoing dramatic changes due to increasing demands from users and also due to technological advances. All consumers have their own specific requirements on the networks in terms of bandwidth, quality of service and network resources. Optical technology has a key role to play enabling that optical networks can support these requirements [1].

The invention of the laser in 1958 and the subsequent demonstration of the optical fiber as a telecommunications transmission medium, in the 1960's, brought a technology platform capable of supporting global communication demands for the 21st century and beyond [2]. In the 1970's, a breakthrough occurred when the optical fibers losses were reduced to below 20 dB/km and, due to its advantages over the copper cables, such as, lower attenuation, broader bandwidth, reduced diameter and weight, and immunity to electromagnetic interference [3, chap. 1], these fibers began to replace coaxial cables as the transmission medium in the trunk systems of telecommunication systems [2]. The deployment of Internet in the mid-80's, sparked a growth of data traffic on the network [2]. During these years, millions of kilometers of optical fiber were deployed world wide [4]. As a result, optical fibers became the dominant transmission medium in the telecommunication networks.

In the 1990's this capacity has been significantly increased due to the technology known as wavelength division multiplexing (WDM). The economic deployment of WDM was only possible due to the introduction of optical amplification with erbium-doped fiber amplifiers (EDFAs). The deployment of optical amplifiers and of WDM strongly contributed, respectively, to the increase of optical transmission reach and to the increase of the amount of traffic carried by an optical fiber. For these reasons, it is desirable for nodes to have switching add/drop capabilities at the optical level. This led to the development of optical add/drop multiplexers (OADMs) and optical cross connects (OXCs). Besides routing the optical paths, these components are also used to protect and restore the optical paths in case of failure, and enable the rapid reconfiguration of lightpaths [2].

Current networks employ bit rates up to 100 Gbps and there are many reasons for believing that the bit rates will continue to increase [1]. However, the increase of the bit rate leads to more demanding requirements in the WDM systems design, due to enhancement of the dispersion effect (chromatic and polarization), of the nonlinear effects and of the crosstalk [3, chap. 3, 4 and 9]. Crosstalk due to the imperfect nature of various WDM components such as optical filters, (de)multiplexers and optical switches, is considered one of the most important physical layer limitation in designing WDM systems [3, chap. 9]. In-band crosstalk is particularly damaging because the crosstalk and the original signal have the same nominal wavelength and in this case the beating terms originated at the receiver cannot be removed by filtering [5].

The increasing of the bit rate and the consequent demanding requirements in the optical communication systems leads to an increasing interest in differential modulation techniques such as differential phase-shift keying (DPSK), which are more robust to transmission impairments than intensity modulation techniques [6]. DPSK modulation has attracted much attention in optical communications, mainly due to its high receiver sensitivity when balanced detection is used, as compared to on-off-keying (OOK) modulation. Using balanced detection, DPSK modulation has the advantage of requiring ~3 dB lower receiver sensitivity than OOK format and offering larges tolerance to signal-power fluctuations in the receiver decision circuit [6].

The influence of in-band crosstalk has been deeply analyzed in optical communication systems using direct-detection with the OOK modulation format [5], [7]. Recently, some crosstalk investigations concerning other modulation formats, such as the DPSK [7], [8], [9] and the differential quadrature phase-shift keying (DQPSK) [10] have also been performed. It has been experimentally found in [9] that the DPSK signal with balanced detection has ~ 6 dB higher tolerance to in-band crosstalk than the OOK signal.

1.2. Objectives and dissertation organization

This dissertation is within the optical communication networks area, in particular the area that studies the impact of the network physical layer constraints. The performance of an optical DPSK communication system with direct detection and using a balanced receiver will be analyzed considering the impact of ASE noise and in-band crosstalk on the performance.

Therefore, a stochastic simulation based on the Monte Carlo (MC) method is implemented to evaluate the performance of the optical DPSK communication system. Different performance measures are used in the MC simulation to evaluate the system performance, such as the bit error probability (BEP), the eye diagrams, the power penalty and the probability density function.

The remainder of this work is organized as follows: the second chapter explains the optical DPSK communication system model with balanced detection, its theoretical concepts and modeling. It also describes the implementation of the MC simulation and the method used to evaluate the BEP.

The third and fourth chapters compare and analyze the performance obtained for the optical DPSK communication system when it is impaired only by ASE noise, or when it is impaired by ASE noise and by in-band crosstalk, respectively. The impact of the imperfections on the performance of the optical DPSK receiver is also investigated in both chapters.

Finally, the fifth chapter outlines the main conclusions derived from this study and provides some ideas for possible future work.

2. Theoretical concepts

2.1. Introduction

In this chapter, the optical DPSK communication system with direct detection is described by: its schematic block diagram, mathematical model and computer model. All programming for implementing the simulation based on the MC method was done in Matlab®.

Figure 2.1 shows the schematic block diagram of an optical DPSK communication system, which includes the transmitter, the fiber transmission and the receiver [8].

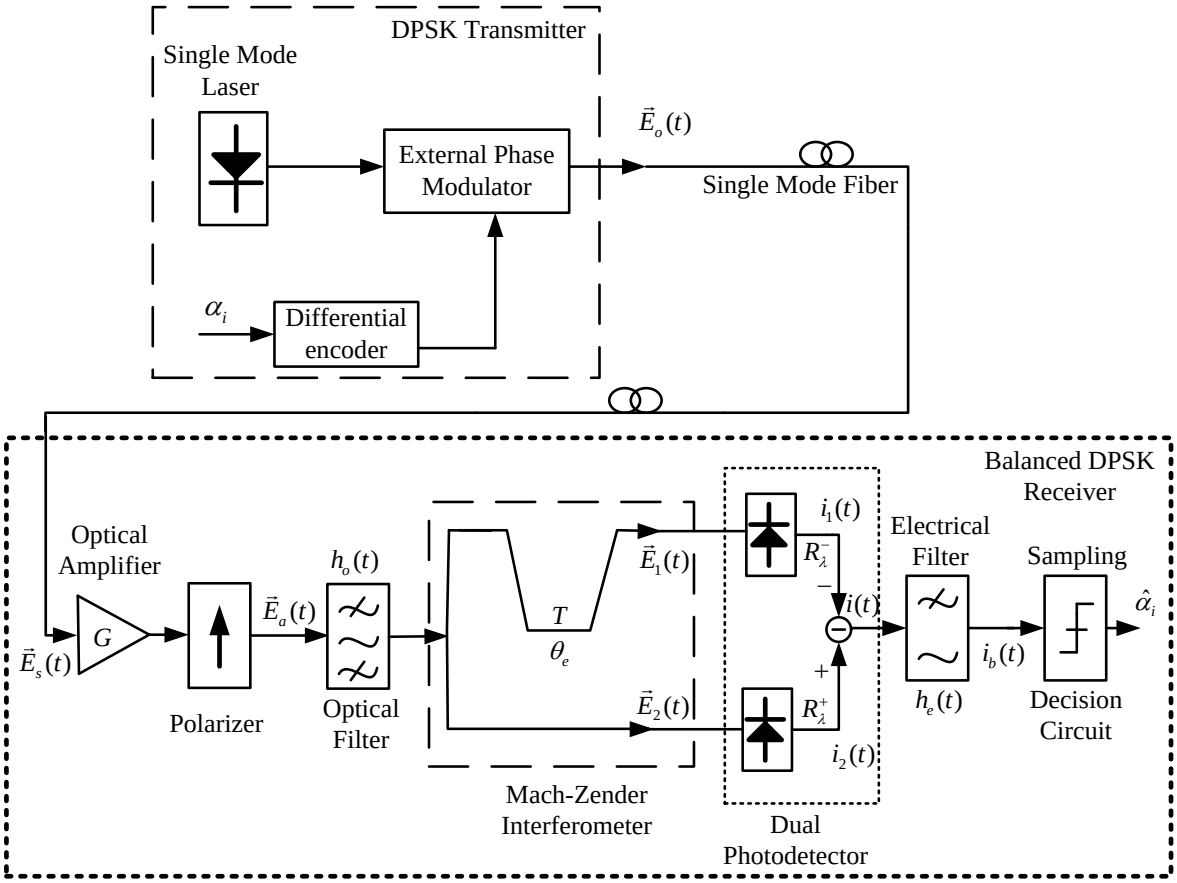

Figure 2.1 - Schematic block diagram of an optical DPSK communication system.

2.2. Transmitter description

The DPSK signal needs to be modulated to the optical domain. This modulation could be accomplished by directly modulating the bias current of the laser, but while being simple and economical, this technique is only implemented for short distances and bit rates below 2.5 Gbps [11]. For higher bit rates, it is more common to modulate the electrical signal using an external phase modulator [11]. Since the bit rate is always assumed to be higher than 2.5 Gbps, the external phase modulator is used in this dissertation.

So, the structure of the DPSK transmitter necessary to obtain a DPSK modulation format for bit rates higher than 2.5 Gbps in the optical domain consists on a single mode laser followed by an external phase modulator.

The most common external phase modulators used are the Mach-Zehnder modulator (MZM), typically based on $LiNbO_3$ technology. A MZM is biased at its null transmission and is driven at twice the required switching voltage. The method to generate the optical DPSK using a MZM and the corresponding DPSK constellation points are shown in Fig. 2.2. The phase of the optical field changes its sign when passing through a minimum in the MZM's power transmission curve and two neighboring intensity transmission maxima have opposite optical phases. Hence, a near-perfect 180º phase shift is obtained, independently of the drive voltage swing [6].

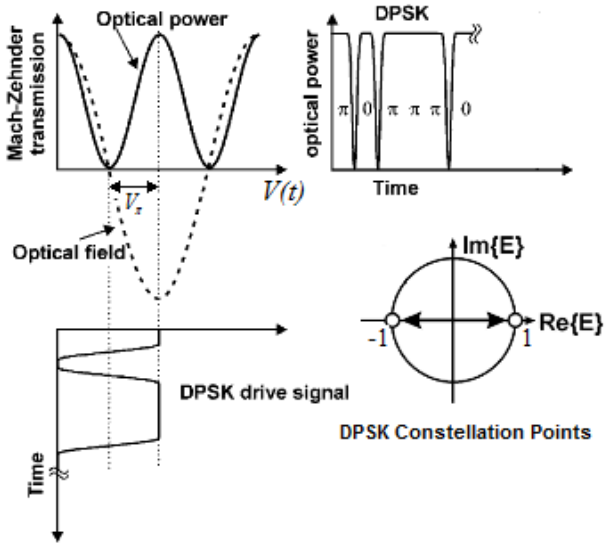

Figure 2.2 - Principle of phase modulation using a MZM (adapted from Fig. 3 of [6]).

The input-output relationship of the electrical fields of the external phase modulator is given by [3, chap. 2]

$$\frac{E_{out}(t)}{E_{in}(t)} = \cos\left(\frac{\pi}{2V_{\pi}}\left(V_b + V(t)\right)\right), \tag{2.1}$$

where V_b is the constant bias voltage of the MZM, $V(t)$ is the alternating current coupled electrical modulating signal, in this case, a DPSK electrical signal, and V_{π} is the voltage required to produce a π phase shift, which is typically between 3 and 5 V [3, chap. 2].

For simulation purposes, the non-return-to-zero (NRZ) signal is encoded differentially (as a DPSK signal) considering that for each bit '1' the optical phase does not change, and for each bit '0' a π-phase change is introduced, forming the DPSK drive signal. Figure 2.3 shows the NRZ signal and the phase of the optical modulated DPSK signal, represented by $\theta(t)$ [rad].

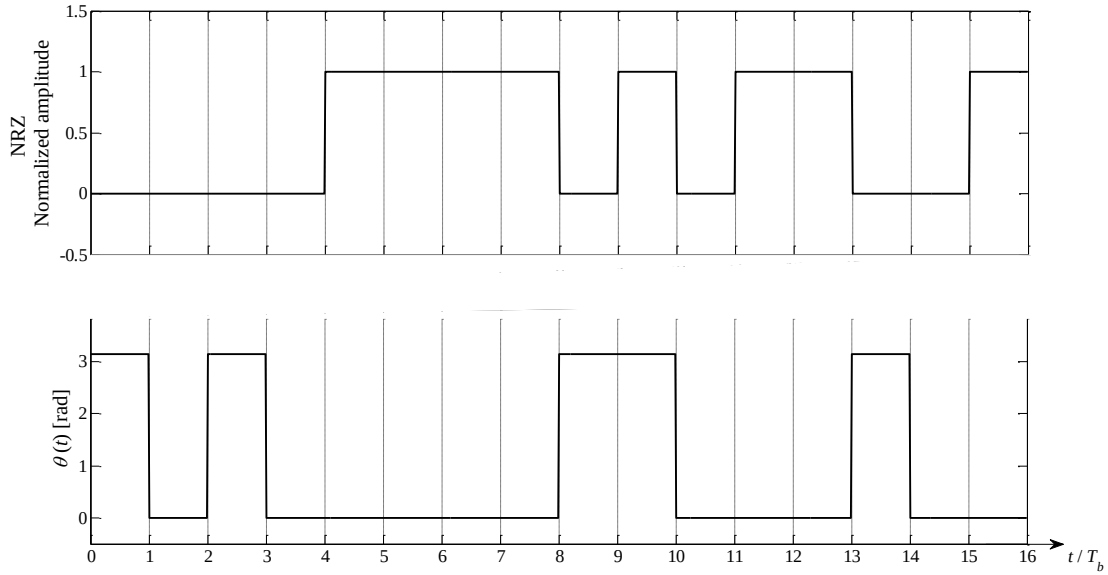

Figure 2.3 –NRZ signal and the phase of the DPSK signal.

The electrical field representing the modulated DPSK signal can be described as

$$\vec{E}_s(t) = E_{os}(t)\, e^{j\theta(t)}\vec{e}_s, \tag{2.2}$$

where $E_{os}(t)$ is assumed as an unitary amplitude and it is considered that the electrical field emitted by the laser is linearly polarized along the direction defined by the unitary vector, $\vec{e}_s$ with ($\vec{e}_s \bullet \vec{e}_s = 1$). The phase $\theta(t)$ is given by

$$\theta(t) = \sum_{i=1}^{N_b} \theta_i\, g(t - iT_b), \tag{2.3}$$

where $g(t)$ is given by

$$g(t) = \begin{cases} 1 & |t| \le T_b/2 \\ 0 & |t| > T_b/2 \end{cases}, \tag{2.4}$$

with N_b and T_b are the number of bits and the bit period, respectively.

The phase in each bit period is calculated by

$$\theta_i = \theta_{i-1} + \frac{\pi}{2}(1-\alpha_i). \tag{2.5}$$

For performing the differential encoding, $\alpha_i = -1$ for a NRZ bit '0' and $\alpha_i = 1$ for a NRZ bit '1'. The phase in the first bit of the DPSK sequence is assumed as $\theta_0 = 0$ [12].

Figure 2.4 shows the power spectral density (PSD) of the NRZ signal (left) and of the DPSK signal (right), where the optical carrier frequency is defined as ν_o.

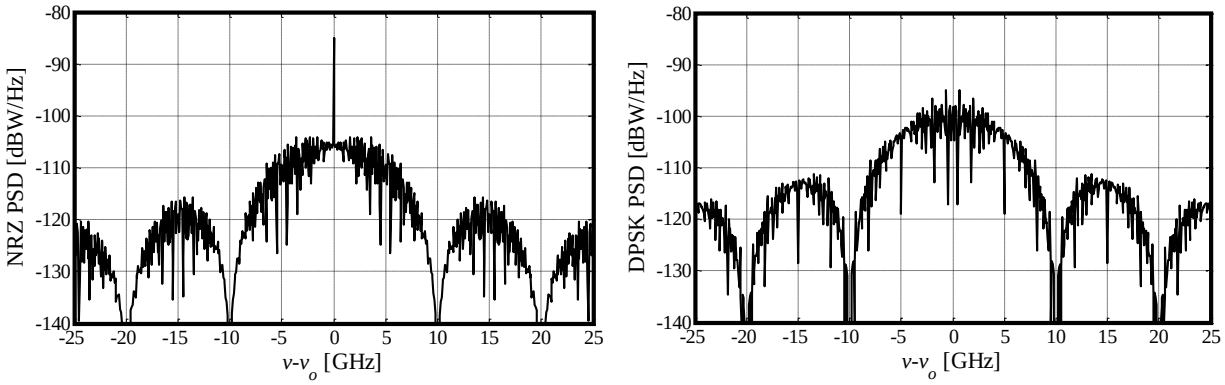

Figure 2.4 – PSDs of NRZ (left) and DPSK (right) signals.

Both signals are obtained with a bit rate of 10 Gbps and, thus, the null points of the principal lobe of the PSDs coincide with the bit rate value. For the PSD of the NRZ signal (left), the presence of the DC component can be detected by the peak of power at the zero frequency. As the DPSK signal average power is twice the NRZ signal power, the PSD of the DPSK signal (right) has an higher amplitude. Both PSDs of NRZ and DPSK signals are in agreement with the signals temporal representation shown in Fig. 2.3.

2.3. Receiver description

The structure of a typically direct-detection DPSK receiver is shown in Fig. 2.1. It consists of an optical pre-amplifier with gain *G*, a polarizer, an optical filter, a Mach-Zehnder delay interferometer (MZDI) with a differential delay *T*, which should be equal to the bit period T_b, a balanced dual photodetector, a post-detection electrical filter and a decision circuit [8].

2.3.1. Optical amplifier, polarizer and optical filter

Optical communication systems require the use of optical amplifiers to restore the optical signal power after long transmission distances. The main types of optical amplifiers (OAs) are Erbium doped fiber amplifier (EDFA), semiconductor optical amplifiers (SOAs) and Raman amplifiers [13], [14].

From the various available amplifiers, EDFAs are the most commonly adopted for optical communications because they operate in the C band (1528-1561 nm) and are able to achieve approximately 30 dB of gain [13]. The OAs can be modeled by an uniform gain across its entire bandwidth, given by

$$G = \frac{P_o}{P_s}, \tag{2.6}$$

where P_s and P_o represent the optical power at amplifier input and output, respectively. However, the OAs has the disadvantage of adding ASE noise. The single-sided PSD of ASE in each polarization at the output of the optical amplifier is represented by [8]

$$S_{ASE} = \frac{F_n}{2}(G-1)hv_o, \tag{2.7}$$

where F_n, G and *h* are the amplifier noise figure, the amplifier gain and the Planck constant, respectively. It is assumed that the gain G is sufficiently high, so that the ASE noise dominates over shot noise power and thermal noise power in the DPSK receiver, allowing the neglect of those noises in the present analysis [8].

The ASE noise power is given by

$$P_{ASE} = S_{ASE}B_{AO}, \tag{2.8}$$

where B_{AO} is the optical amplifier bandwidth. In the simulation, $B_{AO} = B_s$, where B_s is the simulation bandwidth. Thus, the electrical field corresponding to the ASE noise, $\vec{E}_{ASE}(t)$ is modeled by a band-pass Gaussian random process with zero mean and variance equal to P_{ASE}, and is generated on two polarization directions, parallel and perpendicular in relation to the signal. The perpendicular polarization of the ASE noise electrical field is eliminated by the polarizer.

The ASE originating from the EDFAs generates two additional beat noises after photodetection, generally referred as signal-ASE and ASE-ASE beat noises [15]. The beat noises arise after photodetection and this noise dominates the performance degradation.

So, the electrical field at the optical filter input is defined by

$$\vec{E}_a(t) = \left[\sqrt{GP_s}\,\vec{E}_s(t) + \vec{E}_{ASE}(t) \right] \vec{e}_s. \tag{2.9}$$

The optical filter is described by the impulsive response $h_o(t)$ and by the –3 dB bandwidth B_o. At the optical filter output, the electrical field of the DPSK signal is given by

$$\vec{E}_{FO}(t) = \left[\vec{E}_a(t) * h_o(t) \right] \vec{e}_s. \tag{2.10}$$

2.3.2. MZDI and dual photodetector

The differential demodulation is done in the optical domain by the MZDI and the dual photodetector. The delay-interferometer, (see Fig. 2.1) has ideally a differential delay T equal to the bit period, T_b, and acts as an optical demodulator, converting the phase modulation to intensity modulation. The MZDI leads to interference between two adjacent bits at its output ports. This interference leads to the presence (absence) of power at a MZDI output if two adjacent bits interfere constructively (destructively) with each other. Thus, the preceding bit in a DPSK encoded bit stream acts as the phase reference for demodulation of the current bit. Two MZDI output ports generally carry identical, but logically inverted data streams under DPSK modulation. This optical signal preprocessing is necessary in direct-detection receivers to accomplish demodulation, since the photodetection process is insensitive to the optical phase, a detector only converts optical intensity modulation into an electrical current [6].

The demodulated fields at each interferometer arm output are defined by $\vec{E}_1(t)$ and $\vec{E}_2(t)$, and are given by [12]

$$\begin{bmatrix} \vec{E}_1(t) \\ \vec{E}_2(t) \end{bmatrix} = \begin{bmatrix} 1-\varepsilon & -\varepsilon \\ j\sqrt{\varepsilon(1-\varepsilon)} & j\sqrt{\varepsilon(1-\varepsilon)} \end{bmatrix} \begin{bmatrix} \vec{E}_a(t) \\ \vec{E}_a(t-T)e^{j\theta_e} \end{bmatrix} \vec{e}_s, \tag{2.11}$$

where, ε and θ_e define the coupling coefficient and the optical phase error, respectively. The influence of the optical phase error in the performance of the optical DPSK receiver is analyzed in subsection 3.5. Ideally, there is no optical phase error leading to a perfect constructive or destructive interference at the interferometer output ports [6].

Figure 2.5 depicts the PSDs at each interferometer output, the signal $\vec{E}_2(t)$ at the constructive port (left) and the signal $\vec{E}_1(t)$ at the destructive port (right).

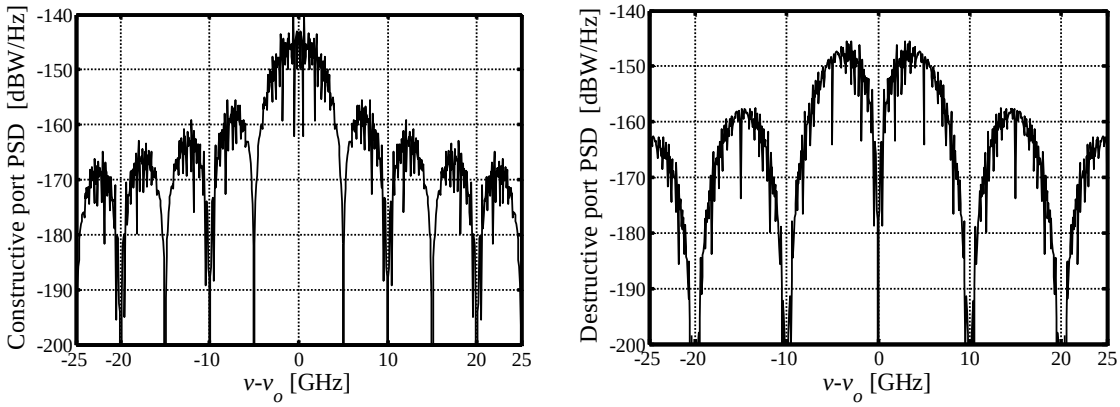

Figure 2.5 – PSDs of signals $\vec{E}_2(t)$ at constructive port (left) and $\vec{E}_1(t)$ at destructive port (right).

The PSDs of both branches are in agreement with the PSDs shown in [6] and indicate that the simulation of the DPSK signaling and detection is implemented correctly.

The dual photodetector uses two positive intrinsic negative (PIN) photodiodes. The function of a photodiode is to convert the optical power into an electrical current in order to recover the transmitted data. A dual photodetector generates two photocurrents, $i_1(t)$ and $i_2(t)$, proportional to the optical powers $p_1(t)$ and $p_2(t)$ incidents in each photodiode of the dual receiver. These photocurrents $i_1(t)$ and $i_2(t)$ are given by

$$\begin{aligned} i_1(t) &= R_\lambda^- p_1(t) \\ i_2(t) &= R_\lambda^+ p_2(t) \end{aligned}, \tag{2.12}$$

where R_λ^+ and R_λ^-, correspond to the responsivity of each photodiode in constructive and destructive branch, respectively, and are expressed in Ampere/Watts (A/W). The responsivity of a photodiode is defined by

$$R_\lambda = \frac{\eta q}{h\nu_o}, \tag{2.13}$$

where η and q are the photodiode quantum efficiency and the electron charge, respectively.

The currents $i_1(t)$ and $i_2(t)$ depend on two signals: the signal at MZDI input, $\vec{E}_a(t)$ and the MZDI input signal with a bit period delay, $\vec{E}_a(t-T)$. At the photodetector output if $\vec{E}_a(t)$ and $\vec{E}_a(t-T)$ are equal, in the constructive port, the expected signal is a bit '1'. Otherwise, in the constructive port, the expected signal is a bit '0'. In the destructive port, the inverse process of the constructive port is observed for the signal.

Accordingly with (2.11), the optical powers at the dual photodetector output in the upper and lower branch, and neglecting the ASE noise, are defined, respectively, by

$$\begin{aligned} &p_1(t) = \vec{E}_1(t).\vec{E}_1^*(t) = \\ &= \left\{ (1-\varepsilon)^2 \left|E_a(t)\right|^2 + \varepsilon^2 \left|E_a(t-T)\right|^2 - 2\varepsilon(1-\varepsilon)\Re\left[\vec{E}_a(t)\vec{E}_a^*(t-T)e^{j\theta_e}\right]\right\} \end{aligned} \tag{2.14}$$

$$\begin{aligned} &p_2(t) = \vec{E}_2(t).\vec{E}_2^*(t) = \\ &= \varepsilon(1-\varepsilon)\left\{ \left|E_a(t-T)\right|^2 + \left|E_a(t)\right|^2 + 2\Re\left[\vec{E}_a(t)\vec{E}_a^*(t-T)e^{j\theta_e}\right]\right\} \end{aligned} \tag{2.15}$$

with

$$\left|E_a(t)\right|^2 = GP_s\left|E_{os}(t)\right|^2 \tag{2.16}$$

and

$$\Re\left[\vec{E}_a(t)\vec{E}_a^*(t-T)e^{j\theta_e}\right] = GP_sE_{os}(t)E_{os}(t-T)\cos\left[\Delta\theta(t)-\theta_e\right], \tag{2.17}$$

where, $\Re[.]$ defines the real part of a complex number and $\Delta\theta(t)$ is given by

$$\Delta\theta(t) = \theta(t) - \theta(t-T). \tag{2.18}$$

The difference between these two photocurrents produces the photocurrent $i(t)$,

$$i(t) = i_2(t) - i_1(t). \tag{2.19}$$

Assuming equal responsivities, $R_\lambda^+ = R_\lambda^- = R_\lambda$, $i(t)$ is given by,

$$i(t) = R_\lambda \left\{ \begin{array}{l} \varepsilon(1-2\varepsilon)\left|E_a(t-T)\right|^2 + (-2\varepsilon^2 + 3\varepsilon - 1)\left|E_a(t)\right|^2 + \\ + 4\varepsilon(1-\varepsilon)GP_s E_{os}(t)E_{os}(t-T)\cos\left[\Delta\theta(t) - \theta_e\right] \end{array} \right\}. \quad (2.20)$$

Considering $\varepsilon = 0.5$, and $E_{os}(t)$ as an unitary amplitude, $i(t)$ is given by,

$$i(t) = R_\lambda GP_s \cos\left[\Delta\theta(t) - \theta_e\right]. \quad (2.21)$$

The signals at the dual photodetector output, $i_1(t)$ and $i_2(t)$, and the photocurrent $i(t)$ are represented in Fig. 2.6, with $\theta_e = 0$.

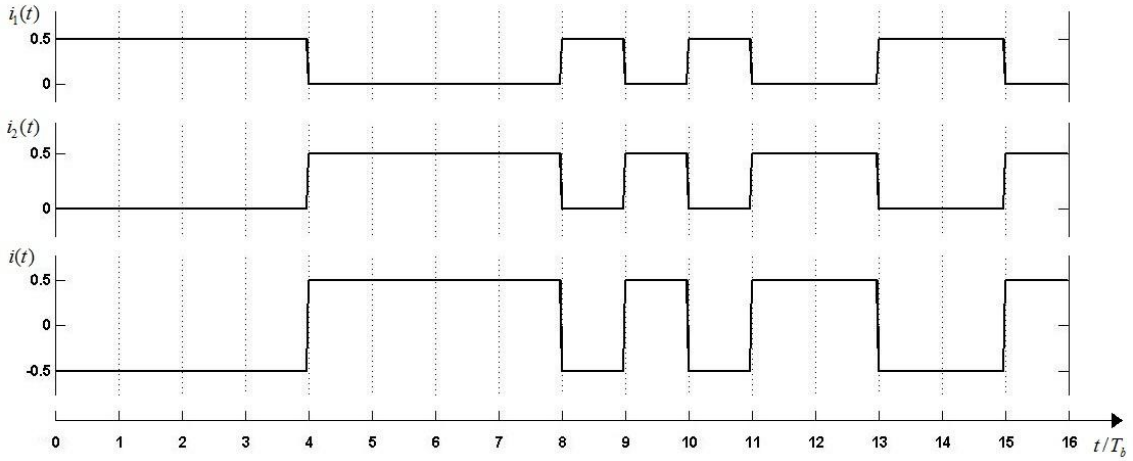

Figure 2.6 – Photocurrents, $i_1(t)$, $i_2(t)$ and $i(t)$.

The signal detection can be done at the constructive port output, accordingly with Fig. 2.6, but for this situation the receiver sensitivity advantage of approximately 3 dB of a balanced DPSK receiver over an OOK reception is lost [6].

2.3.3. Electrical filter and decision circuit

After passing through the MZDI and the dual photodetector, the signal passes by an electrical filter, which can model the frequency limitations of the photodetectors. The electrical filter is described by the impulsive response $h_e(t)$ and by the electrical bandwidth B_e at –3 dB. At the electrical filter output, the current of the signal is given by

$$i_b(t) = i(t) * h_e(t). \quad (2.22)$$

At the decision circuit, the current $i_b(t)$ is sampled every bit period and each sample is compared with a threshold level in order to decide which bit has been transmitted [16]. In a DPSK receiver, the threshold level is typically zero.

The electrical circuitry at the optical receivers generates circuit noise [3, chap. 5]. However, due to the high gain of the optical amplifier, the ASE noise beatings dominate over the circuit noise and, hence, in this work, circuit noise is neglected in the DPSK receiver performance evaluation [17].

Figure 2.7 shows the simulated bits at the decision circuit output.

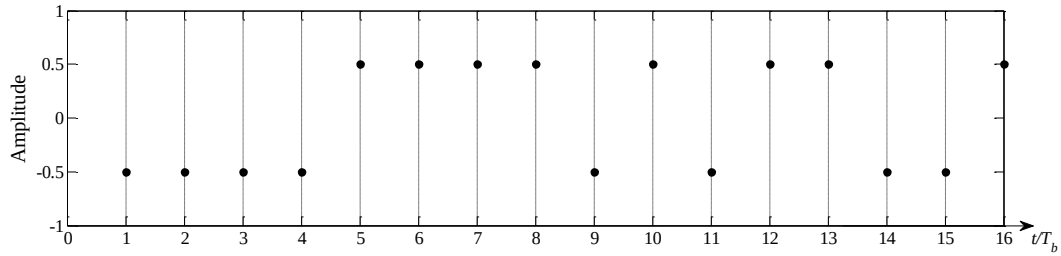

Figure 2.7 – Signal at the decision circuit output.

The signal representation at the DPSK output receiver in Fig. 2.7 is the same as the NRZ signal representation at the DPSK output transmitter in Fig. 2.3.

2.4. Implementation of the Monte Carlo simulator

2.4.1. Signals simulation

The main goal of this work is to create a simulation tool capable of evaluating the performance of the optical DPSK communication system, by calculating its bit error probability (BEP) and the impact of the in-band crosstalk in the system performance. The simulation involves the generation of the signals, its processing and the modeling of several devices.

The simulated signals in Matlab® are represented by discrete vectors, in time and frequency. Each vector position is indexed to a time instant, corresponding to a continuous signal sample. The length of time and frequency vectors is the same, and it is equal to the multiplication of the number of samples per bit (N_a) and the number of bits (N_b) considered in the simulation.

In the simulation, a pseudorandom binary sequence with all possible combinations of b bits and length $N_b = 2^b$ bits is generated using deBruijn sequences [18, chap. 7]. This ensures that all bit patterns of length b are taken into account when studying ISI in a communication system with memory length (measured in bit intervals) of b. If the system memory is higher than b, a higher number of bits must be simulated in order to more rigorously consider the effect of ISI on the system performance. Then, in order to consider ISI inside a bit period of T_b, the bits sequence is sampled N_a times, generating a sampling sequence with $(N_b N_a)$ positions, with a corresponding time length of $(N_b T_b)$. The sampling time is $T_a = T_b / N_a$.

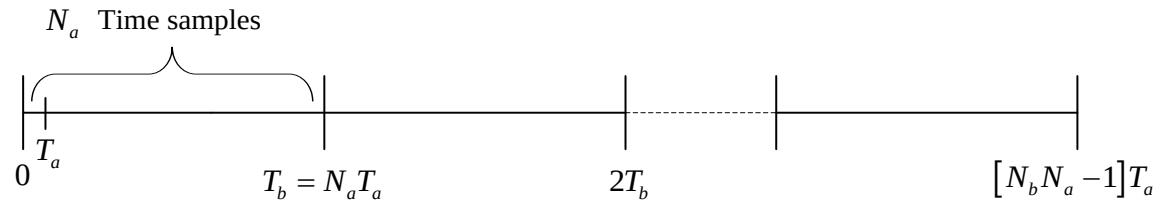

Figure 2.8 – Simulated time vector.

Figure 2.8 shows the simulated time vector. Each n position of the time vector corresponds to the time instant $(n-1)T_a$ at which a sample of the continuous signal is taken.

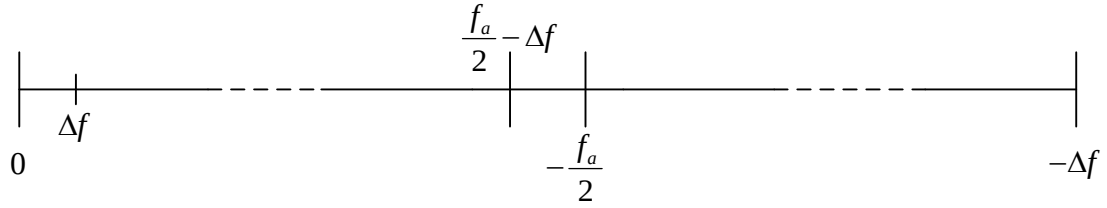

Figure 2.9 – Simulated frequency vector.

Figure 2.9 shows the simulated frequency vector. The signal representation in frequency is obtained using the fast Fourier transform (FFT), an algorithm which calculates the Discrete Fourier Transform (DFT)[1] of the sampled discrete signal [18, chap. 3]. If the vectors lengths are not 2^b, the algorithm used is much slower[2] [18, chap. 3].

[1] The result from the FFT must be multiplied by T_a because the FFT algorithm is not equivalent to the DFT. By the same reason, the result of an inverse fast Fourier (IFFT) must be divided by T_a. If a pair FFT/IFFT is applied, this correction factor is not necessary, since its transform effect is cancelled out.

[2] The FFT requires that the vectors length must be 2^N where N is an integer number, due to the algorithm denominated radix 2 fast, used to calculate the FFT and the IFFT, which gives more celerity to the simulation.

The vector which represents the signal is shifted in frequency. The fftshift Matlab function must be applied to visualize the signal spectrum in its appropriate order. The frequency vector, first shows the positives frequencies $\left[0, \frac{f_a}{2} - \Delta f\right]$ and then the negatives $\left[-\frac{f_a}{2}, \Delta f\right]$, where $f_a = 1/T_a$ is the sampling frequency and Δf is given by

$$\Delta f = \frac{1}{N_b T_b}, \tag{2.23}$$

which defines the resolution of the frequency vector. From (2.23), to increase the resolution in the frequency, a higher number of bits should be simulated. A higher number of samples per bit, N_a increases the sampling frequency and consequently, the frequency window.

2.4.2. Monte Carlo simulation

A MC simulation is a tool that allows the study of a random phenomenon by generating sequences of random numbers that represent the sample functions of the random phenomenon.

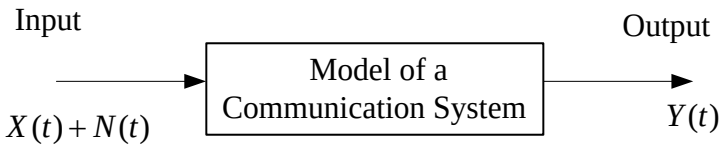

Figure 2.10 – Block diagram of the Monte Carlo simulation.

Figure 2.10 shows the block diagram of a MC simulation, where $X(t)$ is a deterministic signal, $N(t)$ is the random process at the communication system input and $Y(t)$ is the signal obtained at the communication system output. A MC simulation generates random sample functions of $N(t)$, which are added to $X(t)$ and passed through the communication system. The statistical properties (*e.g.* probability density function) of the signal $Y(t)$ are measured at the communication system output [18, chap. 7].

Initially, the random process considered in the simulation is the ASE noise introduced by the EDFAs. The ASE noise field[3] [19], in one polarization, is modeled as an additive white

[3] A common normalization used in the literature consists in the multiplication of the ASE noise field by the factor $\sqrt{2}$. In this situation, the power of the simulated optical signal is the same as the real signal power.

Gaussian noise (AWGN) process with in-phase $N_i(t)$ and quadrature $N_q(t)$ components related by

$$\vec{E}_{ASE}(t) = N(t) = \frac{1}{\sqrt{2}}\left[N_i(t) + jN_q(t) \right]\vec{e}_s. \tag{2.24}$$

Each noise component sample function is generated using a generator of a Gaussian distributed numbers[4], considering a zero mean and a variance equal to $S_{ASE} f_a$, where f_a is equivalent to the simulation bandwidth, B_s. The MC simulation is performed by generating a number of ASE noise sample functions sufficiently high enough to provide an accurate description of the statistical properties of $Y(t)$.

The PSD can be estimated using the periodogram definition [20]. After observing a sample function $Y(t)$ over a long time interval T, the PSD can be estimated by

$$\tilde{G}_y(f) = \frac{1}{T}\left|Y_i(f)\right|^2, \tag{2.25}$$

where $Y_i(f)$ represents one sample function of $Y(t)$ in the frequency domain. The signal average power over a time interval T_s is given by [21]

$$\overline{p} = \frac{1}{T_s}\int_{T_s}\left|Y(t)\right|^2 dt. \tag{2.26}$$

In the MC simulation, the signal average power is determined by the trapezoidal[5] numerical integration.

2.4.3. The Monte Carlo simulation flowchart

The flowchart presented in Fig. 2.11 shows the implemented MC simulator of the optical DPSK receiver impaired by the ASE noise.

Firstly, at the transmitter a pseudorandom binary sequence is generated using deBruijn sequence. This generated sequence is sampled and, then, the angles $\theta(t)$ corresponding to the phase of the DPSK signal are calculated using (2.5). Subsequently, the DPSK signal at the transmitter output is obtained using (2.2).

[4] In Matlab®, this function is implemented using randn.m.
[5] In Matlab®, this function is implemented using trapz.m.

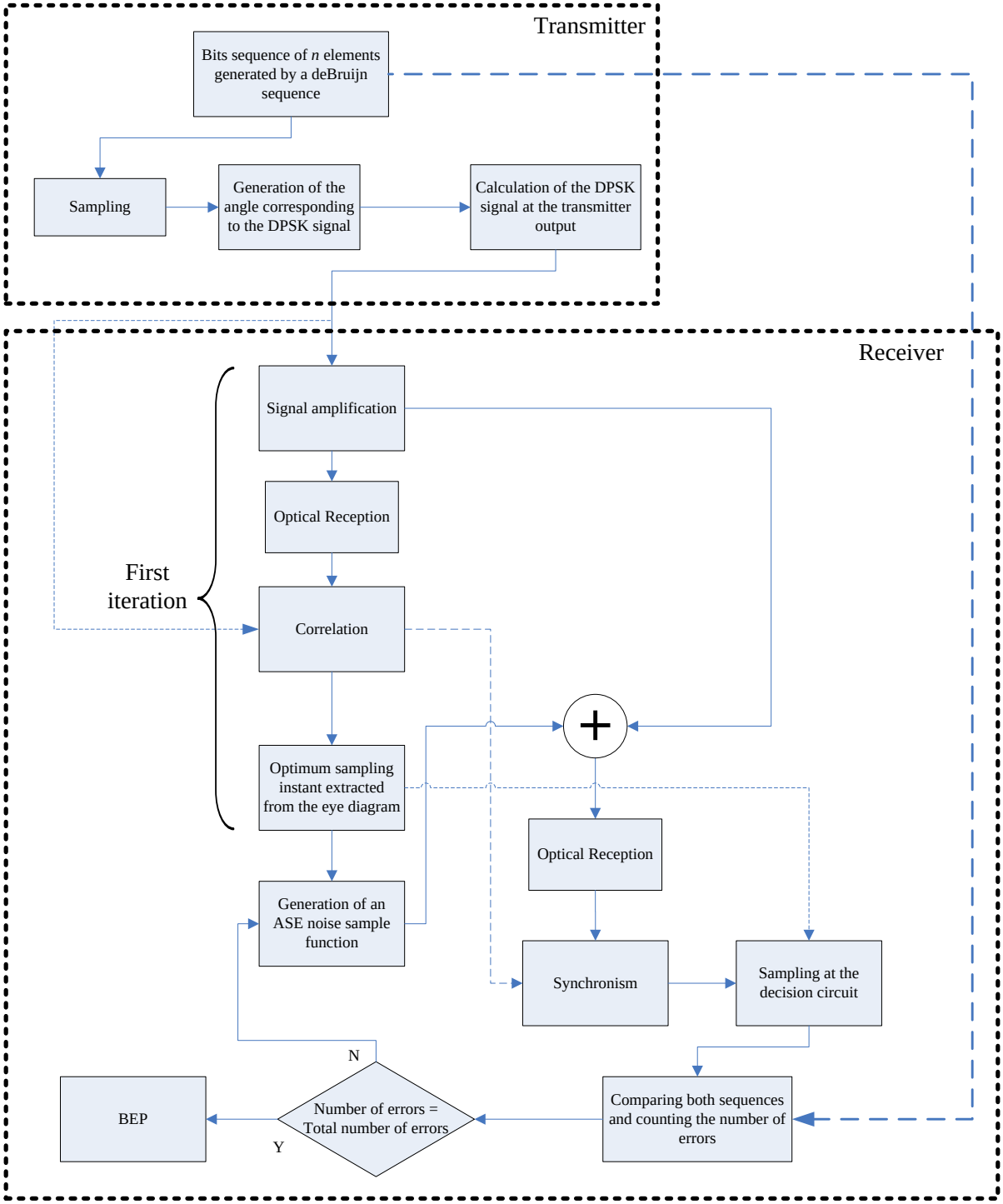

Figure 2.11 – Flowchart of the MC simulation for a back-to-back configuration.

At the receiver input, and considering a back-to-back configuration, the optical signal is amplified. In the first iteration, the MC simulation is performed without noise, and the amplified signal passes through the optical receiver. The received signal is then correlated with the signal at the optical amplifier input, in order to identify the time propagation delay of the optical receiver, and after that the optimum sampling time is extracted from the eye

diagram. Then, a new random ASE noise sample function is generated and added to the amplified signal. The ASE noise sample added to the amplified signal passes through the optical receiver and is synchronized using the estimated propagation delay and the optimum sampling time. After synchronization and sampling, each received bit is compared with the bit of the deBruijn sequence to determine the number of errors, N_e. In the next iterations, the number of errors from the previous iterations is added to the number of errors obtained in the current iteration. The cyclical process ends when the number of erroneous bits is the same as the total number errors, N_e, initially imposed for a specific accuracy of the MC simulation. The simulation process ends with the calculation of the BEP.

Correlation and Synchronization

The correlation process which is imposed at the first iteration on the receiver is necessary to determine the time propagation delay along the optical reception and allows to construct the eye diagram at the decision circuit input. This delay is used to synchronize the received sequence with the original sequence, in order to decide if the received bit has an error. The optimum sampling instant is extracted from the eye diagram considering the maximum eye opening and it is used in the decision to sample the received DPSK signal.

Calculation of the Bit Error Probability

In the MC simulation, the BEP is estimated through direct-error counting by

$$BEP = \frac{N_e}{N_{it}(N_b - 1)}, \tag{2.27}$$

where N_{it} is the number of iterations of the MC simulator.

In the MC simulation, the first bit of the received DPSK signal is excluded, since it depends on a previous bit, which is outside the time window of the simulator.

3. Optical DPSK communication system impaired by ASE noise

3.1. Introduction

In this chapter, the performance of an optical DPSK communication system impaired by ASE noise is investigated in a back-to-back configuration using MC simulation. Section 3.2 presents the model and characterization of the filters considered in the simulations. In section 3.3, the implementation of the MC simulation is validated by comparison of its BEP estimates, with the estimates of the analytical formulation proposed in [7], developed to assess the performance of optical DPSK communication systems. Notice that the analytical formulation [7] is derived for an isolated DPSK symbol, while the MC simulation is run with a sequence of N_b bits. Section 3.4 shows the performance of the optical DPSK balanced receiver studied for different optical and electrical filter combinations. In section 3.5, two DPSK receiver imperfections are studied: the interferometer detuning and the responsivity imbalance. The MC simulation is validated once again by comparison of its BEP estimates, with the estimates of the analytical formulation developed in [7] and with the results obtained in [22]. Table 3.1 shows the parameters considered to evaluate the performance of the optical DPSK communication system. Unless stated otherwise, these parameters are used throughout this chapter.

Table 3.1. Parameters of the simulated optical DPSK communication system impaired by ASE noise.

Parameter	Value
Number of bits (N_b)	64
Number of samples (N_a)	256
Number of erroneous bits (N_e)	100
EDFA gain (G)	30 dB
Responsivity (R_λ^+, R_λ^-)	1A/W
Amplified noise figure (F_n)	5 dB
Bit period (T_b)	0.1 ns
Polarizer	Present
Phase error of the interferometer (θ_e)	0º

3.2. Filters characterization

In this section, the filters used in the simulation are described and its main characteristics are analyzed. B_o is defined as the –3 dB bandwidth of the optical filter and B_e is the –3 dB bandwidth of the electrical filter.

3.2.1. Ideal filter

The impulse response of an ideal optical filter (lowpass equivalent definition) is given by [23],

$$h_o(t) = B_o \text{sinc}(B_o t), \tag{3.1}$$

and its transfer function is given by,

$$H_o(f) = \text{rect}\left(\frac{f}{B_o}\right). \tag{3.2}$$

An ideal optical filter passes exactly all the signal frequencies inside its passband bandwidth and completely rejects the others. Figure 3.1 represents the ideal optical filter transfer function for $B_o T_b = 100$.

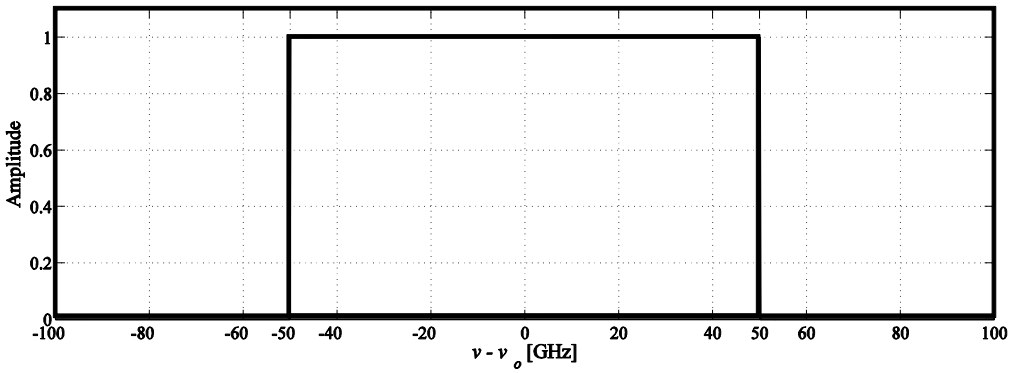

Figure 3.1 – Ideal filter transfer function for $B_o T_b$ = 100.

3.2.2. Gaussian filter

The Gaussian filter is used as an optical filter and as an electric filter, where $B_e = 2B_o$. The impulse response of an optical Gaussian filter is given by [24],

$$h(t) = \sqrt{\frac{2\pi}{\ln 2}} . \frac{B_o}{2} e^{-\frac{2\pi^2}{\ln 2}.(\frac{B_o}{2}t)^2}, \tag{3.3}$$

with transfer function given by,

$$H(f) = \exp\left[-\frac{f^2}{B_o^2} \frac{2}{\ln 2} \right]. \tag{3.4}$$

Notice that the Gaussian filter has a zero phase response and is usually used in the optical communication systems, because its frequency response is similar with the transfer function of an arrayed-waveguide grating [24].

3.2.3. Lorentzian filter

The impulse response of a Lorentzian optical filter is given by [25],

$$h(t) = \pi B_o e^{-\pi B_o t}, t \geq 0 \tag{3.5}$$

where its transfer function is given by,

$$H(f) = \frac{1}{1 + 2j\frac{f}{B_o}}. \tag{3.6}$$

Fabry-Perot filters are widely used in optical transmission systems and their response can be approximated by a Lorentzian impulse response [26].

3.2.4. Integrator filter

The integrator filter is only used as an electrical filter. The impulse response of an integrator filter is given by [7],

$$h(t) = rect\left(\frac{t}{T_b} \right) \tag{3.7}$$

where its transfer function is given by,

$$H(f) = T_b \text{sinc}(fT_b). \tag{3.8}$$

Figure 3.2 shows the transfer function of an integrator electrical filter.

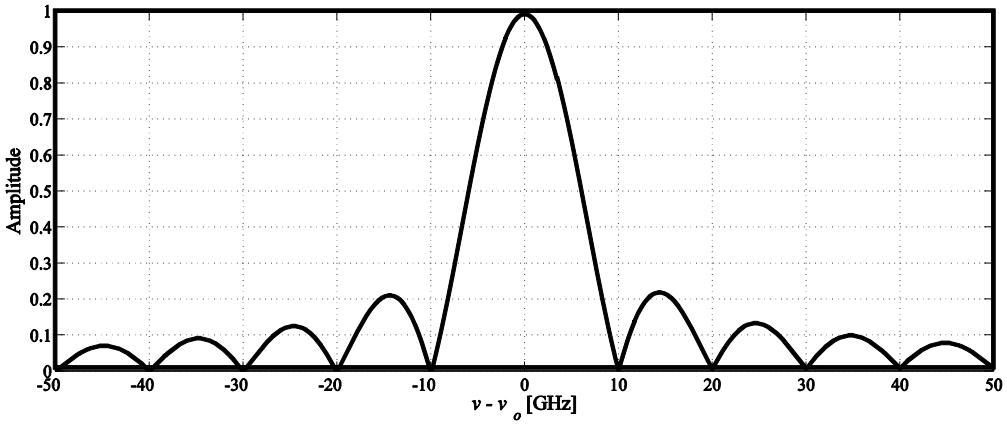

Figure 3.2 – Electrical integrator filter transfer function for B_eT_b = 1.

3.2.5. RC filter

The RC filter is an electrical filter with impulse response given by [7],

$$h(t) = 2\pi B_e e^{-2\pi B_e t},\ t \geq 0 \tag{3.9}$$

with transfer function defined by,

$$H(f) = \frac{1}{1 + j\dfrac{f}{B_e}}. \tag{3.10}$$

Figure 3.3 depicts the amplitude response of the Gaussian and Lorentzian optical filters with a –3 dB bandwidth $B_o = 100$ GHz.

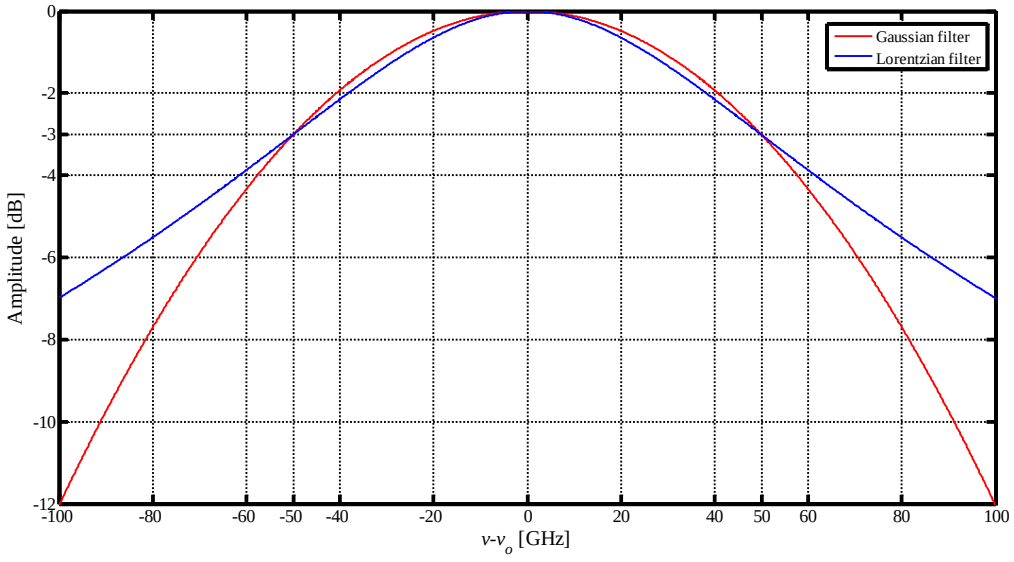

Figure 3.3 – Amplitude response of the Gaussian and Lorentzian optical filters.

Accordingly with Fig. 3.3, it can be visualized that the Gaussian optical filter is more selective than the Lorentzian optical filter because its amplitude response is flatter inside its passband and exhibits a highest rejection.

Figure 3.4 presents the amplitude response of the Gaussian and RC electrical filters, for a –3 dB bandwidth of $B_e = 7$ GHz.

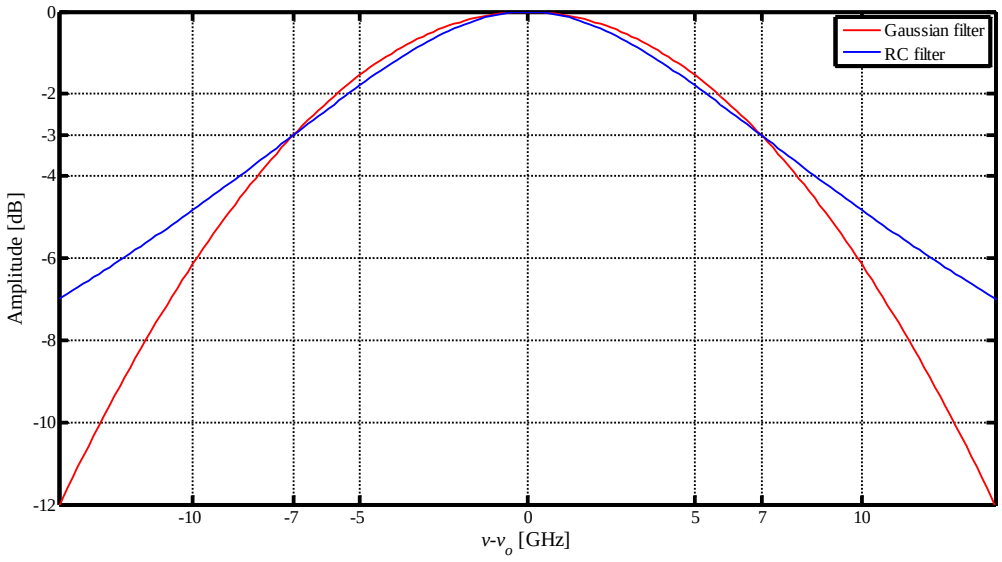

Figure 3.4 – Amplitude response of the Gaussian and RC electrical filters.

From Fig. 3.4, it can be concluded that the Gaussian electrical filter is again more selective than the RC electrical filter because the Gaussian filter has a flatter amplitude response in the cut-off frequency. The RC filter presents a lowest rejection in the amplitude response, which can lead to more degradation in the simulation, due to higher filtered ASE noise power.

The Lorentzian and RC filters are the only filters considered in this work that have a phase response, and consequently a delay response. Although, the Lorentzian filter being an optical filter and the RC filter an electrical filter, they exhibit the same response since their definition is identical [see (3.6) and (3.10)].

Figure 3.5 shows the group delay response of a RC electrical filter, for the –3 dB bandwidths $B_e = 3.5$, 7, 10 and 13 GHz.

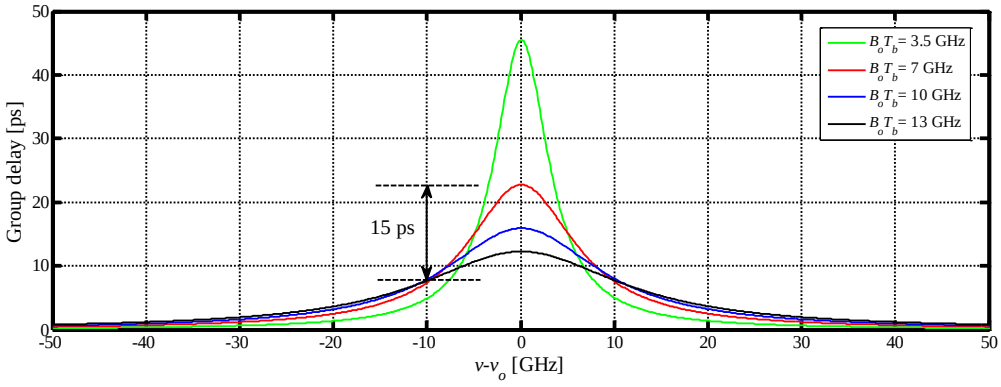

Figure 3.5 – Group delay of the RC filter for different electrical filter –3 bandwidths.

From Fig. 3.5, it can be concluded that RC electrical filter with smaller bandwidths exhibit a higher group delay. As the bit rate considered in this work is 10 Gbps, electrical filters with a –3 dB bandwidth of 3.5 GHz would lead to a severe signal degradation due to their higher delay distortion. Even for $B_e = 7\,\text{GHz}$, the delay distortion (inside the bandwidth of 10 GHz) is about 15 ps, i.e., about 15% of the bit period, and so a higher performance degradation is expected.

3.3. Validation of the Monte Carlo simulation

In this section, the MC simulation is validated by comparison with the analytical formalism developed in [7] for an isolated DPSK symbol. This analytical formalism can consider arbitrary optical and electrical filtering at the optical DPSK receiver. Notice that this validation is accomplished by comparison of BEP estimates obtained using the MC simulation with the estimates calculated by the analytical formalism [7]. The accuracy of the MC simulation BEP estimates with the number of bits and the number of errors used in the simulation is also studied. In this subsection, all the MC simulations are obtained for an ideal optical filter (OF) and an integrator electrical filter (EF). The bandwidth of the electrical filter is always the same, B_e = 10 GHz.

In this section, the BEP estimates obtained from the MC simulation are depicted with a solid line or with a legend (S), while the BEPs obtained with the analytical formalism are depicted with a dashed line or with a legend (A).

Figure 3.6 shows BEP estimates of the MC simulation, as a function of the optical signal power for different optical filter –3 dB bandwidths, compared with the BEP estimates of the analytical formalism [7]. The optical signal power is obtained at the optical pre-amplifier input.

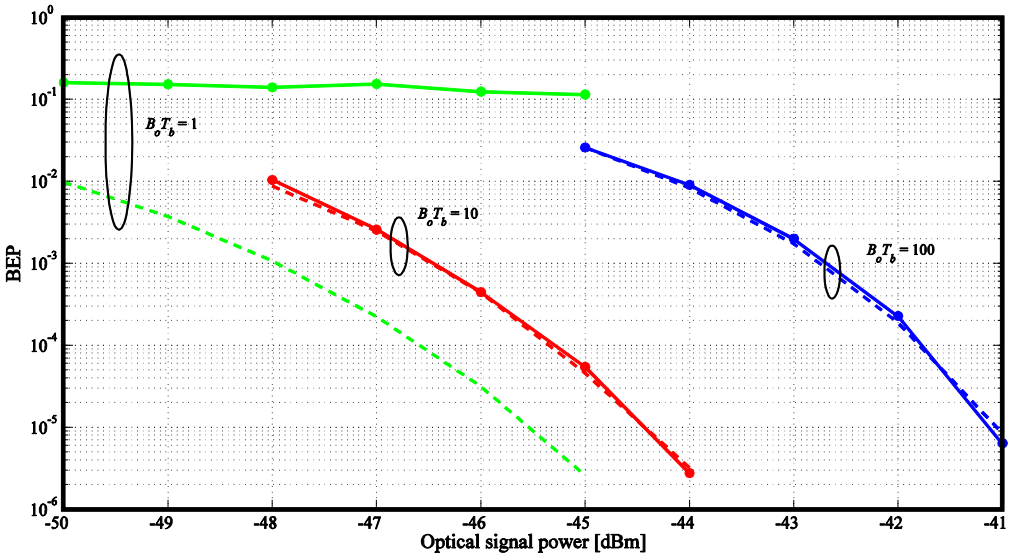

Figure 3.6 – BEP as a function of the optical signal power, for the ideal OF and the integrator EF combination, considering B_oT_b = 1, 10 and 100.

As the MC simulation is obtained with a sequence of bits, it takes into account the ISI effect on the DPSK receiver performance. As the analytical formulation neglects this effect, for smaller normalized optical filter bandwidths $(B_oT_b = 1)$, the BEPs estimated from the MC simulation and the analytical formulation are very discrepant. For normalized higher optical filter bandwidths $(B_oT_b = 10, 100)$, the simulated results are very similar to the results obtained with the analytical formulation, and the MC simulator can be considered validated for this situation.

Figure 3.6 also shows that, for the same optical signal power, there is a severe increase of the BEP with the optical filter bandwidth enlargement. This occurs because with the increase of the optical filter bandwidth, the filtered ASE noise power is higher, and the receiver performance is degraded.

Figure 3.7 depicts the BEPs obtained with the MC simulation and with the analytical formalism [7], for normalized optical filter bandwidths, where the ISI effect on the performance is relevant [$B_oT_b \leq 2$].

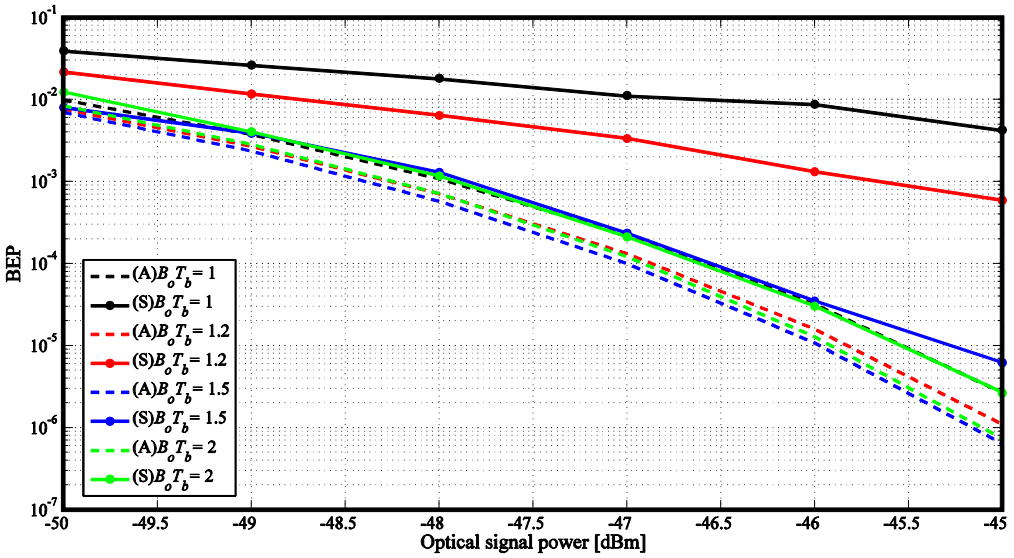

Figure 3.7 – BEP as a function of the optical signal power, for the ideal OF and the integrator EF combination considering smaller normalized optical filter bandwidths.

Accordingly with Fig. 3.7, it can be assumed that the simulated results become similar to the analytical results above $B_oT_b = 2$. This means that the ISI effect starts to lose its influence as the dominant source of performance degradation and provides a reference for the optical filter bandwidth above which, the precision of the analytical formalism (that neglects ISI) is ensured. It is important to notice that the ISI effect on the performance depends on the optical and electrical filters combination.

Figure 3.8 depicts the probability density function (PDF) for B_oT_b equal to 1 (red), 5 (blue) and 10 (green), using an optical signal power of –47dBm.

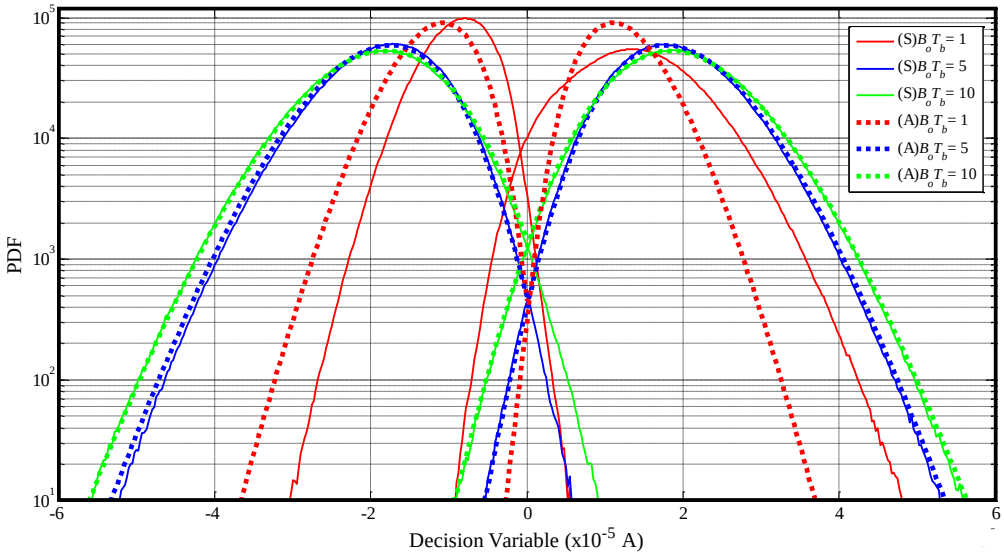

Figure 3.8 – PDF of the decision variable, for the ideal OF and the integrator EF combination, considering an optical signal power with –47 dBm and B_oT_b = 1, 5 and 10.

The estimates of the MC simulation and the analytical formalism from [7] are represented by the solid and dashed curves, respectively. Accordingly with Fig. 3.8, a very good agreement is found between the PDFs estimated using both methods, for B_oT_b = 5 and B_oT_b = 10, which ensures again the validation of the MC simulation implementation. Only for smaller normalized optical filter bandwidths, near B_oT_b = 1 there exists a difference between the PDFs of the bits '0' and '1', calculated using MC simulation and the PDFs estimated analytically. The ISI effect on the PDFs assumes the highest relevance with the decrease of the bandwidth of the optical filter, especially for smaller normalized optical filter bandwidths, $B_oT_b = 1$, which leads to a growing asymmetry between the PDFs of the bits '0' and '1' and to an optimum decision threshold deviation from zero to negative values. This asymmetric behavior does not occur on the analytical formalism [7], because this formalism assumes an isolate DPSK symbol and neglects the ISI effect. The PDFs asymmetric behavior (observed in the MC simulation) is in agreement with the results presented in [27], which also consider a sequence of bits to obtain the PDFs.

Figure 3.8 also shows that for $B_oT_b > 1$, the optimum decision threshold is near zero and the PDFs crossing points increases with the increase of B_oT_b, which means that higher BEPs are achieved due to the higher ASE noise power.

Figure 3.9 shows the eye diagrams at the decision circuit input for the ideal OF and the integrator EF, consudering B_oT_b equal to 1 (left), 5 (middle) and 10 (right), using an optical signal power of –47dBm.

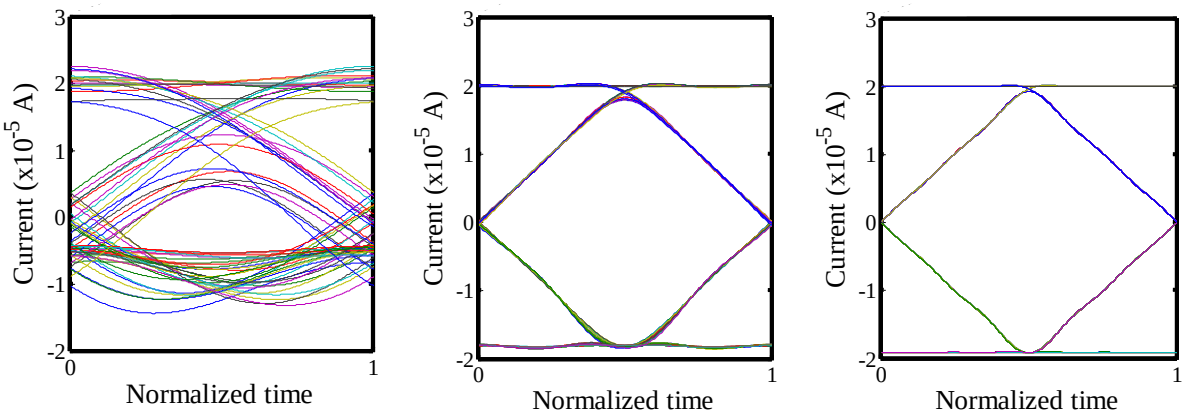

Figure 3.9 – Eye diagram at the decision circuit input for the ideal OF and the integrator EF combination, considering B_oT_b equal to 1 (left), 5 (middle) and 10 (right).

From Fig. 3.9, one can visualize the growth of the ISI effect with the decrease of B_oT_b. Furthermore, the amplitude of the received current of the bit '0' is also reduced, with the optical filter bandwidth decrease, which is in agreement with the shift of the PDFs corresponding to bits '0' to lower values. By inspection of the eye patterns depicted in Fig. 3.9 and the PDFs shown in Fig. 3.8, it can be concluded that the asymmetry of the PDF is caused by the asymmetry of the received eye patterns, when the ISI effect is enhanced.

As the MC simulation accuracy depends on the length of the bits sequence, N_b, Fig. 3.10 shows the BEP as a function of B_oT_b, for different bits sequence lengths, considering the highest ISI effect ($1 < B_oT_b < 2$). For a higher accuracy of the MC simulation, the number of errors considered was 1000.

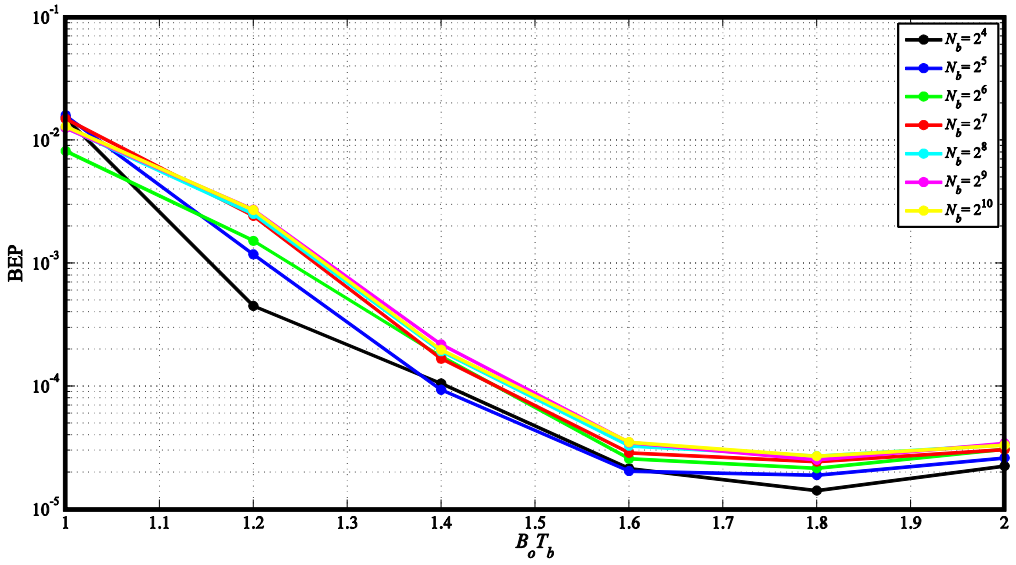

Figure 3.10 – BEP as a function of B_oT_b, considering the ideal OF and the integrator EF combination tested for different number of bits.

From Fig. 3.10, it can be concluded that the achieved BEP stabilizes when the number of bits is higher than 2^6. Notice that for N_b lower than 2^6, some BEP instabilities can be visualized. For example, for $B_oT_b = 1.2$, a number of bits equal to 2^4 leads to a prediction of the BEP with an error of a factor of almost 10 in comparison with the BEPs obtained for a higher number of bits. So, $N_b = 2^6$, seems a safe choice for the bits sequence length and unless otherwise stated, it is used throughout this work.

Table 3.2 shows the evolution of the BEP and the corresponding simulation time in accordance with the increase of the number of errors N_e on the MC simulation, for two scenarios: a normalized optical filter bandwidth equal to 100 and an optical signal power equal to –41 dBm; and a normalized optical filter bandwidth equal to 10 and an optical signal power equal to –44 dBm.

Table 3.2. The evolution of the BEP estimates and the simulation time with the increase of the number of errors, N_e, of the MC simulation.

	B_oT_b = 100 and P_s = –41 dBm		B_oT_b = 10 and P_s = –44 dBm	
Analytical formalism				
$\log_{10}$(BEP)	–5.07		–5.59	
MC simulation formalism				
Number of errors (N_e)	$\log_{10}$(BEP)	Simulation time [seconds]	$\log_{10}$(BEP)	Simulation time [seconds]
20	–5.2118	868	–5.6695	1629
40	–5.231	1498	–5.5297	2126
60	–5.1178	3043	–5.5620	3728
80	–5.0249	5093	–5.6052	4652
100	–5.1955	6256	–5.5081	5764
120	–5.049	7858	–5.5183	5939
140	–5.0849	8454	–5.5853	9776
160	–5.1053	9252	–5.5647	9396
180	–5.1035	10396	–5.5344	10754
200	–5.1026	12760	–5.5437	10526
500	–5.0969	30653	–5.5396	26836
1000	–5.0934	56470	–5.5499	46817

From Table 3.2, a higher number of errors tend to approximate the MC simulation BEPs to the analytical BEPs. However, a very high number of errors can lead to a MC simulation with an unfeasible computational time. So, it is important to determine which N_e leads to a reasonably sufficiently accurate BEP. In several works, MC simulations are typically performed with 100 errors because in agreement with Table 11.1 of [18, chap. 11], for a 99% confidence level, the BEP estimated by the MC simulation is between 0.762p and 1.118p, where p is the real error probability. This provides BEP estimates with a reasonable accuracy without demanding a significant computation time. So, running MC simulations with $N_e = 100$ offers a good compromise between accuracy and simulation time.

3.4. Performance evaluation for different optical and electrical filters combinations

In this section, the performance of the optical DPSK balanced receiver will be studied and compared with the analytical formalism proposed in [7] for different combinations of the optical filter (OF) and electrical filter (EF): an ideal OF and an integrator EF, a Gaussian OF and an integrator EF, a Lorentzian OF and an integrator EF, a Gaussian OF and a Gaussian EF and a Gaussian OF and a RC EF.

3.4.1. Ideal optical filter and integrator electrical filter

In this subsection, the performance of an optical DPSK receiver is evaluated for an ideal OF and an integrator EF combination and compared with the performance obtained from the analytical formalism [7]. The performance of the DPSK receiver is studied for different optical filters –3 dB bandwidths and considering different optical signal powers.

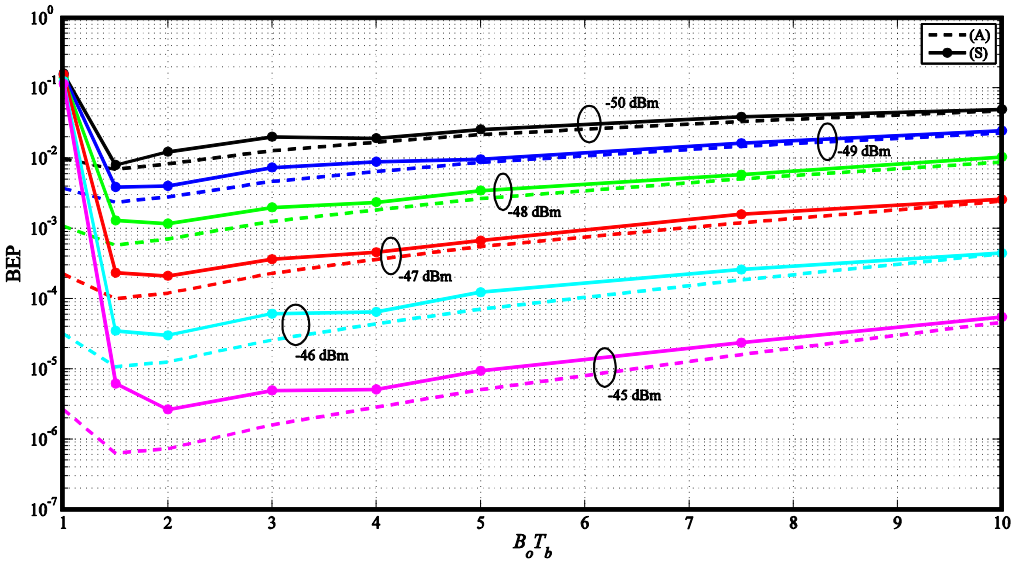

Figure 3.11 – BEP as a function of B_oT_b, for the ideal OF and the integrator EF combination, considering different optical signal powers.

Figure 3.11 shows the BEP estimates as a function of B_oT_b, considering different optical signal powers. The increase of B_oT_b leads to an increase of the ASE noise power and to a reduction of the ISI effect and the BEPs estimated through MC simulation tend to values similar to the analytical BEPs.

For low B_oT_b, the BEP estimated through MC simulation and analytically become discrepant due to the enhanced ISI effect. Additionally, the optimum optical filter bandwidth predicted by the two methods is discrepant. The BEP obtained from MC simulation is more realistic due to the inclusion of the ISI effect.

Figure 3.12 shows the PDFs of the current at the decision circuit input, for a B_oT_b equal to 1 (red line), 1.1 (blue line), 1.2 (green line), 1.3 (black line), 1.4 (yellow line) and 1.5 (magenta line) for an optical signal power of –47dBm.

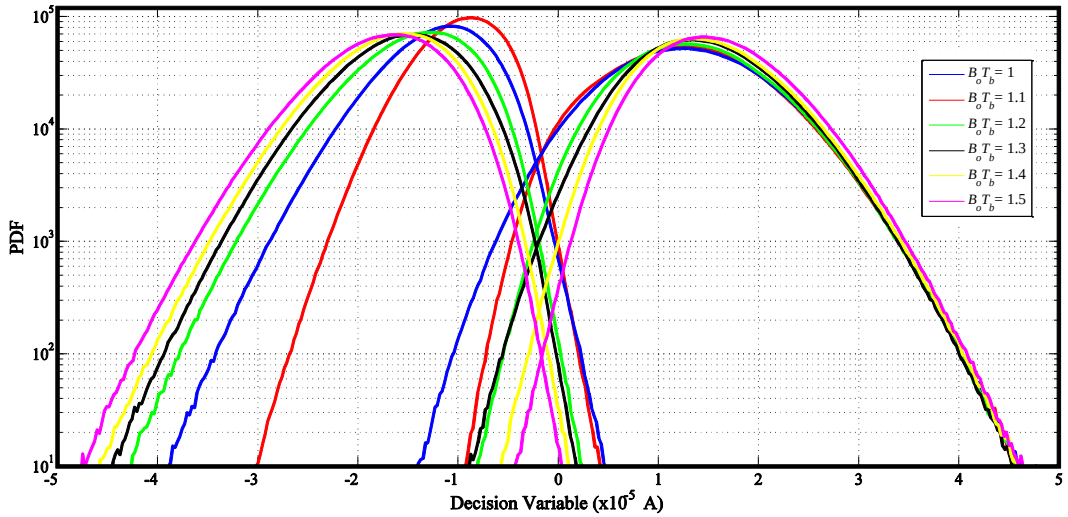

Figure 3.12 – PDF of the decision variable, for an ideal OF and an integrator EF combination, considering an optical signal power with –47 dBm for B_oT_b = 1, 1.1, 1.2, 1.3, 1.4 and 1.5.

Figure 3.12 focuses on the PDFs obtained for different normalized optical filters bandwidths that lead to a higher ISI effect. From the inspection of Fig. 3.12, it can be concluded that the asymmetry is more relevant for the normalized bandwidths $B_oT_b = 1$ (red line) and 1.1 (blue line), where the impact of the ISI effect is higher. As already observed, the PDFs crossing point which defines the decision threshold, deviates from zero to negative values due to the ISI effect, and higher BEPs are obtained. When the PDFs are symmetric, the PDFs crossing point (optimum threshold) is near zero, and due to the increase of the optical filter bandwidth (ISI less significant), lower BEPs are achieved.

3.4.2. Gaussian optical filter and integrator electrical filter

In this subsection, the performance of the optical DPSK receiver is investigated for the Gaussian OF and the integrator EF combination.

Figure 3.13 shows the BEP as a function of B_oT_b, considering different powers of the optical signal.

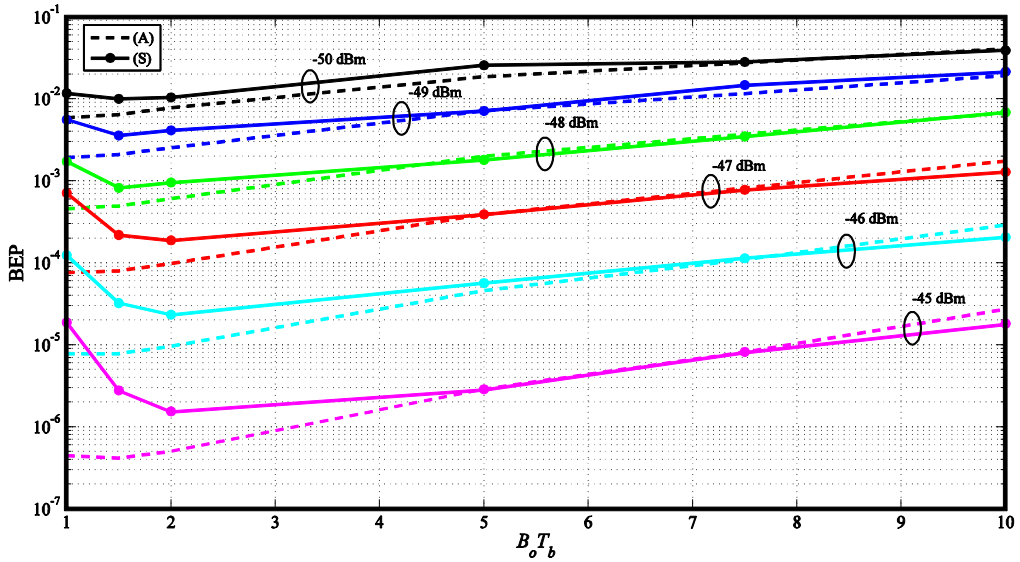

Figure 3.13 – BEP as a function of B_oT_b, for the Gaussian OF and the integrator EF combination, considering different optical signal powers.

According to Fig. 3.13, for B_oT_b higher than 2, the BEP estimates obtained through the MC simulation are very similar with the BEP estimates obtained analytically. For normalized optical filter bandwidth smaller than 2, due to the ISI effect, the BEPs estimated using both methods become discrepant.

Although the ISI effect is present for the lowest optical filters bandwidths $(B_oT_b < 2)$, the performance degradation is not so high as in the case of an ideal OF and integrator EF. In general, it can be concluded that a Gaussian OF and an ideal EF combination enhances the accuracy of the BEP estimates obtained from the MC simulation with the analytical formalism presented in [7].

Figure 3.14 depicts the eye diagrams at the decision circuit input for different optical filter bandwidths.

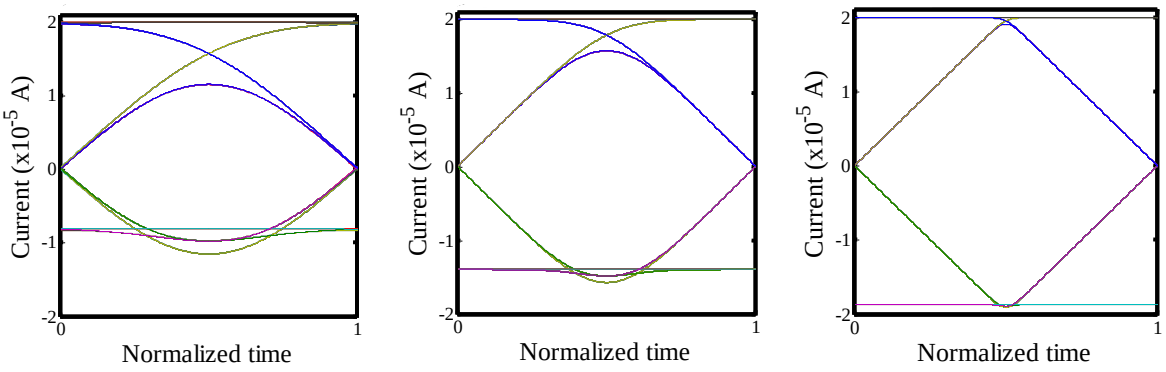

Figure 3.14 – Eye diagram at the decision circuit input for the Gaussian OF and the integrator EF combination, considering B_oT_b equal to 1 (left), 2 (middle) and 10 (right).

By comparing the eye diagrams from Fig. 3.14 with the eye diagrams obtained for the ideal OF and integrator EF combination presented in Fig. 3.9, a reduction of the ISI effect on the optical DPSK system performance is observed for lower optical filters bandwidths, which leads to an approximation between the BEPs calculated using the analytical formalism with the estimates obtained using the MC simulation.

3.4.3. Lorentzian optical filter and integrator electrical filter

In this subsection, the performance of the optical DPSK receiver is assessed for the Lorentzian OF and the integrator EF combination.

Figure 3.15 shows the BEP as a function of B_oT_b considering different powers of the optical signal.

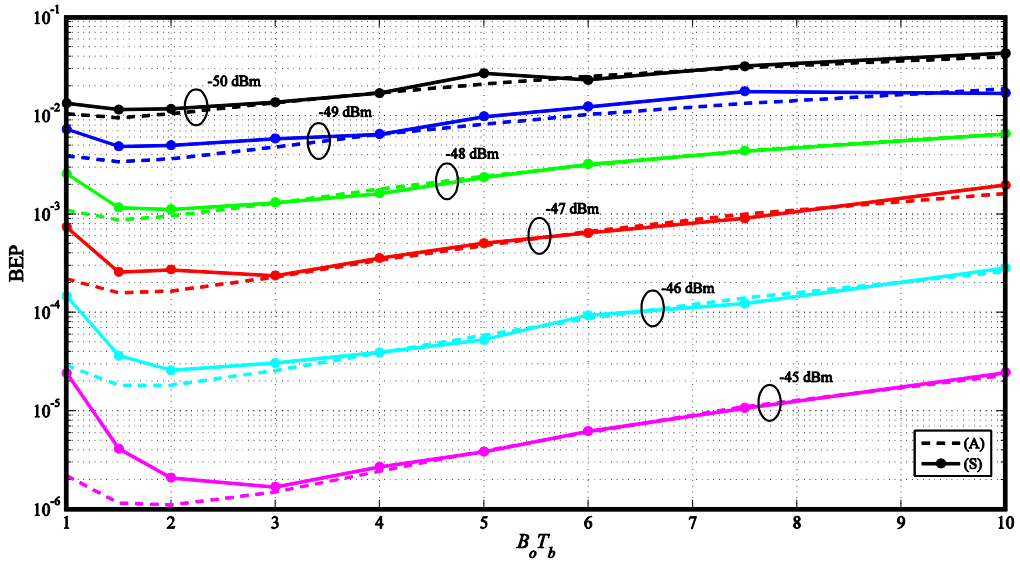

Figure 3.15 – BEP as a function of B_oT_b, for the Lorentzian OF and the integrator EF combination, considering different optical signal powers.

The performance of the MC simulation in this filter combination is similar with the performance obtained for the Gaussian OF and integrator EF combination presented in subsection 3.4.2 because, the ISI effect is not so predominant for lower optical filters bandwidth, as in the ideal OF and integrator EF combination. Again, with the increase of the B_oT_b, the BEP estimates of the MC simulation approach the BEP estimates of the analytical formalism [7].

Figure 3.16 illustrates the PDFs for the normalized optical filter bandwidth equal to 1 (red), 2 (blue), 5 (green) and 10 (black), using an optical signal power with –47 dBm, for the Lorentzian OF and the integrator EF.

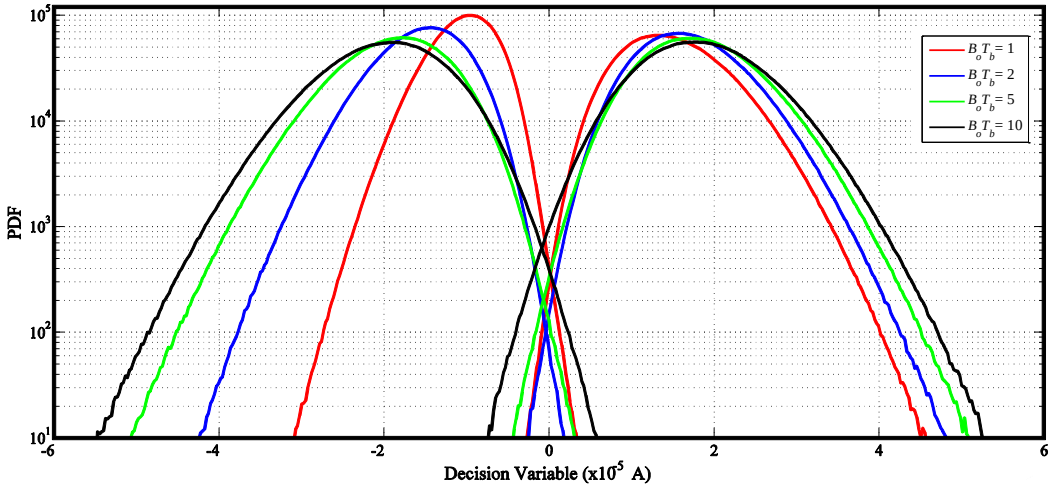

Figure 3.16 – PDF of the decision variable, for the Lorentzian OF and the integrator EF combination, considering an optical power with -47dBm for B_oT_b = 1, 2, 5 and 10.

By inspection of Fig. 3.16, the asymmetric effect on the PDFs introduced by the ISI can be observed, as previously shown for the ideal OF and integrator EF combination. With the optical filters bandwidth broadening, the PDF crossing points increase, leading to higher error probabilities due to the higher impact of the ASE noise on the performance of the optical DPSK system.

3.4.4. Gaussian optical filter and Gaussian electrical filter

The next performance assessment considers a Gaussian OF combined with a Gaussian EF. The normalized electrical filter bandwidth is assumed as $B_eT_b = 0.7$. Figure 3.17 shows the BEP estimates as a function of B_oT_b, considering different optical signal powers.

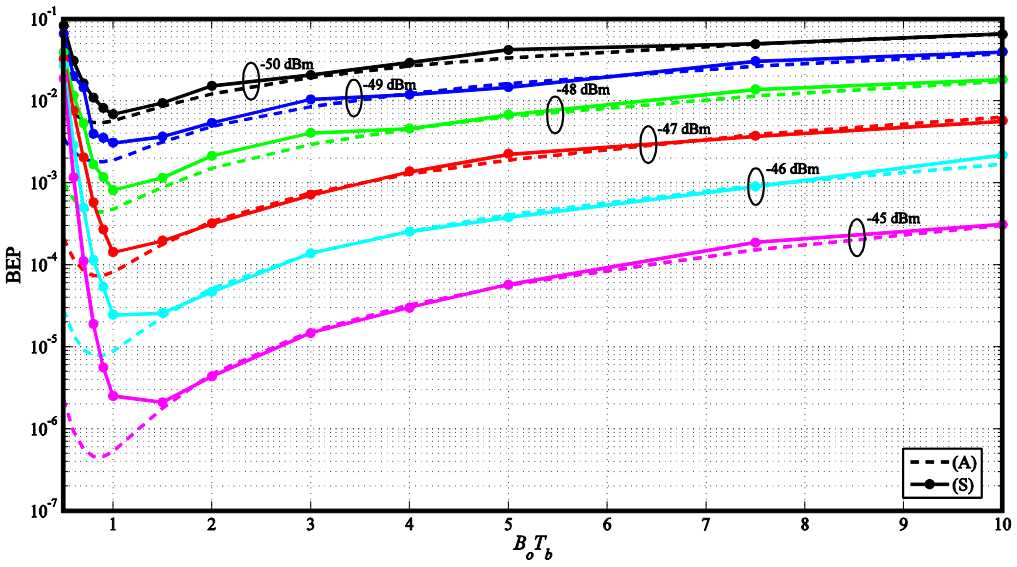

Figure 3.17 – BEP as a function of B_oT_b, for the Gaussian OF and the Gaussian EF combination, considering different optical signal powers.

From Fig. 3.17, the simulated BEPs are very near to the BEPs estimated analytically, for $B_oT_b > 1.5$. Due to the normalized electrical bandwidth reduction (to $B_eT_b = 0.7$), the optimum optical filter –3 dB bandwidth is slightly reduced to lower values (below $B_oT_b = 1.5$), in comparison with the others filters combinations.

The utilization of an electrical filter different from the ideal integrator filter case, and the matching between the BEPs estimates using MC simulation and the analytical formalism, supports the use of both methods to assess the performance in more realistic scenarios.

3.4.5. Gaussian optical filter and RC electrical filter

The next combination of filters that is analyzed is the Gaussian OF and the RC EF combination. The electrical filter bandwidth is assumed as $B_eT_b = 0.7$.

Figure 3.18 shows the BEP estimates as a function of B_oT_b considering different optical signal powers.

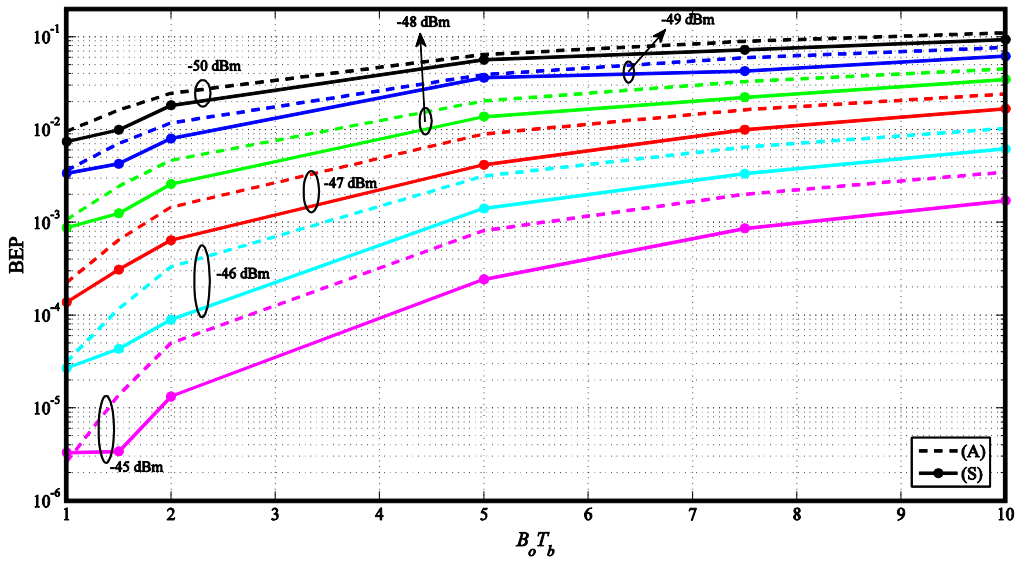

Figure 3.18 – BEP as a function of B_oT_b, for a Gaussian OF and a RC EF combination, considering different optical signal powers.

Figure 3.18 shows that, for the first time, the BEPs obtained through the MC simulation are always lower than the BEPs obtained with the analytical formalism. This behavior occurs only with this combination of filters and can be justified because the sampling time used in the analytical formalism [7] is always at the middle of the bit period, while in the MC simulation the optimal sampling time is obtained for the largest eye opening.

Figure 3.19 depicts the eye diagram at the decision circuit input, considering an optical signal power equal to –47 dBm for $B_oT_b = 2$ and $B_oT_b = 10$.

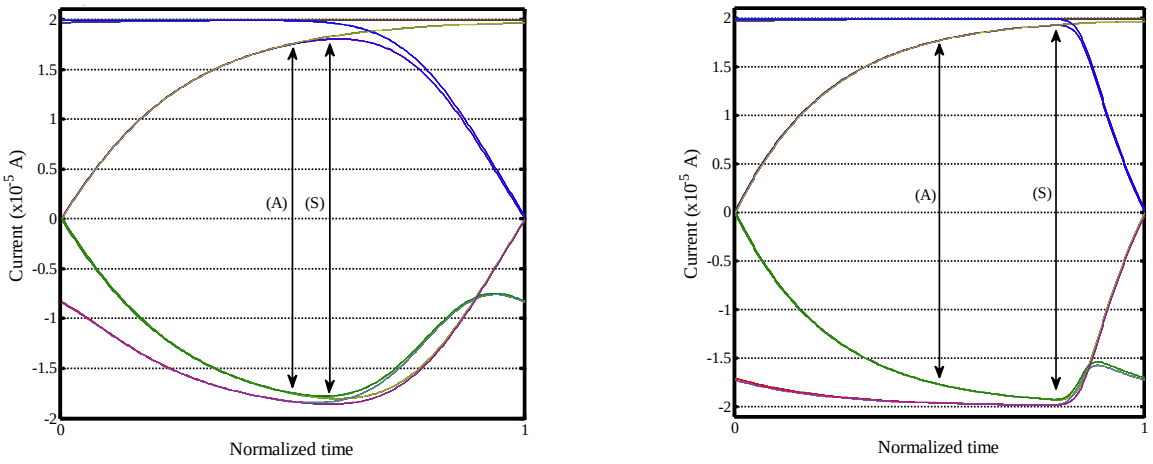

Figure 3.19 – Eye diagram at the decision circuit input, considering a Gaussian OF and a RC EF combination, an optical signal power equal to –47 dBm, for B_oT_b = 2 (left) and B_oT_b = 10 (right).

Figure 3.19 shows that the analytical results are obtained for a sampling time with a much smaller eye-opening than the maximum eye-opening. The MC simulation, by its

correlation process, guarantees that the sampling time occurs always in the largest eye opening, which can lead to BEPs obtained in the MC simulation lower than the BEPs obtained using the analytical formalism.

Hence, the MC simulation was run without synchronism and with the sampling time equal to half bit period, in order to achieve the same conditions as the analytical formalism [7]. Figure 3.20 depicts the BEP estimates of the MC simulation as a function of B_oT_b, considering different optical signal powers.

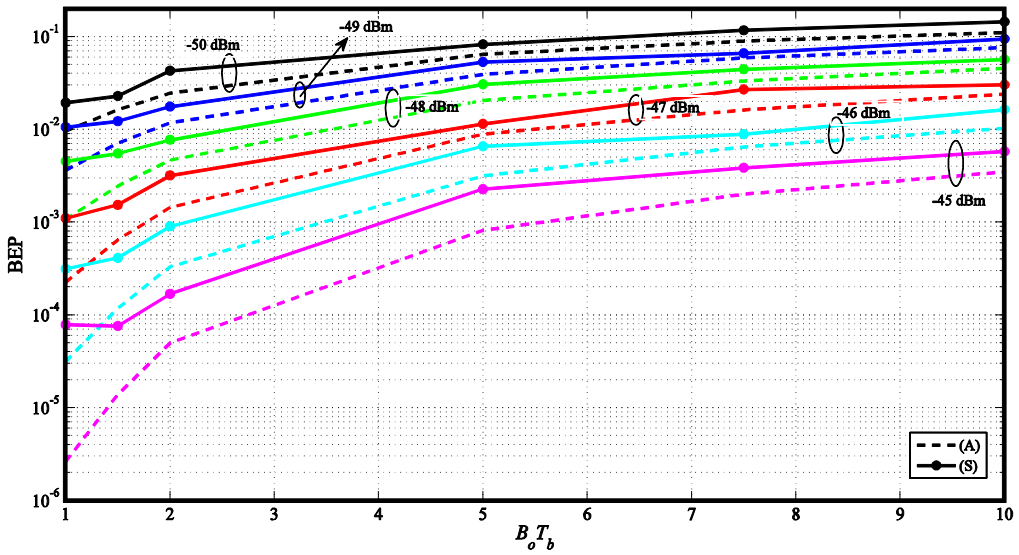

Figure 3.20 – BEP estimates as a function of B_oT_b, for a Gaussian OF and a RC EF combination, considering different signal optical powers and for a sampling time equal to half bit period.

Figure 3.20 shows that the BEP estimates obtained from the analytical formalism are lower than the simulated BEPs, when considering the same sampling time in both formalisms. This behavior is attributed to the ISI introduced by the RC electrical filter.

3.4.6. Comparison of the different filters combinations

Finally, the performance of the optical DPSK communication system is simultaneously analyzed for all the optical and electrical filters combinations studied in section 3.4. Figure 3.21 shows the BEP obtained from the MC simulation and the analytical formalism [7], as a function of the optical signal power for a normalized optical filter bandwidth equal to 5, considering different optical and electrical filters combinations.

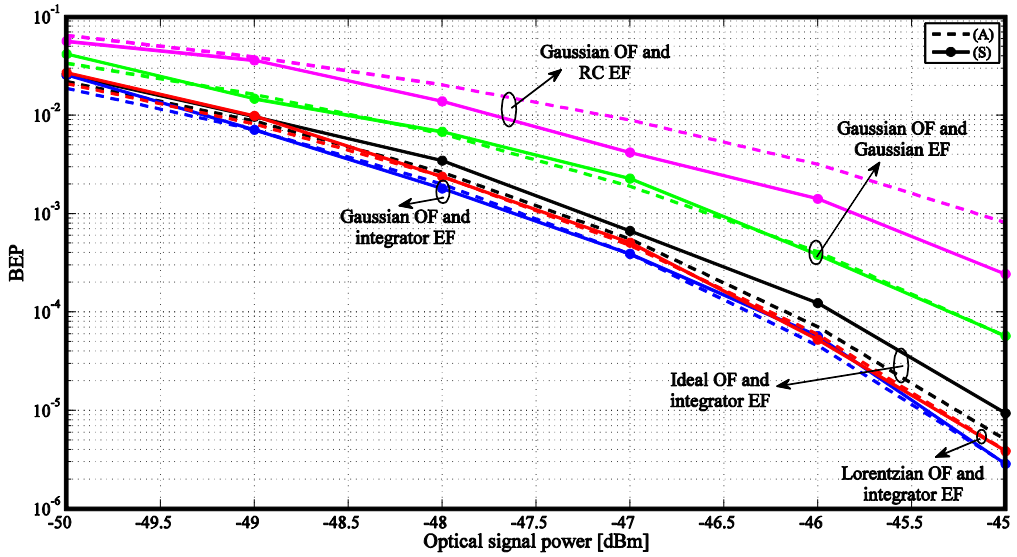

Figure 3.21 – BEP as function of the optical signal power for B_oT_b = 5, considering different filters combinations.

Fig. 3.21 shows that the lower BEPs are achieved with the use of an integrator electrical filter. However, since the integrator electrical filter represents an ideal filter, this implies a situation far from reality. Considering all the optical and electrical filters combinations, all the BEPs achieved by the MC simulation are relatively approximated to the BEPs obtained through the analytical formalism [7], except for the Gaussian OF and RC EF combination, due to the reasons explained previously. As shown in all section 3.4, the analytical formalism can be applied without loss of precision, for normalized optical filter bandwidths above $B_oT_b = 2$. For lower bandwidths, ISI plays its role and the analytical method loses accuracy. So, it can be concluded that from all the filters combinations studied, the ones which assumes an integrator EF represents an ideal filter, corresponding to performances deviated from a real scenario. So, the DPSK receiver performances obtained with the filters combinations which do not include an integrator EF may be closer to more realistic scenarios.

3.5. Impact of the DPSK receiver imperfections

The goal of this section is to analyze the effects of the receiver imperfections on the performance of the optical DPSK receiver. Due to these imperfections, the receiver sensitivity advantage over the conventional OOK might be lost [28]. DPSK reception needs a rather

complex receiver that requires an asymmetric MZDI and a balanced photodetector. To achieve balanced detection, the MZDI needs to be accurately phase-tuned and the dual photodetector should have a perfect responsivity matching between its two arms. However, these requirements are difficult to satisfy in practice, due to the imperfect fabrication of the receiver components [22].

So, the receiver imperfections analyzed on the performance of an optical DPSK receiver are the responsivity imbalance between the two arms of the dual photodetector $\left(R_\lambda^+ \neq R_\lambda^-\right)$ and the frequency offset between the transmit laser frequency and the frequency that originates a perfect constructive/destructive interference at the MZDI output, which is modeled by a nonzero interferometer phase error $\left(\theta_e \neq 0\right)$ [22], [29]. Other imperfections can play a harmful role in the performance of the optical DPSK receiver [29].

The study of the performance of the optical DPSK receiver imperfections is also validated by comparison of the MC simulation results with the results presented in [7], [22].

Ideally, for an optimal DPSK receiver $R_\lambda^+ = R_\lambda^-$. The responsivity imbalance is defined as [7]

$$K = 10\log\left(\frac{R_\lambda^+}{R_\lambda^-}\right). \tag{3.11}$$

When studying the impact of the responsivity imbalance on the performance, as the optimum decision threshold deviates from zero [22], in the MC simulation, the decision threshold is estimated by the PDFs crossing point.

The interferometer detuning leads to an optical phase error at the DPSK receiver, leading to imperfect constructive or destructive interference at the interferometer output ports. The interferometer detuning can be characterized by the offset in transmitter laser frequency Δf, given by [22]

$$\Delta f = \frac{\theta_e}{2\pi T_b}. \tag{3.12}$$

3.5.1. Validation of the MC simulation

In this subsection, the impact of the receiver imperfections in the performance of the optical DPSK receiver is validated by comparison of the MC simulation results, with the

results presented in [22], which are obtained from an analytical formalism that considers a sequence of bits on the DPSK signal.

Figure 3.22 shows the BEP as a function of the responsivity imbalance for different values of the interferometer detuning, for a matched optical filter, absence of electrical filter and an optical signal-to-noise ratio equal to 7.5 dB (as defined in [22]).

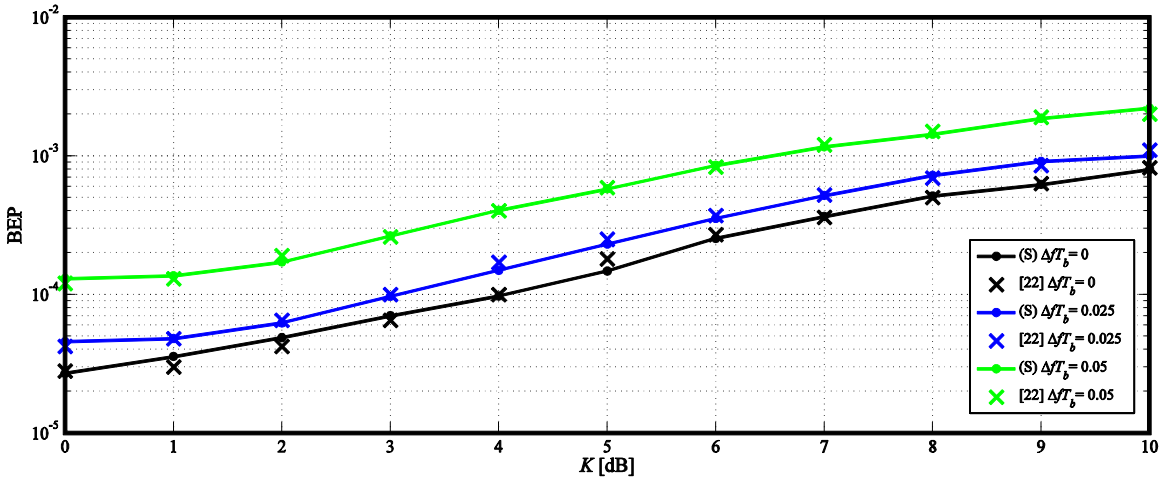

Figure 3.22 – BEP as a function of the responsivity imbalance for a matched optical filter and absence of electrical filter, considering different values of the interferometer detuning.

Figure 3.22 corresponds to Fig. 2 of [22] and shows that the BEPs estimated using MC simulation are in very good agreement with the results presented in [22], hence validating the MC simulation for both optical DPSK receiver impairments, and also for a sequence of bits on the DPSK signal.

3.5.2. Performance evaluation for different optical and electrical filter combinations

In this subsection, the performance of the optical DPSK receiver is analyzed in presence of the receiver imperfections for three filters combinations: the ideal OF and integrator EF, the Lorentzian OF and integrator EF and the Gaussian OF and Gaussian EF. The results obtained with the ideal OF and integrator EF combination are compared with the analytical formalism developed in [7].

Figure 3.23 depicts the power penalty as a function of the responsivity imbalance for different B_oT_b, considering an ideal OF and an integrator EF combination, compared with the power penalty obtained analytically [7]. The power penalty is calculated with the signal

power that gives a BEP of 10^{-3} as a reference, for the ideal optical DPSK receiver ($K = 0$ dB). Optical communication systems usually use forward error correction to guarantee the maximum accuracy on data transmissions. The forward error correction decoder can improve BEPs from its original value of 10^{-3} to 10^{-13}, as is presented in Fig. 6 of [30]. The power penalties are obtained considering $K = 0$ dB and no detuning and for a BEP equal to 10^{-3}, the optical signal powers are equal to –47.1 dBm, –46.4 dBm and –42.7 dBm for the normalized optical filter bandwidths equal to 5, 10 and 100, respectively.

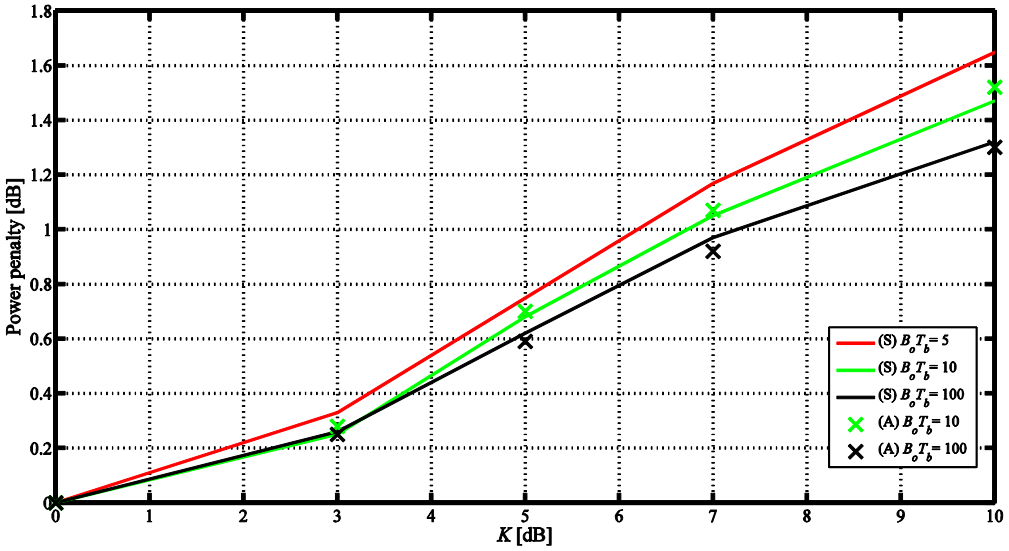

Figure 3.23 – Power penalty as a function of the responsivity imbalance for an ideal OF and integrator EF combination, considering different values of B_oT_b.

Accordingly with Fig. 3.23, it can be concluded that the achieved power penalties obtained by the MC simulation, for the different optical filter bandwidth are in agreement with the results presented in [7], hence validating the MC simulation. The power penalty tends to decrease with the broadening of the optical filter bandwidth. This reduction can be explained by the growing impact of the ASE noise power in the system performance as B_oT_b increases, which masks the impact of this impairment. Numerical results for B_oT_b lower than 5 were not obtained, since the ISI severely deteriorates the receiver performance for these bandwidths, and could mask the impact of the responsivity imbalance on the performance. The variation of K is achieved by changing the value of R_λ^-, while the value of R_λ^+ is kept constant.

Figure 3.24 shows the eye diagrams at the decision circuit input for an ideal OF and an integrator EF combination, considering three different values of the responsivity imbalance [

$K = 0$ dB (left), $K = 5$ dB (middle) and $K = 10$ dB (right)], for a normalized optical filter bandwidth equal to 10 and an optical signal power equal to –47 dBm.

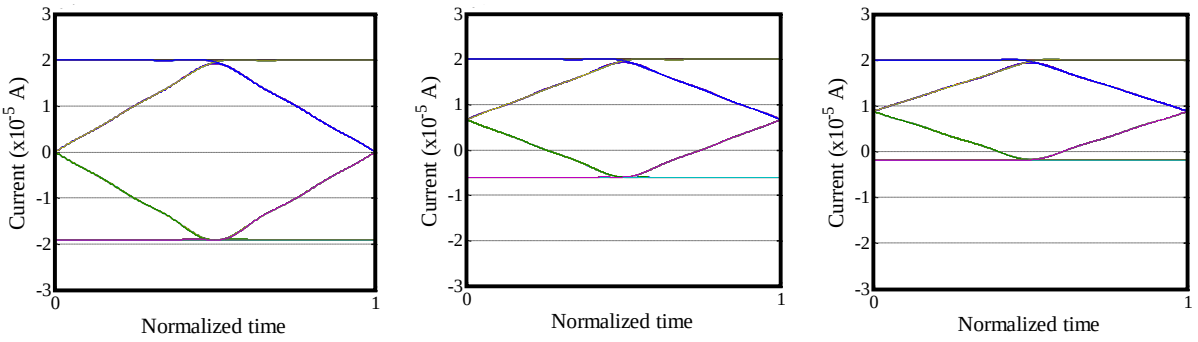

Figure 3.24 – Eye diagram at the decision circuit input for an ideal OF and integrator EF, considering *K* = 0 dB (left), *K* = 5 dB (middle) and *K* = 10 dB (right).

Accordingly with Fig. 3.24, it can be concluded that the decision threshold deviates from zero with the increase of the responsivity imbalance. This behavior is caused by the increase of the current corresponding to the bits '0' towards zero due to the reduction of R_λ^- and the constancy of the current for the bits '1' (R_λ^+ constant). Figure 3.25 depicts the PDFs of the decision variable for the same conditions of Fig. 3.24.

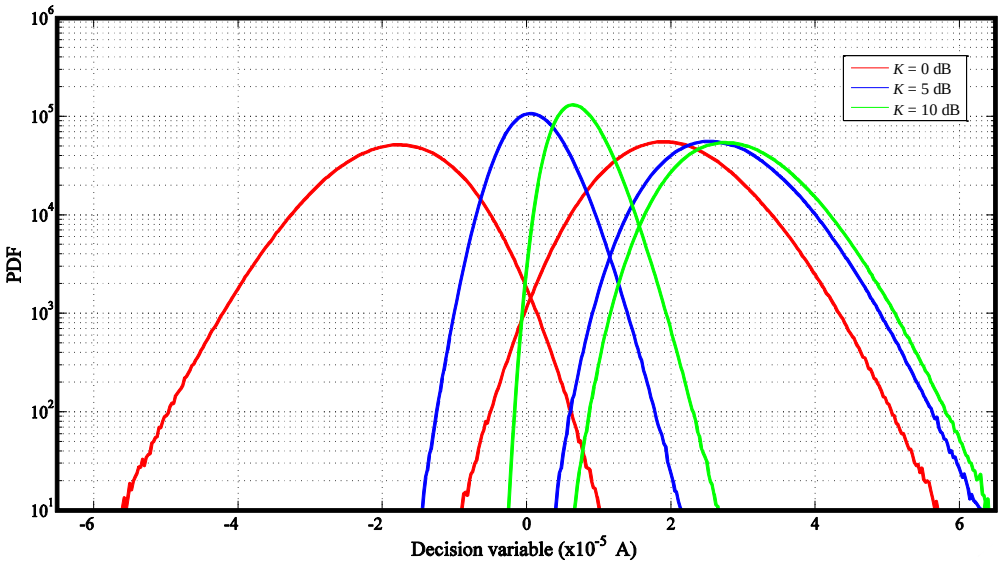

Figure 3.25 – PDFs of the decision variable, for an ideal OF and integrator EF, considering *K* = 0 dB (red), *K* = 5 dB (blue) and *K* = 10 dB (green).

Due to the responsivity imbalance, the PDFs of the bits '0' deviate from the Gaussian behavior to a "more" Chi-squared behavior. This Chi-squared behavior presented in the PDFs of the bits '0' becomes more significant with the increase of responsivity imbalance due to the enhancement of the impact of the ASE-ASE beat noise on the performance over the impact of

the signal-ASE beat noise [15]. This is in agreement with the shift of the current of the bits '0' towards zero, due to the enhancement of the responsitivity imbalance, depicted in Fig. 3.24.

Accordingly with Fig. 3.25, it can be also visualized that the PDFs, for $K > 0$ dB, have its crossing point deviating from zero, which justifies the deviation in the decision threshold. Additionally, the PDFs corresponding to bits '0' and '1' are no longer symmetrical, due to the increase of the responsivity imbalance. A similar behavior has also been observed in [7] and [27]. The difference in the PDF curves for bit '1' is almost negligible, whereas the curves for bit '0' for $K = 5$ dB and $K = 10$ dB present visible differences in comparison with the curve representing a balanced responsivity. These differences are justified since the responsivity R_λ^+ is kept constant and the responsivity R_λ^- varies when the imbalance is taken into account. Once the value of the PDF in the crossing points increases with the responsivity imbalance augmentation, it is expectable that the BEP is also deteriorated.

Figure 3.26 depicts the power penalty as a function of the responsivity imbalance for different B_oT_b, considering a Lorentzian OF and an integrator EF combination (left) and a Gaussian OF and a Gaussian EF combination (right) for $B_eT_b = 0.7$. In the Lorentzian OF and integrator EF combination (left), the power penalties are obtained for a BEP equal to 10^{-3}, and considering $K = 0$ dB and no detuning, the optical signal powers are equal to –47.3 dBm, –46.6 dBm and –43.2 dBm, for B_oT_b equal to 5, 10 and 100, respectively. For the Gaussian OF and Gaussian EF combination (right), the optical signal powers are equal to –46.4 dBm, –45.6 dBm and –42.2 dBm, for B_oT_b equal to 5, 10 and 100, respectively.

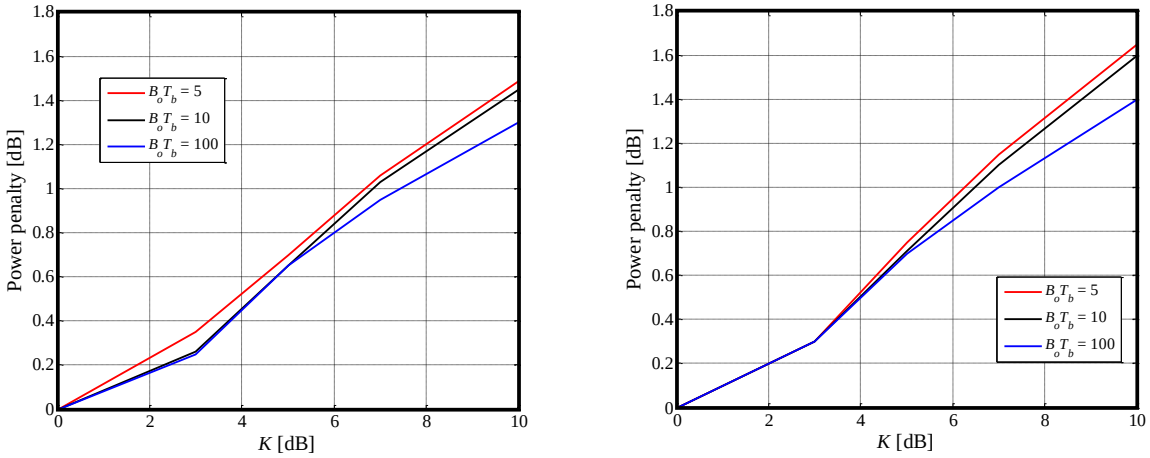

Figure 3.26 – Power penalty as a function of the responsivity imbalance for different values of B_oT_b, considering a Lorentzian OF and integrator EF combination (left) and a Gaussian OF and a Gaussian EF combination (right).

Accordingly with the power penalties depicted in Fig. 3.26, a similar behavior of the power penalty for both filter combinations can be detected. The Lorentzian OF and integrator EF combination achieves slightly lower power penalties. This improvement is related to the use of the ideal integrator EF, which gives better receiver performance.

By inspection of Fig. 3.23 and Fig. 3.26, it can be concluded that the adopted filters combinations do not have a considerable influence in the performance of the optical DPSK receiver in presence of the responsivity imbalance, since all the power penalties exhibit a similar behavior. For example, considering a normalized optical filter bandwidth equal to 10, the power penalty is equal to 1.45 dB, for a $K = 10\,\text{dB}$, in the ideal OF and integrator EF combination. In the Lorentzian OF and integrator EF combination and in the Gaussian OF and Gaussian EF combination, for a $K = 10\,\text{dB}$, the power penalties are equal to 1.45 dB and 1.6 dB, respectively.

The impact of the interferometer detuning in the optical DPSK receiver will now be analyzed. Figure 3.27 shows the power penalty as a function of the normalized interferometer detuning $\Delta f\, T_b$, for an ideal OF and an integrator EF combination, considering different optical filters bandwidths.

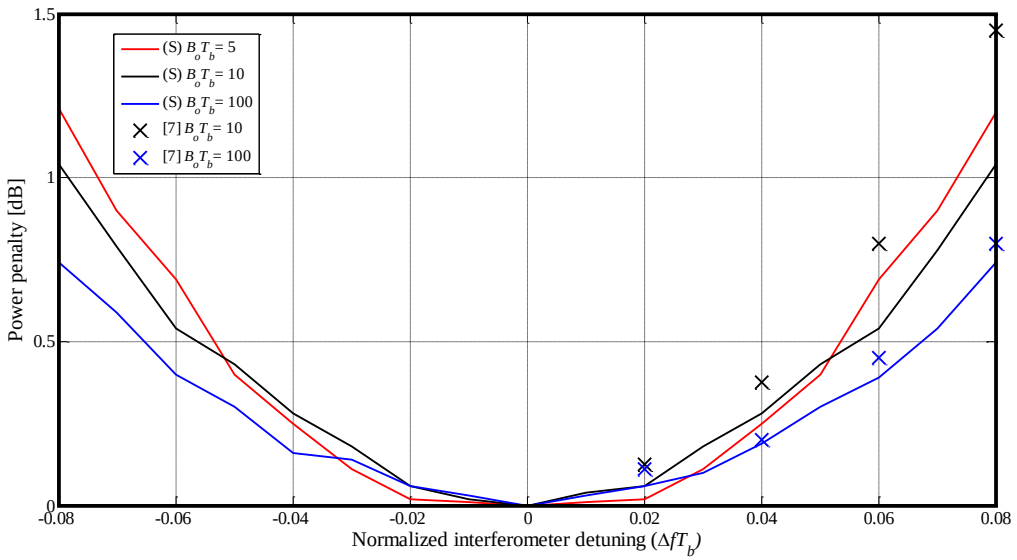

Figure 3.27 – Power penalty as a function of the normalized interferometer detuning for an ideal OF and integrator EF combination, considering different values of B_oT_b.

As in the analytical formalism [7], the power penalty of the MC simulation when the optical DPSK receiver is impaired by the interferometer detuning tends to increase with the

decreasing of the optical filter bandwidth. From Fig. 3.27, it can be concluded that a 8% detuning results in a power penalty of approximately 1.2 dB, when $B_oT_b = 5$.

Figure 3.27 exhibits a small difference between the power penalties obtained using the analytical formalism and the obtained using the MC simulation. This difference increases with the decrease of B_oT_b. A maximum difference of approximately 0.5 dB, when $B_oT_b = 10$ is found for a 8% detuning. This difference might be caused by the consideration of an isolate DPSK symbol on the analytical formulation, while the MC simulation considers a sequence of bits.

Figure 3.28 shows the eye diagrams at the decision circuit inpnut for an ideal OF and an integrator EF combination, considering three different values of the normalized interferometer detuning [$\Delta f\, T_b = 0$ (left), $\Delta f\, T_b = 0.04$ (middle) and $\Delta f\, T_b = 0.08$ (right)], for a $B_oT_b = 10$ and an optical signal power equal to –47 dBm.

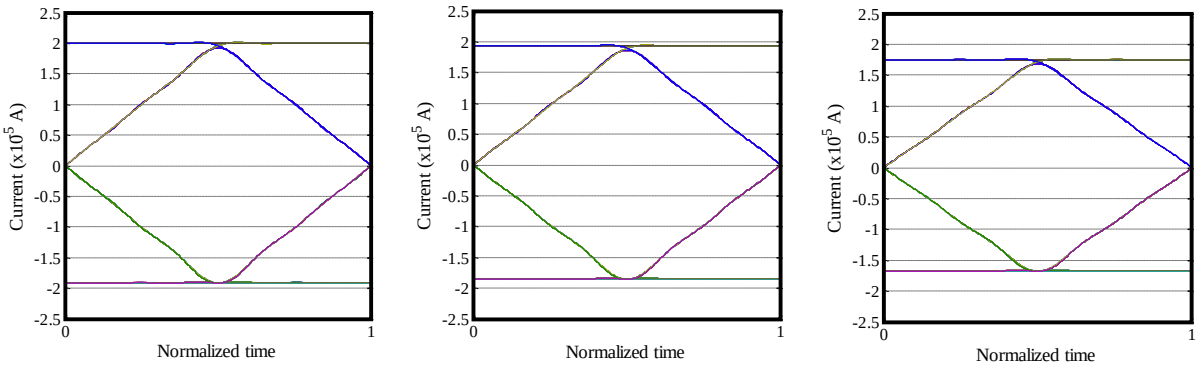

Figure 3.28 – Eye diagram at the decision circuit input for an ideal OF and integrator EF, considering $\Delta f\, T_b$ = 0 (left), $\Delta f\, T_b$ = 0.04 (middle) and $\Delta f\, T_b$ = 0.08 (right).

Figure 3.28 shows that the amplitude of the current corresponding to the bits ‘0’ and bits ‘1’ is reduced, with the increase of the interferometer detuning. The ISI on the optimum sampling instant seems to be similar for the different interferometer detunings.

As the ISI effect is constant with the interferometer detuning, the difference between the analytical and the simulated results, might be related in part with some loss of accuracy of the MC simulation when calculating the power penalty.

Figure 3.29 presents the power penalty as a function of the normalized interferometer detuning for different B_oT_b, considering a Lorentzian OF and an integrator EF combination (left) and a Gaussian OF and a Gaussian EF combination (right).

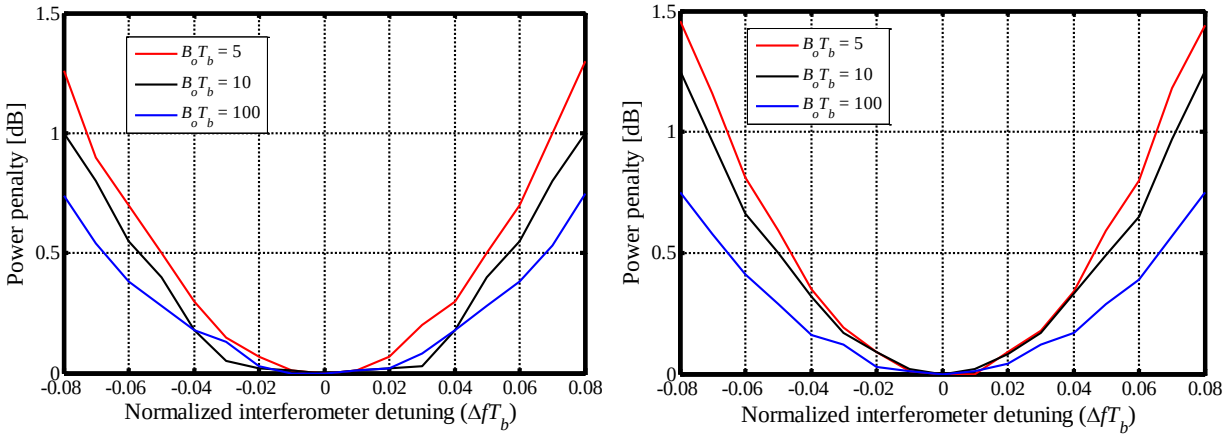

Figure 3.29 – Power penalty as a function of the normalized interferometer detuning considering different values of B_oT_b, for a Lorentzian OF and integrator EF combination (left) and for a Gaussian OF and a Gaussian EF combination (right).

By inspection of Fig. 3.27 and Fig. 3.29, it can be concluded once again, that the adopted filters combinations have a negligible influence in the performance of the optical DPSK receiver in presence of the interferometer detuning. In the filters combination presented above, the power penalties have an approximated behavior. For example, considering $B_oT_b = 10$, the power penalty is equal to 1 dB, for a 8% detuning, in the ideal OF and integrator EF combination. In the Lorentzian OF and integrator EF combination and in the Gaussian OF and Gaussian EF combination, for a 8% detuning, the power penalties are equal to 1 dB and 1.25 dB, respectively.

In a realistic scenario, typically, an interferometer can be 5% detuned and the responsivity imbalance is below $K = 1$ dB [32]. By considering that and from the previous analyzes, the interferometer detuning leads to higher performance degradation than the responsivity imbalance. For example, considering Fig. 3.26 (right), the power penalty for $B_oT_b = 10$ and $K = 1$ dB is 0.1 dB. Accordingly with Fig. 3.29 (right), for an interferometer detuning of 5% and $B_oT_b = 10$, the power penalty is 0.5 dB.

3.6. Conclusions

In this chapter, the performance of an optical DPSK communication system impaired by ASE noise has been investigated in a back-to-back configuration using a MC simulation. The MC simulation was validated by comparison of its BEP estimates with the estimates of the analytical formalism proposed in [7] and with the analytical results presented in [22]. The

performance of the optical DPSK communication was analyzed for different optical and electrical filter combinations and when impaired by receiver imperfections.

The number of bits and the number of errors used in the MC simulation were also tested in order to reach stabilized values of the BEP. It has been seen that a safe choice for the number of bits is 2^6 and, according with the confidence ratio presented in [18, chap. 11] and our simulation results, a number of errors equal to 100 provides sufficiently accurate estimates of the BEP.

As shown in all section 3.4, the analytical formalism [7] can be applied without loss of precision, for normalized optical filter bandwidths generally above 2. For lower bandwidths, ISI becomes dominant and the analytical method loses accuracy, since it has been derived for an isolated DPSK symbol. From all the filters combinations studied, it has been seen that the combinations with the integrator EF provide the best DPSK receiver performance. However, the integrator filter is an ideal filter, and the corresponding performance predictions might deviate a little from a real system. In that case, the DPSK receiver performance obtained with the others filters combinations may be of more practical interest.

For the Gaussian OF and RC EF combinations, it was observed that the MC simulation can predict lower BEPs than the analytical formulation. This behavior was caused by the use of different sampling instants on the MC simulation (at the largest eye-opening) and on the analytical work (at the middle of the bit period). Even when, in the MC simulation, a sampling instant at half of the bit period has been considered, the BEP estimated by MC simulation is slight lower than the estimated analytically. In this case, the difference has been attributed to the ISI introduced by the RC electrical filter.

It has been shown that, by MC simulation, the ISI leads to a growing asymmetry between the PDFs of the bits ‘0’ and ‘1’, for narrower optical filter bandwidths. This asymmetric behavior in not predicted by the analytical formalism [7], because this formalism assumes an isolated DPSK symbol and neglects ISI. The PDFs asymmetric behavior (observed in the MC simulation) is in agreement with the results presented in [27], which also consider a sequence of bits to obtain the PDFs.

The effect of receiver imperfections on the performance of the optical DPSK communication system has been also studied. Considering the different filter combinations, it can be concluded that they have a negligible influence in the performance of the optical

DPSK receiver in presence of the responsivity imbalance or of the interferometer detuning. With the responsivity imbalance increase, the mean of the PDFs of the bits ‘0’ deviates to higher values and its Gaussian behavior is substituted by a “more” Chi-squared behavior. Consequently, the decision threshold deviates also from zero to positive values. This Chi-squared behavior becomes more significant with the increase of the responsivity imbalance due to the enhancement of the impact of the ASE-ASE beat noise in comparison with the signal-ASE beat noise impact on the performance.

Discrepancies that can reach 0.5 dB between the power penalties obtained using MC simulation and the analytical formalism have been observed for higher interferometer detunings. The reason for such discrepancies is still to be explained, however, might be caused by the consideration of an isolate DPSK symbol on the analytical formulation.

4. Optical DPSK communication system impaired by in-band crosstalk

4.1. Introduction

In this chapter, the performance of an optical DPSK communication system impaired by in-band crosstalk is analyzed in a back-to-back configuration using MC simulation. In section 4.2 a theoretical introduction about the different crosstalk types and the implementation of the in-band crosstalk on the MC simulator are described. Section 4.3 presents the model of the random phase noise used in this work [31] to characterize the random fluctuations on the crosstalk signal. Section 4.4 shows the numerical results obtained with the MC simulation developed to investigate the impact of in-band crosstalk in the optical DPSK receiver performance and its respective validation by comparison with the analytical formalisms [7] and [32]. Section 4.5 contains the analysis of the performance of the optical DPSK receiver impaired by in-band crosstalk when considering some particular aspects in the optical DPSK receiver model, such as: a delay between the original signal and the crosstalk signal, different sequences of bits on the DPSK crosstalk signal and receiver imperfections. Table 4.1 shows the parameters used to evaluate the performance of the optical DPSK communication system impaired by in-band crosstalk. Unless stated otherwise, these parameters are used throughout this chapter.

Table 4.1. Parameters of the simulated optical DPSK communication system impaired by in-band crosstalk.

Parameter	Value
Number of bits (N_b)	64
Number of samples (N_a)	256
Number of errors (N_e)	100
EDFA gain (G)	30 dB
Responsivity (R_λ^+, R_λ^-)	1A/W
Amplified noise figure (F_n)	5 dB
Bit period (T_b)	0.1 ns
Polarizer	Present
Spectral width of the laser ($\Delta\nu$)	10 MHz
Interfering terms (M)	1
Phase error of the interferometer (θ_e)	0

4.2. In-band crosstalk model

In optical networks, the isolation of optical components, such as optical filters, switches and (de)multiplexers is not ideal, leading to performance degradation due to crosstalk. The principal sources of crosstalk in optical networks with direct detection are summarized in Table I of [33].

The crosstalk signals may arise from distinct sources or from the same source as the original signal. When the crosstalk signal arises from distinct sources, it may have the same wavelength as the original signal or a different wavelength, giving rise to in-band crosstalk and inter-band crosstalk, respectively. In-band and inter-band crosstalk may be classified as incoherent crosstalk, since the crosstalk signal is statistically independent of the original signal, [7], [33], [34]. When the crosstalk signal arises from the same source, it has always the same wavelength as the original signal, giving rise to coherent or incoherent crosstalk. In the case of coherent crosstalk, the differential delay between the signal and the delayed replicas is much smaller than the coherence time of the source and the crosstalk signal is statistically dependent on the original signal. In the case of incoherent crosstalk, the crosstalk signal becomes statistically independent on the original signal, since the differential delay is much greater than the coherence time of the source, [7], [33], [34].

In-band crosstalk, from distinct sources, is one of the most severe impairments in optical transparent networks, because the signal-crosstalk beating terms originated at the receiver cannot be removed by filtering [32], [34]. This is the case studied in this work.

Several works analyzed the impact of in-band crosstalk on optical receivers using direct detection and with different modulation formats: 1) OOK [5], [7]; 2) DPSK [7], [8], [9] and [32] or 3) DQPSK [10]. In [9], Liu *et al*, experimentally found that the DPSK signal with balanced detection has ~6 dB higher tolerance to in-band crosstalk than the OOK signal.

In this chapter, the impact of in-band crosstalk on the optical DPSK receiver performance is investigated using MC simulation and a performance comparison with the results obtained from the analytical formalism proposed in [7], [8] is performed.

Figure 4.1 shows the schematic block diagram of an optical DPSK balanced receiver with direct detection impaired by ASE noise and by in-band crosstalk. The only particularity is the addition of the in-band crosstalk electrical field to the original signal before being optically amplified in the receiver.

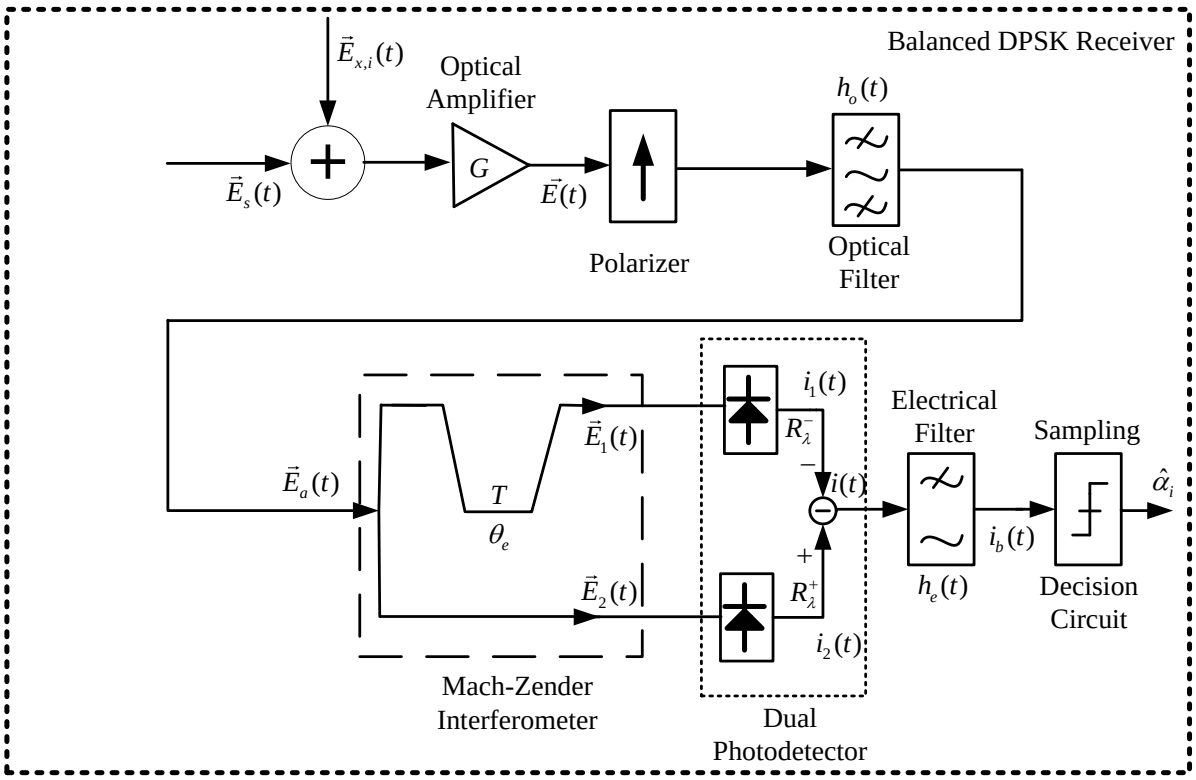

Figure 4.1 – Schematic block diagram of an optical DPSK balanced receiver impaired by in-band crosstalk.

The electrical field at the optical amplifier output can be expressed as [35]

$$\vec{E}(t) = \left[\vec{E}_s(t) + \sum_{i=1}^{M} \vec{E}_{x,i}(t) + \vec{E}_{ASE}(t) \right] \vec{e}_s, \tag{4.1}$$

where the first term corresponds to the original signal, the second term to the in-band crosstalk and the third to the ASE noise originated from the optical pre-amplifier. The in-band crosstalk effect occurs due to the interference from *M* different DPSK signals with the same wavelength and the same bit rate of the original signal. The complex envelope of the *i*-th crosstalk signal field can be represented as [35]

$$\vec{E}_{x,i}(t) = \sqrt{GP_{x,i}} \exp\left[j\left(\theta_{x,i}(t) + \phi_{x,i}(t)\right)\right] \vec{e}_s, \tag{4.2}$$

where $P_{x,i}$ is the crosstalk power, $\phi_{x,i}(t)$ is a random phase noise, and $\theta_{x,i}(t)$ is the crosstalk phase that carries the binary information and is given by

$$\theta_{x,i}(t) = \theta_{x,i}(t-T) + \frac{\pi}{2}\left(1-\alpha_{x,i}\right), \tag{4.3}$$

with $\alpha_{x,i}=1$ for the bit '1' and $\alpha_{x,i}=-1$ for the bit '0'. The crosstalk level of the *i*-th interferer, ε_i, is defined as the ratio of crosstalk power to signal power, and is given by

$$\varepsilon_i = \frac{P_{x,i}}{P_s}, \tag{4.4}$$

while, the total crosstalk level, ε is defined by

$$\varepsilon = \sum_{i=0}^{M} \varepsilon_i. \tag{4.5}$$

Unless otherwise stated, throughout this chapter, it is considered that the original and the in-band crosstalk signal fields are co-polarized and temporally aligned, which leads to a worst case performance [36]. It is also assumed throughout this chapter that the number of interfering terms (*M*) is always one, $M=1$.

4.3. Implementation of the random phase noise

This section describes the implementation of the random phase noise on the MC simulator. This randomness is a result of spontaneous photon emissions during the laser operation [27].The conventional model employed to generate the random phase noise in a semiconductor laser is the Brownian motion model [27], [37].

The temporal derivative, $\phi^{\bullet}(t)$, of the random phase, $\phi(t)$, is modeled as a stationary Gaussian process with zero mean and constant power spectral density [27], [37], given by

$$\phi(t) = \int_0^t \phi^{\bullet}(u)du. \tag{4.6}$$

To simulate (4.6), it is necessary to perform a temporal discretization, so that the random phase noise[6] is described by,

$$\phi(n) = \sigma_{\phi^{\bullet}} \sum_{k=1}^{n} \mu_k, \tag{4.7}$$

[6] In Matlab, this summation is implemented using cumsum.m.

where μ_k are independent Gaussian random variables with zero mean and unitary variance, n are the number of samples of the vector used in the simulation which corresponds to $n = N_a N_b$ and $\sigma_{\phi\bullet}$ is the standard deviation, defined by

$$\sigma_{\phi\bullet} = \sqrt{2\pi\Delta\nu T_a}, \tag{4.8}$$

where $\Delta\nu$ is the spectral width of the laser and T_a is a sampling time defined in subsection 2.4.1. The spectral width of the laser is assumed as 10 MHz [3, chap. 2]. As the variables μ_k are independent,

$$\sigma_\phi^2 = n\sigma_{\phi\bullet}^2 . \tag{4.9}$$

So, $\phi(n)$ is a non-stationary Gaussian process whose variance grows with n, or its equivalent time continuous representation, $\phi(t)$ is a non-stationary Gaussian process whose variance grows with time.

Figure 4.2 depicts the temporal evolution of the Brownian motion random phase noise for two independent sample functions.

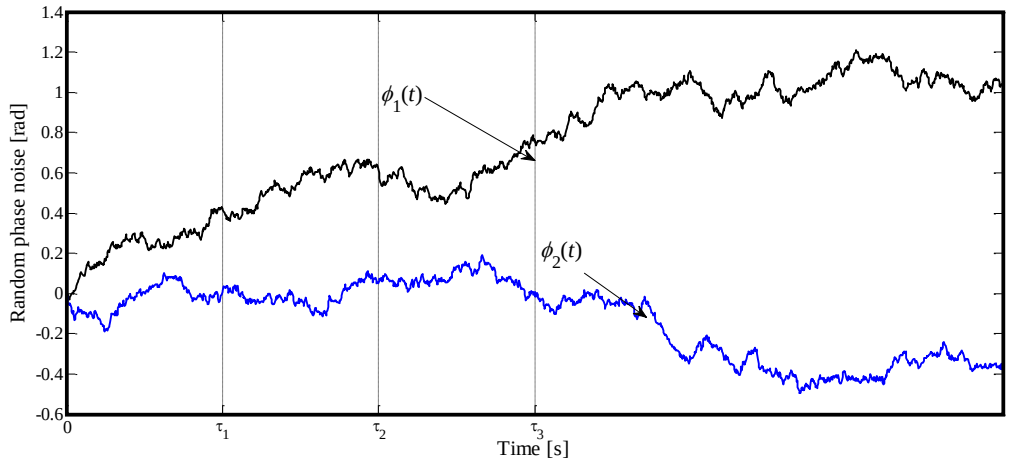

Figure 4.2 – Temporal evolution of the Brownian motion random phase noise, for two independent sample functions.

Figure 4.3 shows the PDFs of the random phase noise $\phi(t)$, considering specific temporal instants, $\tau_1 = T_b$, $\tau_2 = 2T_b$, and $\tau_3 = 3T_b$.

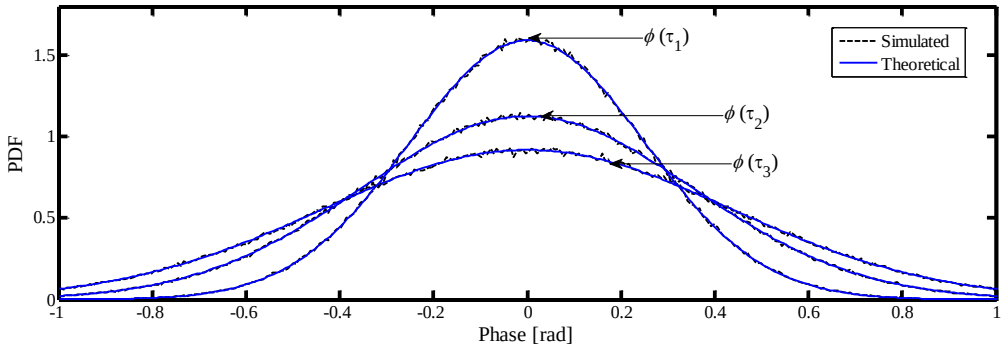

Figure 4.3 – PDF of random phase considering different temporal instants.

Accordingly with Fig. 4.3, from the theoretical PDFs, it can be concluded that the distribution of the Brownian motion random phase noise is indeed Gaussian with variance given by (4.9) [38] and the correctness of the implementation of the random phase noise on the MC simulator is verified.

In order to completely check the MC simulator, its results are compared with the results presented in [37] for the random phase noise difference. The expression that represents the random phase noise difference is given by [37]

$$\Delta\phi(\tau) = \phi(\tau + NT_a) - \phi(\tau), \tag{4.10}$$

or equivalently, in a discrete temporal representation,

$$\Delta\phi(n, N) = \phi(n + N) - \phi(n), \tag{4.11}$$

where N is the number of samples between two instantaneous values of the random phase noise. The standard deviation of the random phase noise difference is given by

$$\sigma^2_{\Delta\phi(n,N)} = N\sigma^2_{\phi}. \tag{4.12}$$

Figure 4.4 shows the PDFs of the theoretical and the simulated random phase noise difference when the delays between the signals are $N = 1$, $N = 3$ and $N = 7$.

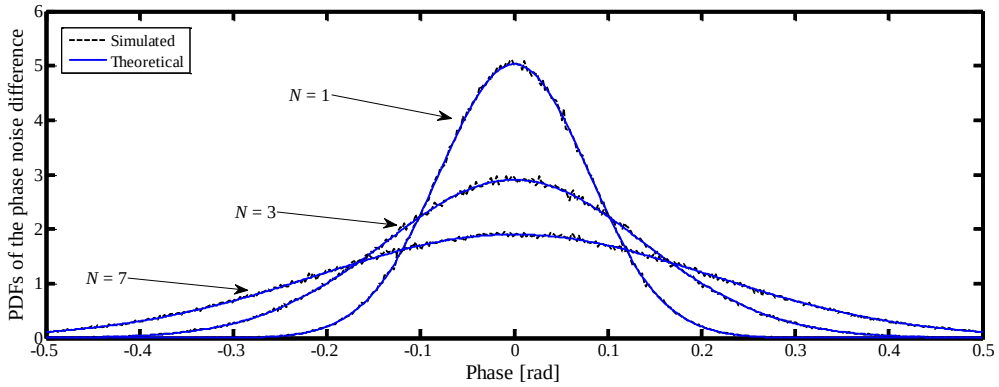

Figure 4.4 – PDF of the random phase noise difference.

A very good agreement between the MC simulated curves and the theoretical obtained using the Gaussian distribution is found in Fig. 4.4, which further validates the MC simulation of the random phase noise.

4.4. Validation of the Monte Carlo simulation

In this section, the MC simulation is validated by comparison of its BEP estimates with the results obtained from the analytical formalism developed in [7]. The MC simulation is analyzed for different optical and electrical filter combinations as a function of the optical signal power and of the crosstalk level. The performance of the optical DPSK communication system impaired by in-band crosstalk when affected by optical DPSK receiver imperfections is also studied and compared with the analytical results presented in [32].

In this section, the BEP estimates obtained from the MC simulation are depicted with a solid line or with a legend (S), while the BEPs obtained with the analytical formalism are depicted with a dashed line or with a legend (A).

Figure 4.5 shows the BEP estimates from the MC simulation and from the analytical formalism [7] as a function of the optical signal power, considering an ideal OF and an integrator EF and a crosstalk level equal to –12 dB, for different normalized optical filter bandwidths.

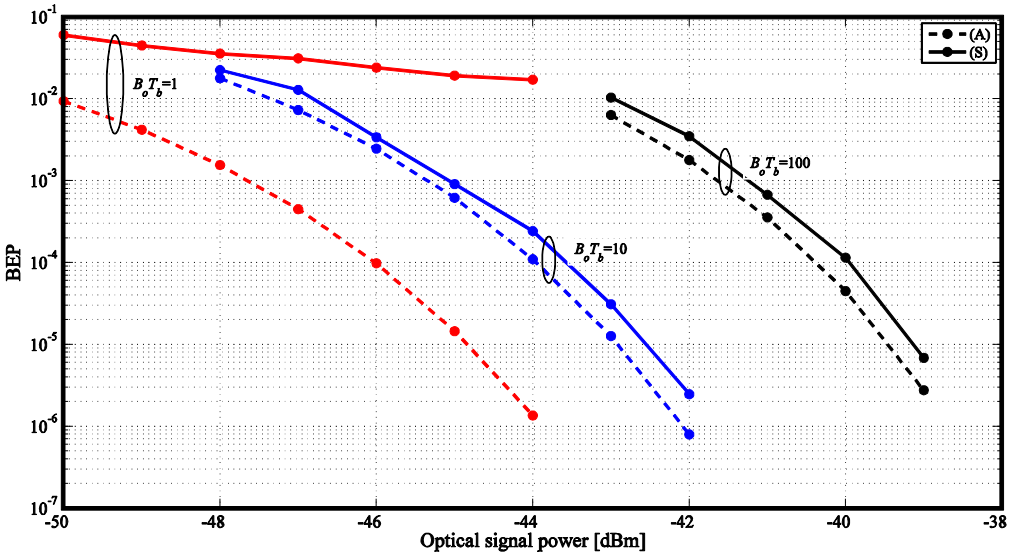

Figure 4.5 – BEP as a function of the optical signal power, for an ideal OF and an integrator EF, considering B_oT_b = 1, 10 and 100 and the crosstalk level equal to -12 dB.

Figure 4.5 can be compared with Fig. 3.6 presented in section 3.3 and obtained without in-band crosstalk. For smaller optical filter bandwidths, the ISI effect is predominant and, again, enhances the difference between the BEPs obtained using the MC simulation and the analytical BEPs. For higher normalized optical filter bandwidths (B_oT_b = 10 and 100), the BEPs obtained using the MC simulation with in-band crosstalk are relatively discrepant to the BEPs obtained with the analytical formalism. The BEPs obtained by both formalisms are not so precise as the ones observed in Fig. 3.6 in the absence of in-band crosstalk.

This difference might be attributed to the fact the MC simulation assumes a Brownian motion model for the random phase noise and the analytical formalism considers that random phase noise has an uniform distribution and is constant along the overall bit period, or also, due to the fact that the MC simulation considers a random sequence of bits on the DPSK crosstalk signal and the BEPs obtained by the analytical formalism [7] are estimated by averaging the BEP obtained with a DPSK symbol on the crosstalk signal equal to the symbol on the original signal and the BEP obtained with the negated symbol (in relation to the original signal) on the crosstalk signal. The influence of the different sequence of bits in the DPSK crosstalk sequence is investigated in subsection 4.5.2.

Figure 4.6 shows the BEP as a function of the crosstalk level for the ideal OF and the integrator EF combination and an optical signal power of –46 dBm (left) and the Gaussian OF and the RC EF combination and an optical signal power of –45 dBm (right), both filter combinations with B_eT_b = 0.7, considering different normalized optical filters bandwidths.

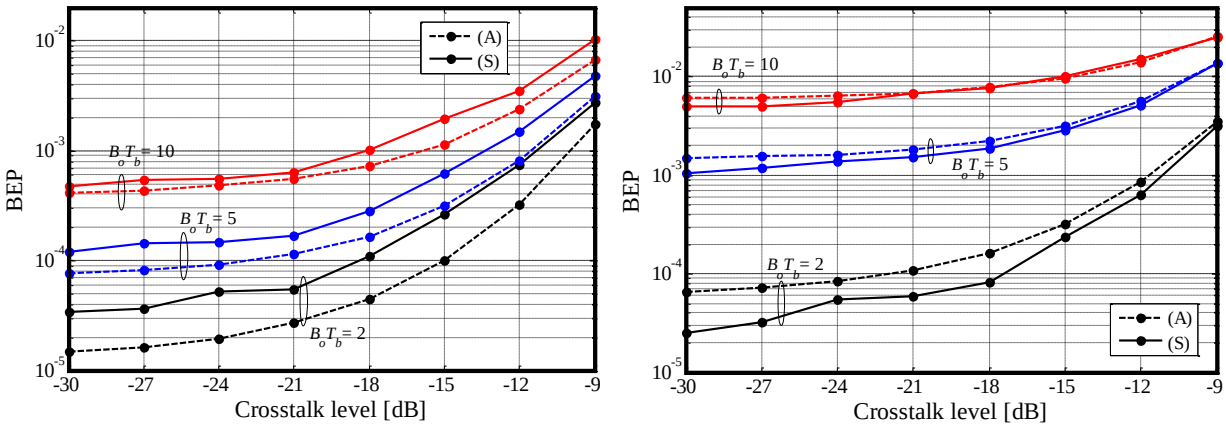

Figure 4.6 – BEP as a function of the crosstalk level, considering the ideal OF and the integrator EF combination (left) and the Gaussian OF and the RC EF combination (right), for different normalized optical filter bandwidths.

In accordance with Fig. 4.6, it can be concluded that the BEPs obtained through the MC simulation are in agreement with the BEPs obtained analytically by the formalism proposed in [7], although the slight discrepancy (observed also in Fig. 4.5) between the estimates of both methods, which increases with the optical filter –3 dB bandwidth narrowing, i.e., with the ISI enhancement. Although these slightly discrepancies, the MC simulator can be considered validated. The increase of the crosstalk level leads to an expectable increase of BEP and the broadening of the normalized optical filter bandwidths implies a lower influence of the ISI effect and higher influence of the ASE noise. The discrepancies of BEPs are related with the reasons explained previously in Fig. 4.5.

The distinction between the results obtained for the two filters combinations is that the MC simulation performed with the Gaussian OF and RC EF combination (right) achieves lower BEP when compared with the analytical formalism. This behavior occurs once again in these filters combination because the optimal sampling time in the MC simulation is obtained for the largest eye opening, instead of the sampling time at the middle of the bit period used in the analytical formalism [7].

Figure 4.7 shows the eyes diagrams at the decision circuit input for the ideal OF and the integrator EF, for an optical signal power of –45 dBm, $B_oT_b = 10$ and considering different crosstalk levels.

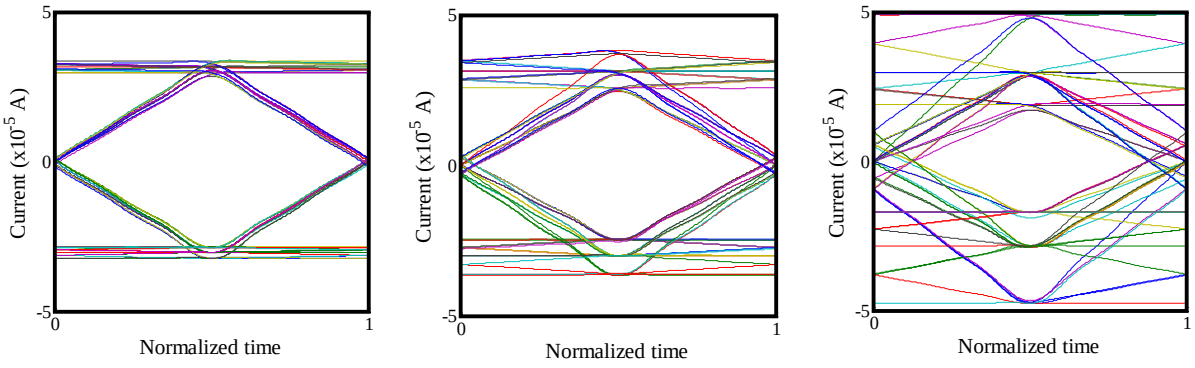

Figure 4.7 – Eye diagrams at the decision circuit input for the ideal OF and the integrator EF, for an optical signal power of –45 dBm, B_oT_b = 10 and considering a crosstalk level equal to –30 dB (left), –20 dB (middle) and –12 dB (right).

Notice that in Fig. 4.7, with the enhancement of the crosstalk level, the eye-pattern becomes more distorted and the ISI on the optimum sampling instant is enhanced. It is the effect of this ISI on the performance that also can lead to the discrepancies observed in Figs. 4.5 and 4.6 between the estimates of the analytical formalism and the MC simulation.

The MC simulator is also validated when impaired by in-band crosstalk and in the presence of DPSK receiver imperfections. Their power penalties are compared to the results obtained in [32] with the analytical formalism.

Figure 4.8 depicts the power penalty as a function of the responsivity imbalance with different interferometer detunings, considering a Gaussian OF and a Gaussian EF, a normalized optical filter bandwidth equal to 5, a $B_eT_b = 0.7$ and a crosstalk level of –15 dB. The power penalty is obtained for a BEP of 10^{-3}, considering the absence of crosstalk and receiver imperfections as a reference.

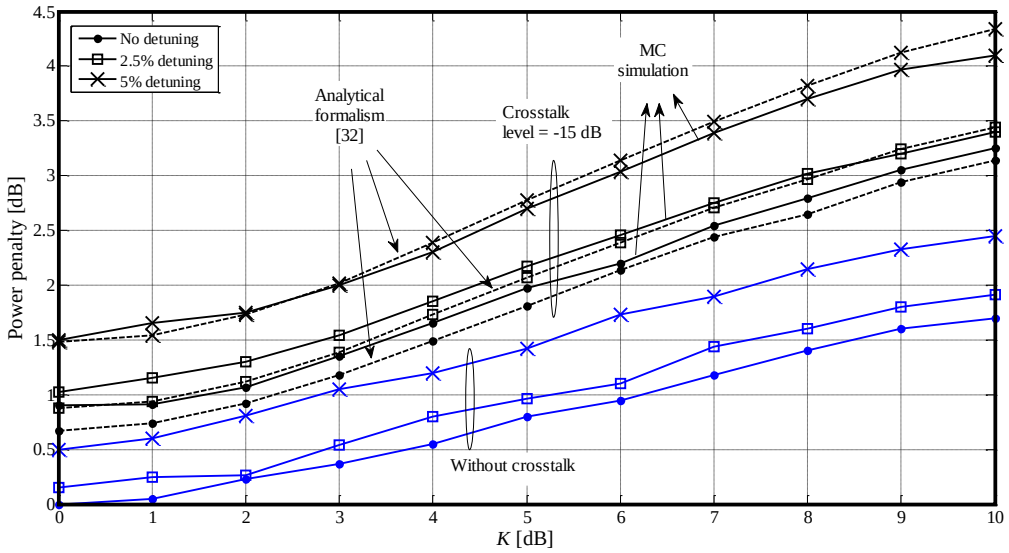

Figure 4.8 – Power penalty as a function of the responsivity imbalance with different interferometer detunings, for the Gaussian OF and the Gaussian EF with a crosstalk level of -15 dB, considering a normalized optical filter bandwidth equal to 5.

Accordingly with Fig 4.8, it can be concluded that there is a good approximation between the power penalties obtained with the analytical formalism and the MC simulation. The small differences between the performances might be related with the reasons previously explained. The graphical behavior from the MC simulation is in agreement with the power penalties presented for the analytical formalism, hence validating the MC simulation for both optical DPSK receiver imperfections. For power penalties obtained for a BEP of 10^{-9} (Fig. 4 b) of [32]), the performance degradation with the increase of the responsivity imbalance is higher than the one shown in Fig. 4.8.

4.5. Performance evaluation

In the results presented in the previous section, it was assumed a random bits sequence on the DPSK crosstalk signal and that the crosstalk and original signal are synchronized (aligned). This section analyzes the performance of the optical DPSK balanced receiver impaired by in-band crosstalk when considering: 1) a delay between the original signal and the crosstalk signal; 2) different sequences of bits on the DPSK crosstalk signal, and 3) receiver imperfections with other filter combinations.

4.5.1. Delay between the original signal and the crosstalk signal

The influence of a delay between the crosstalk signal and the original signal on the optical DPSK receiver performance is analyzed in this subsection. In Fig. 4.9, the BEP is illustrated as a function of the optical signal power for different crosstalk signal delays, considering an ideal OF and an integrator EF combination, a crosstalk level of –12 dB and $B_oT_b = 10$ (left) and $B_oT_b = 100$ (right).

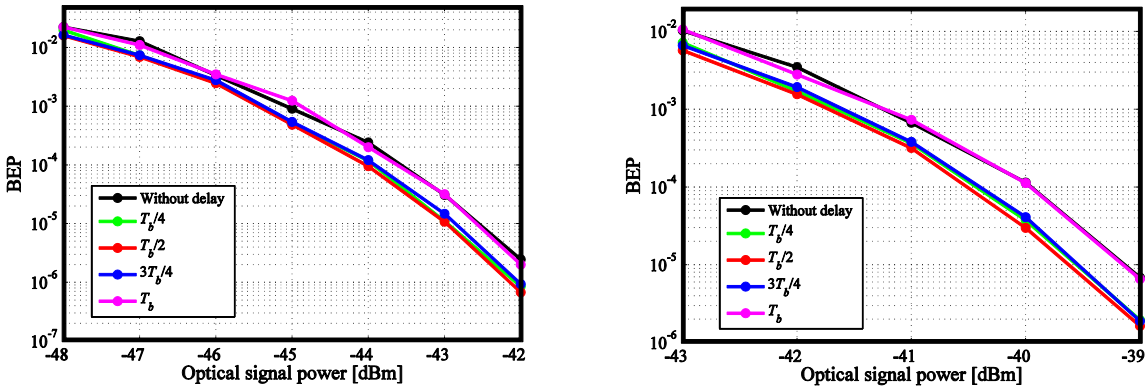

Figure 4.9 – BEP as a function of the optical signal power, for an ideal OF and an integrator EF combination, a crosstalk level of -12 dB and a normalized optical filter bandwidth equal to 10 (left) and 100 (right), considering different crosstalk signal delays.

Figure 4.9 shows that the delay applied in the crosstalk signal does not introduce a significant impact on the performance of the optical DPSK receiver in comparison with the aligned case for both B_oT_b, because the difference between the BEPs estimated using the several delays is almost irrelevant. However, all crosstalk signal delays provide a slightly better BEP, being the better performance achieved with a delay of $T_b / 2$.

Figure 4.10 shows the BEP as a function of the delay between the original and crosstalk signals for two filter combinations: a Gaussian OF and a RC EF combination with an optical signal power equal to –45 dBm (left) and an ideal OF and an integrator EF combination with an optical signal power equal to –46 dBm (right), considering a normalized optical filter bandwidth equal to 2 and a crosstalk level of –12 dB. To achieve better accuracies, a value of 1000 erroneous bits was assumed in the MC simulation.

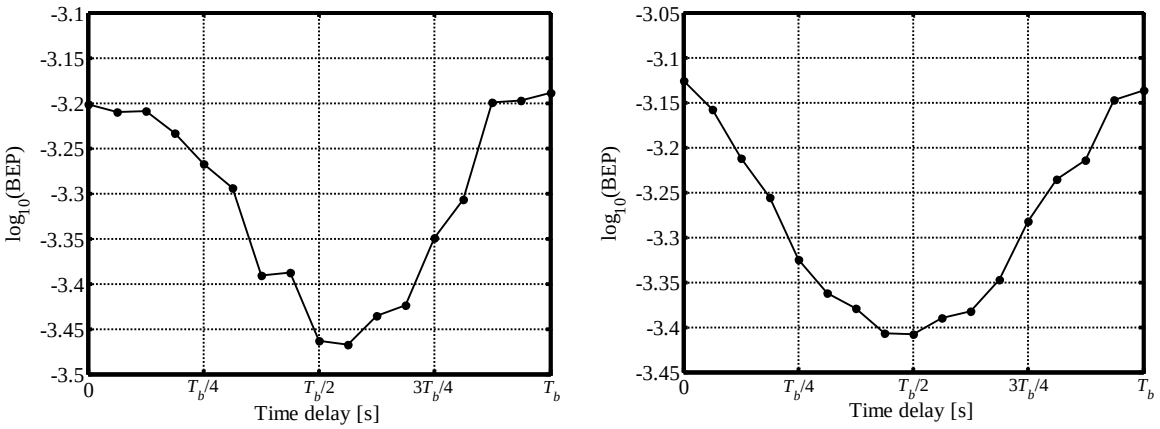

Figure 4.10 – BEP as a function of the delay between the crosstalk and the original signals, considering a Gaussian OF and a RC EF combination (left) and an ideal OF and an integrator EF combination (right), both for a crosstalk level of -12 dB and $B_oT_b = 2$.

Although the influence of the delay between the crosstalk signal and the original signal on the performance of the optical DPSK receiver is small, Fig. 4.10 shows for both filter combinations that the best BEP is achieved for a delay of half bit period, and that the BEP has a symmetric behavior around this point, with the worst BEP obtained for delays multiple of the bit period.

This behavior can be explained from the eye diagrams shown in Fig 4.11 for an ideal OF and an integrator EF combination with an optical signal power equal to –46 dBm, a crosstalk level of –12 dB and considering three crosstalk signals delays [without delay (left), $T_b/2$ (middle) and T_b (right)] for a normalized optical filter bandwidth equal to 10.

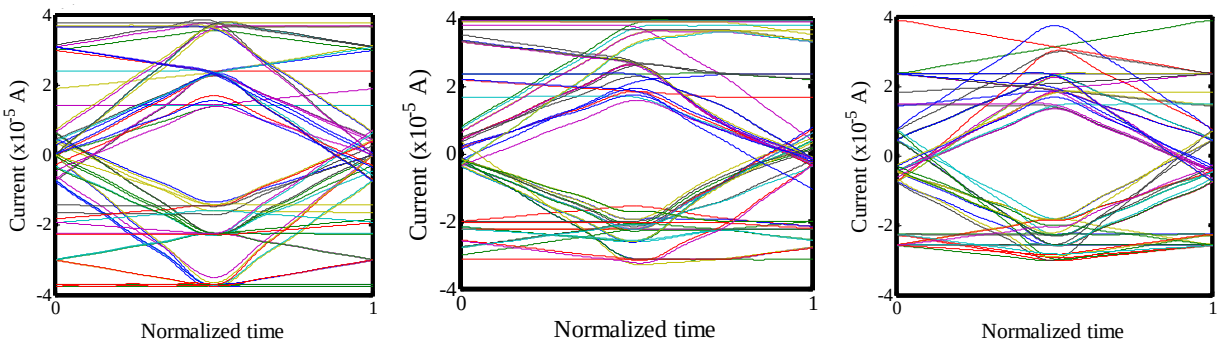

Figure 4.11 – Eye diagram at the decision circuit input considering an ideal OF and an integrator EF combination, for three crosstalk signals delays equal to 0 (left), $T_b/2$ (middle) and T_b (right).

By inspection of the eye diagrams depicted in Fig. 4.11, it can be concluded that there is a slightly larger eye opening when the crosstalk signal is delayed by $T_b/2$ (middle), allowing achieving a lower BEP than for a delay multiple of T_b. Figures 4.9 to 4.11 confirm that the aligned case is a worst-case situation for a single interferer.

4.5.2. Different bits sequences on the DPSK crosstalk signal

In this subsection, the performance of the optical DPSK receiver is investigated for different bits sequences on the DPSK crosstalk signal.

Until now, in the MC simulator, it was assumed that the bits sequence on the DPSK crosstalk signal is random. The next studies aim to analyze and compare the performance of the optical DPSK receiver for specific bits sequence on the DPSK crosstalk signal: 1) bits sequence equal to the sequence of bits on the original DPSK signal; 2) the negation of the sequence of bits on the original DPSK signal; 3) a sequence with only bits '1', and 4) a sequence with only bits '0'.

Figure 4.12 shows the BEP as a function of the crosstalk level, considering an ideal OF and an integrator EF with an optical signal power of –46 dBm (left) and a Gaussian OF and a RC EF with an optical signal power of –45 dBm (right), for different bits sequences on the DPSK crosstalk signal, considering a $B_oT_b = 2$ and $B_oT_b = 10$.

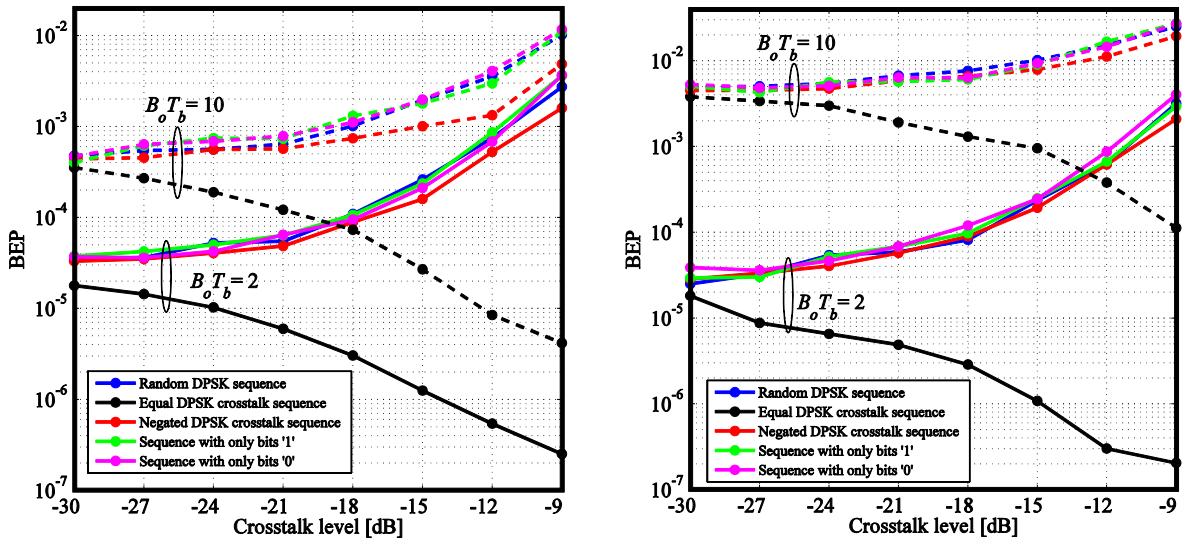

Figure 4.12 – BEP as a function of the crosstalk level, considering an ideal OF and an integrator EF combination with an optical signal power of -46 dBm (left) and a Gaussian OF and a RC EF combination with an optical signal power of -45 dBm (right), for different sequence of bits on the DPSK crosstalk signal, considering a normalized optical filter bandwidth equal to 2 and 10.

As shown in Fig. 4.12, except for the situation where the sequence of bits on the DPSK crosstalk signal is equal to the original DPSK signal, the BEP estimated through the MC simulation, when impaired by the other DPSK crosstalk signals achieves approximated the same values, for both filter combinations. When the bits sequence on the DPSK crosstalk

signal is equal to the original DPSK signal, an increase of the crosstalk level results in an improvement of the performance of the DPSK optical receiver, because as the DPSK crosstalk signal is added in-phase to the original signal, there is a signal power reinforcement leading to an signal enhancement and consequently the BEP is reduced.

Accordingly with Fig. 4.12 and considering the fact that the DPSK crosstalk signal in the analytical formalism [7] is obtained by averaging the BEP obtained with a DPSK symbol on the crosstalk signal equal to the symbol on the original signal and the BEP obtained with the negated symbol (in relation to the original signal) on the crosstalk signal, it may be concluded that this average is approximately equal to the negated DPSK crosstalk sequence, because the equal DPSK crosstalk sequence has significantly lower BEPs. Considering the same scenario on Fig. 4.5 and Fig. 4.12 (left), i.e., the ideal OF and integrator EF, an optical signal power equal to –46 dBm, $B_oT_b = 10$ and a crosstalk level of –12 dB, it can be concluded that the difference between the BEPs of the analytical formalism [7] and the MC simulation in Fig. 4.5 is the same as the difference between the BEPs of the negated DPSK crosstalk sequence and the random DPSK crosstalk sequence in Fig. 4.12 (left). So, the discrepancies between the BEPs of the analytical formalism [7] and the MC simulation are related with the difference between the DPSK crosstalk signal adopted analytically and in the MC simulation.

In order to understand the influence of the bits sequences on the DPSK crosstalk signal, the eye diagrams of the desired signal impaired by different bits sequences on the DPSK crosstalk signal are shown in Fig. 4.13, considering a random bit sequence (left), a bit sequence equal to the original signal (middle) and the negated bits sequence (right), considering a Gaussian OF and a RC EF combination with B_oT_b = 2 and B_eT_b = 0.7, considering an optical signal power equal to –45 dBm and a crosstalk level of –12 dB.

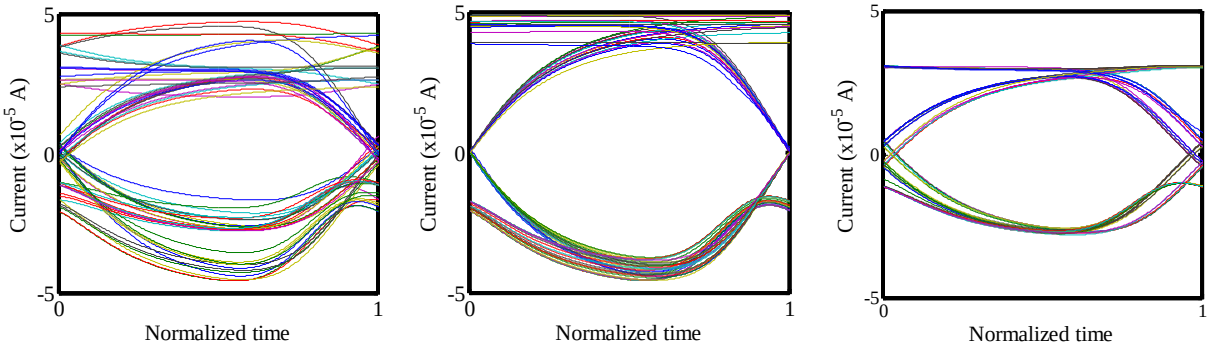

Figure 4.13 – Eye diagrams at the decision circuit input considering a Gaussian OF and a RC combination, for a random bits sequence on the DPSK crosstalk signal (left), an equal bits sequence (middle) and a negated bits sequence (right).

Accordingly with Fig. 4.13, it can be concluded once again, that the eye diagram of the random bits sequence (left) contain all bit transitions, and, hence, it contains the eye diagrams obtained for specific bits sequences as the ones represented in Fig. 4.13 (middle) and (right). As the eye opening obtained with the negated bits sequence is similar to the eye opening obtained for a random bits sequence, the BEP is similar for both cases.

When the bits sequence of the DPSK crosstalk signal is equal to the bits sequence of the original signal, Fig. 4.13 (middle), the eye pattern shows only the transitions that lead to larger eye opening. As a consequence, the BEP achieves lower values, as shown in Fig. 4.12.

Figure 4.14 shows the PDFs as a function of the decision variable, for a random bits sequence on the DPSK crosstalk signal (blue), an equal DPSK crosstalk sequence (red) and a negated DPSK crosstalk sequence (green) and is obtained for the same conditions than the considered in Fig. 4.13, except for the optical signal power, which is equal to –40 dBm.

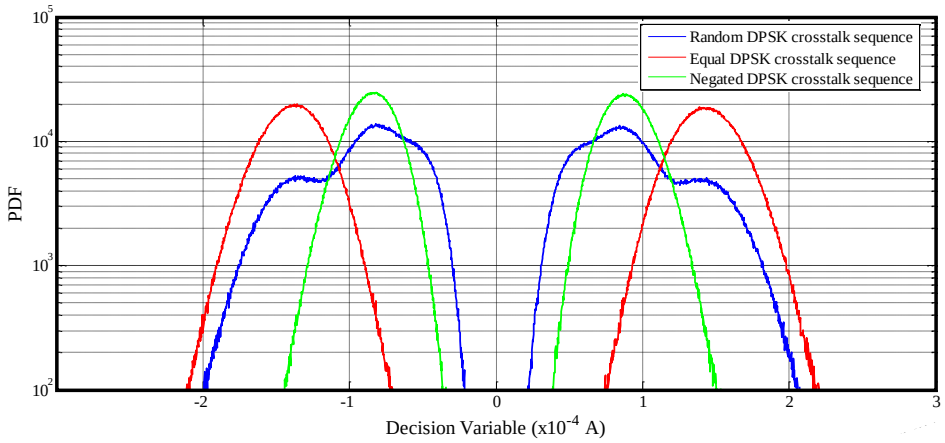

Figure 4.14 – PDFs of the decision variable, considering a Gaussian OF and a RC EF, for a random bits sequence on the DPSK crosstalk signal (blue), an equal bits sequence (red) and a negated bit sequence (green).

From Fig. 4.14, the PDF of the random bits sequence (blue) seems to contain the PDFs variations corresponding to the equal DPSK crosstalk sequence and the negated DPSK crosstalk sequence. The optical signal power is equal to –40 dBm, in order to compare Fig. 4.14 with the Figs. 2 and 3 of [32] obtained with the analytical formalism, and also, to reduce the impact of ASE noise and to visualize the variations on the top of the PDFs. The "flat-top" behavior shown in [32] seems to be characteristic of an isolated DPSK symbol, since it does not appear on the PDFs of Fig. 4.14 obtained with several bits sequences.

4.5.3. Receiver imperfections

This subsection analyzes the impact of the receiver imperfections in the performance of the optical DPSK communication system impaired by in-band crosstalk. A Gaussian OF and a Gaussian EF combination is assumed.

Figure 4.15 illustrates the BEP estimates as a function of the responsivity imbalance (left) and of the interferometer detuning (right), for different crosstalk levels, considering a normalized optical filter bandwidth equal to 5 and an optical signal power of –45 dBm.

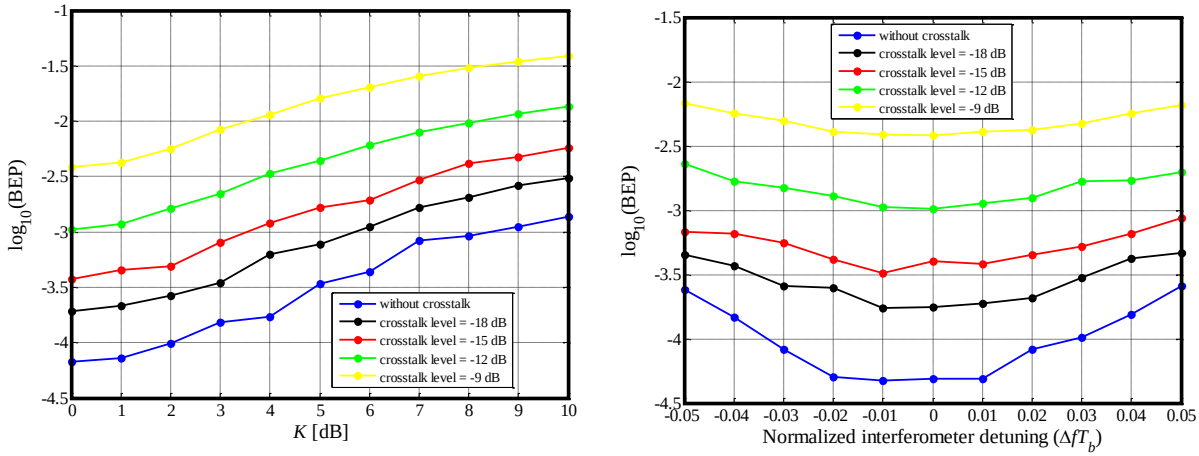

Figure 4.15 – BEP as a function of the responsivity imbalance (left) and of the interferometer detuning (right), for different crosstalk levels, considering a Gaussian OF and a Gaussian EF combination, a normalized optical filter bandwidth equal to 5 and an optical signal power of -45 dBm.

By inspection of Fig. 4.15, although the increase of the crosstalk level degrades the receiver performance, the graphical behavior of the BEP with the responsivity imbalance and with the interferometer detuning in the presence of crosstalk is similar to the graphical behavior without crosstalk. Hence, it can be concluded that the performance degradation due to receiver imperfections is not enhanced with the increase of the crosstalk level.

Figure 4.16 depicts the PDFs of the decision variable for an optical DPSK receiver impaired by the responsivity imbalance (left) and by the interferometer detuning (right), assuming a Gaussian OF and a Gaussian EF combination, a crosstalk level of –12 dB, a normalized optical filter bandwidth equal to 5 and an optical signal power equal to –40 dBm (as defined in Fig. 2 and Fig. 3 of [32]).

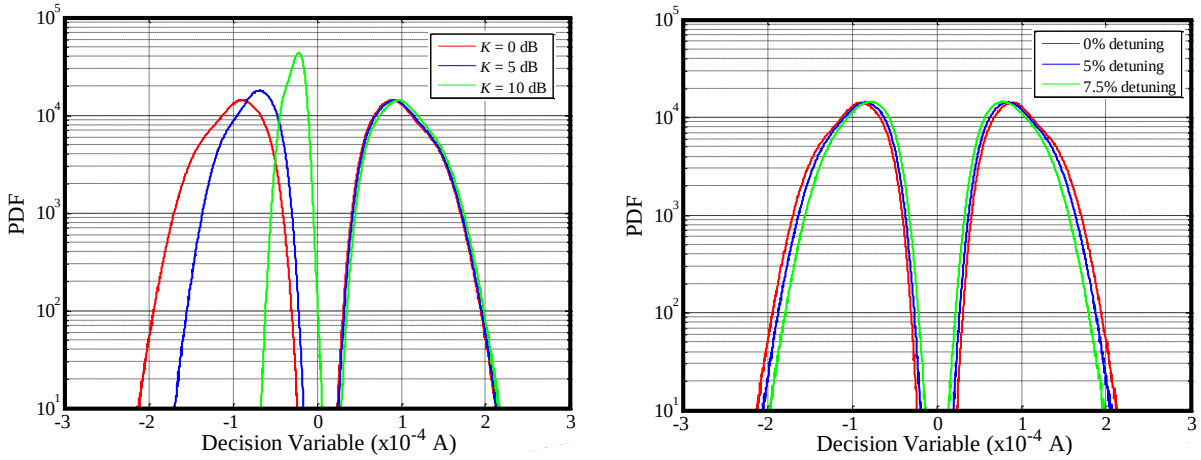

Figure 4.16 – PDF of the decision variable, considering responsivity imbalance (left) and of the interferometer detuning (right), for a crosstalk level of –12 dB, considering a Gaussian OF and a Gaussian EF combination, B_oT_b = 5 and an optical signal power of -40 dBm.

As can be observed in Fig. 4.16 (right), the PDFs of the bits '1' and '0' for different interferometer detunings are identical and symmetrical around the optimum decision threshold. With the increase of the detuning, the inner tails of the PDFs always stays above the PDFs tails of the receiver without imperfections, leading to an increase of the PDFs crossing points. The PDFs crossing points cannot be visualized in Fig. 4.16 because the signal optical power used –40 dBm, is too high and demands a considerable increase of the duration of the MC simulation to reach the PDF crossing points.

In Fig. 4.16 (left), the PDFs are plotted for different values of the responsivity imbalance. It can be seen that the PDF corresponding to bits '0' and '1' become asymmetrical with the increase of *K*. The PDFs of the bit '0' for $K = 5$ dB (blue line) and $K = 10$ dB (green line) present visible differences in comparison with the PDF obtained without imperfections (red line). The mean is diminishing towards zero and the variance is reducing with the increase of K. The difference in the PDF curves of Fig. 4.16 (left) for the bit '1' is almost negligible. These behaviors are in agreement with the PDFs behavior observed in [32]. As has already been shown in Fig. 3.25, the PDF of the optical DPSK receiver when impaired by responsivity imbalance has its crossing points deviating from zero, which results in a decision threshold different from zero and the achievement of higher BEPs.

Furthermore, the MC simulation shows that the PDF do not exhibit the "flat-top" behavior depicted in Figs. 2 and 3 of [32], because they are obtained for a random bits sequence, while in [32] the PDFs are obtained for an isolated DPSK symbol and considering the same symbol on the crosstalk signal.

4.6. Conclusions

In this chapter, the performance of the optical DPSK balanced receiver with direct detection, when impaired by in-band crosstalk was investigated for a single interferer term.

At first, the estimates of the BEP obtained using the MC simulation have been compared with the BEP estimates obtained using the analytical formalism [7], in order to validate the simulator. In this case, however, even for large optical filter bandwidth $(B_o T_b = 10)$, a slight discrepancy has been observed between the BEP estimates of both methods. This discrepancy has been attributed to the different DPSK crosstalk signal considered in the MC simulation and in the analytical work. For lower optical filter bandwidths, the ISI introduced by the electrical filtering enhances the discrepancies between the estimates of both methods, as already was observed in chapter 3, for the DPSK receiver case without crosstalk. The power penalty of the DPSK receiver impaired by in-band crosstalk and receiver imperfections using MC simulation was shown to be in agreement with the analytical BEPs.

The impact of in-band crosstalk on the performance of the optical DPSK receiver was also analyzed for different delays between the crosstalk and original signals, different bit sequences on the DPSK crosstalk signal and receiver imperfections. It was concluded that the influence of a delay in the crosstalk signal on the performance of the optical DPSK receiver is small. However, the aligned case seems to be a worst-case scenario, as usually stated in the literature [11]. It has been shown that different bit sequences on the DPSK crosstalk signal may introduce significant differences in the performance of the optical DPSK receiver, and, so, the performance should be analyzed for all possible bits sequences. For example, the assumption of a bit sequence on the DPSK crosstalk signal equal to the original DPSK signal, considerably improves the performance of the optical DPSK receiver when the crosstalk level is increased due to a reinforcement of the power of the original signal. This signal reinforcement has been observed on the PDFs of the decision variable and on the corresponding eye-diagrams.

It was also noticed that the PDFs nearly “flat-top” behavior observed for a high crosstalk level and reported in [7], [32], appears only when an isolated DPSK symbol is considered. When the DPSK crosstalk signal consists of a sequence of bits, the mentioned “flat-top” behavior is not much pronounced.

It was shown that the degradation introduced by receiver imperfections is not enhanced due to the presence of in-band crosstalk. Its behavior is similar to the case without crosstalk. Again, it was confirmed that the increase of the responsivity imbalance increases the mean of the PDFs corresponding to the bits ‘0’ towards positive values due to an enhancement of the power of the ASE-ASE beat noise in comparison with the signal-ASE beat noise power.

5. Conclusions and future work

In this work, the performance of an optical DPSK communication system with balanced reception and direct detection has been investigated. The goal was to create a MC simulation tool capable of analyzing the impact of some performance impairments in the optical DPSK communication system, such as the ASE noise introduced by the optical amplifiers, the in-band crosstalk due to the imperfect isolation of optical components and the distortion introduced by filtering.

Chapter 2 has presented the theoretical concepts dealing with the optical DPSK signal (its transmission and reception) and the implementation of the stochastic simulation based on Monte Carlo method was described.

In chapter 3, the performance of the optical DPSK receiver impaired by ASE noise and without crosstalk was studied. The MC simulation was compared to an analytical formalism [7] and the MC simulator was considered validated because the BEPs obtained using both methods were in very good agreement. Only in the cases where the ISI is enhanced (lower optical and electrical filter bandwidths), discrepancies between the MC simulation and the analytical results have been found, which become significant for very strong ISI. Our results have shown that, when the electrical filter is an integrator, the DPSK receiver achieves its best performance. However, the integrator is an ideal filter and its corresponding performance predictions might differ from those obtained in a real system. It was also shown that for lower optical filter bandwidths, due to ISI, the PDFs of the bits ‘0’ and ‘1’ become asymmetric, and that this asymmetry is enhanced with the ISI increase. The analytical formalism [7] does not predict this behavior, however, this asymmetric behavior is in agreement with the results presented in [27].

The DPSK receiver imperfections were also analyzed and validated by comparison of the BEPs obtained using MC simulation with the BEPs obtained from the analytical formalisms [7] and [22]. Two receiver imperfections were studied, the responsivity imbalance and the interferometer detuning. A maximum discrepancy of 0.5 dB has been obtained between the power penalties obtained with the MC simulation and with the analytical formalism proposed in [7]. This difference might be caused by the consideration of an isolated DPSK symbol on the analytical formulation, while the MC simulation considers a sequence of bits. In comparison with the results of [22], an excellent agreement has been

found. While the responsivity imbalance increases, the PDFs of the bits ‘0’ shift to higher values and its Gaussian behavior tend to a “more” Chi-squared behavior. The chosen filter combination does not particularly influence the performance of the optical DPSK receiver when impaired by receiver imperfections.

In chapter 4, the performance of the optical DPSK receiver impaired by in-band crosstalk was analyzed. The MC simulation was validated by comparison of its results with the results obtained using the analytical formalism [7], however, for high normalized optical filter bandwidths, the MC simulation results with in-band crosstalk were not so precise, as in the validations performed in the absence of in-band crosstalk. This difference might be attributed due to the fact that the MC simulation considers a random sequence of bits on the DPSK crosstalk signal and the analytical formalism estimates the BEPs by averaging the BEP obtained with a DPSK symbol on the crosstalk signal equal to the symbol on the original signal and the BEP obtained with the negated symbol on the crosstalk signal, in relation to the original signal.

The system performance due to the impact of in-band crosstalk was analyzed for different delays between the crosstalk and original signals, different bits sequences on the DPSK crosstalk signal and two receiver imperfections. It was concluded that a delay in the crosstalk signal does not have a considerable influence in the performance of the optical DPSK receiver. However, as usually stated in the literature, the aligned case seems to be the worst-case scenario. Furthermore, different bits sequences on the DPSK crosstalk signal may introduce significant differences in the performance of the optical DPSK receiver, and, so, the performance should be analyzed for all possible bits sequences. The performance of the optical DPSK receiver considerably improves with the assumption of a bit sequence on the DPSK crosstalk signal equal to the original DPSK signal. Finally, it was also shown that the performance degradation introduced by receiver imperfections is not much dependent on the increase of the crosstalk level.

5.1. Future work

Some suggestions for future work are presented here:

- Studying the performance of the optical DPSK receiver for other filters combinations and other optical DPSK receiver imperfections;
- Analyzing the effect of multiple interfering terms and the impact of other crosstalk types in the performance of the optical DPSK receiver;
- Investigating the performance of an optical DQPSK communication system with direct detection impaired by in-band crosstalk;
- Investigating the impact of in-band crosstalk when the modulation format on the crosstalk signal is different from the modulation of the original signal;
- Studying the impact of in-band crosstalk on the performance of optical networks based on DPSK transmission, with a particular emphasis on the architecture of the optical node.

6. References

[1] O. Gerstel, M. Jinno, A. Lord and S. J. Yoo, "Elastic Optical Networking: A New Dawn for the Optical Layer?", *IEEE Commun. Mag.*, vol. 50, pp. s12-s20, Feb. 2012.

[2] M. O'Mahony, C. Politi, D. Klonidis, R. Nejabati and D. Simeonidou, "Future Optical Networks", *J. Lightw. Technol.*, vol. 24, no. 12, pp. 4684-4696, Dec. 2006.

[3] G. P. Agrawal, "Lightwave Technology – Telecommunication Systems", John Wiley & Sons, 2005.

[4] E. Desurvire, "Capacity Demand and Technology Challenges for Lightwave Systems in the Next Two Decades", *J. Lightw. Technol.*, vol. 24, no. 12, pp. 4697-4710, Dec. 2006.

[5] J. C. Attard, J. E. Mitchell and C. J. Rasmussen, "Performance Analysis of Interferometric Noise Due to Unequally Powered Interferers in Optical Networks", *J. Lightw. Technol.*, vol. 23, no. 4, pp. 1692-1703, Apr. 2005.

[6] A. H. Gnauck and P. J. Winzer, "Optical Phase-Shift-Keyed Transmission", *J. Lightw. Technol.*, vol. 23, no. 1, pp. 115-130, Jan. 2005.

[7] L. Cancela, "Análise do impacto do crosstalk em matrizes de comutação óptica espacial", PhD in Science and Information Technology – Telecommunications Specialization", ISCTE – IUL, 2007.

[8] J. Pires and L. Cancela, "Estimating the Performance of Direct-Detection DPSK in Optical Networking Environments Using Eigenfunction Expansion Techniques", *J. Lightw. Technol.*, vol. 28, no. 13, pp. 1994-2003, Jul. 2010.

[9] X. Liu, Y.-H. Kao, M. Movassaghi and R. C. Giles, "Tolerance to In-Band Coherent Crosstalk of Differential Phase-Shift-Keyed Signal with Balanced Detection and FEC", *IEEE Photon. Technol. Lett.*, vol. 16, no. 4, pp. 1209-1211, Apr. 2004.

[10] A. Agarwal, P. Toliver, T. Banwell, R. Menendez, J. Jackel and S. Etemad, "Impact of Coherent Crosstalk on DQPSK in a Coherent OCDM System", *in Proc. Conference on Optical Fibre Communication (OFC)*, USA, Mar. 2008.

[11] I. Monroy and E. Tangdiongga, "Crosstalk in WDM Communication Networks", Kluwer Academic Publishers, 2002.

[12] P. A. C. Monteiro, "Aspectos do desempenho de um sistema DPSK com pré-amplificação e desmodulação óptica", Msc. dissertation on Electrical and Computers Engineering, IST, 1995.

[13] G. P. Agrawal, "Lightwave Technology – Components and Devices", John Wiley & Sons, chapt. 3, 2004.

[14] M. N. Islam, "Raman Amplifiers for Telecommunications", *IEEE J. Sel. Topics Quantum Electron.*, vol. 8, no. 3, pp. 548-559, May/Jun. 2002.

[15] B. Chan and J. Conradi, "On the Non-Gaussian Noise in Erbium-Doped Fiber Amplifiers", *J. Lightw. Technol.*, vol. 15, no. 04, pp. 680-687, Apr. 1997.

[16] Keang-Po Ho, "Phase-Modulated Optical Communication Systems", Springer, chapt. 2, 2005.

[17] P. J. Winzer, S. Chandrasekhar and X. Liu, "Modulation Formats and Receiver Concepts for Optical Transmission Systems", *Short Course 105, OFC/NFOEC*, Los Angeles, CA, Mar. 2012.

[18] M. C. Jeruchim, P. Balaban and K. S. Shanmugan, "Simulation of Communication Systems" *Modeling, Methodology, and Techniques*, Kluwer Academic Publishers, Second edition, 2002.

[19] R. Ribeiro, J. Ferreira da Rocha and J. Pinto, "Performance Evaluation of EDFA Preamplified Receivers Taking into Account Intersymbol Interference", *J. Lightw. Technol.*, vol. 13, no. 2, pp. 225-232, Feb. 1995.

[20] A. Carlson, "Communication Systems", McGraw-Hill, Third edition, chapt. 5, 1986.

[21] A. Carlson, P. Crilly and J. Rutledge, "Communication Systems", McGraw-Hill, Fourth edition, chapt. 2, 2002.

[22] G. Bosco and P. Poggiolini, "The Impact of Receiver Imperfections on the Performance of Optical Direct-Detection DPSK", *J. Lightw. Technol.*, vol. 23, no. 2, pp. 842-848, Feb. 2005.

[23] W. Davenport and W. Root, "An Introduction to the Theory of Random Signals and Noise", Wiley – Interscience, 1987.

[24] H. Takahashi, K. Oda, H. Toba and Y. Inoue, "Transmission Characteristics of Arrayed Waveguide NxN Wavelength Multiplexer", *J. Lightw. Technol*, vol. 13, no. 3, pp. 447-455, Mar. 1995.

[25] C. Lawetz and J. Cartledge, "Performance of Optically Preamplified Receivers with Fabry-Perot Optical Filters", *J. Lightw. Technol*, vol. 14, no. 11, pp. 2467-2474, Nov. 1996.

[26] I. T. Monroy and G. Einarsson, "Bit Error Evaluation of Optically Preamplified Direct Detection Receivers with Fabry-Perot Optical Filters", *J. Lightw. Technol*, vol. 15, no. 8, pp. 1546-1553, Aug. 1997.

[27] Q. Zhang, C. R. Menyuk, R. Bajracharya, H. W. Huang, A. Miner, "On the Gaussian Approximation and Margin Measurements for Optical DPSK Systems With Balanced Detection", *J. Lightw. Technol.*, vol. 28, no. 12, pp. 1752-1760, Jun. 2010.

[28] G. Bosco and P. Poggiolini, "The Effect of Receiver Imperfections on the Performance of Direct-Detection Optical Systems using DPSK Modulation", *in Proc. Conference on Optical Fibre Communication (OFC'03)*, Paper ThE6, EUA, Mar., 2003.

[29] P. J. Winzer and H. Kim, "Degradations in Balanced DPSK Receivers", *IEEE Photon. Technol. Lett*, vol.15, no. 9, pp. 1282-1284, Sep. 2003.

[30] T. Mizuochi, Y. Miyata, T. Kobayashi, K. Ouchi, K. Kuno, K. Kuno, K. Shimizu, H. Tagami, H. Yoshida, H. Fujita, M. Akita, K. Motoshima, "Forward Error Correction Based on Block Turbo Code With 3-Bit Soft Decision for 10-Gb/s Optical Communication Systems", *IEEE J. Sel. Topics Quantum Electron.*, vol. 10, no. 2, pp. 376-386, Mar/Apr. 2004.

[31] M. Azizoglu and P. A. Humblet, "Optical DPSK with Generalized Phase Noise Model and Narrowband Reception", in *Proc. IEEE ICC 93*, Geneva, vol. 3, pp. 1591-1596, May 1993.

[32] L. Cancela and J. Pires, "Crosstalk Tolerance of Direct Detection DPSK Optical Systems in Presence of Receiver Imperfections", *IET Optoelectron.*, vol. 6, no. 2, pp. 94-101, Apr. 2012.

[33] P. J. Legg, M. Tur, I. Andonovic, "Solution Paths to Limit Interferometric Noise Induced Performance Degradation in ASK/Direct Detection Lightwave Networks", *J. Lightw. Technol.*, vol. 14, no. 9, pp. 1943-1954, Sep. 1996.

[34] T. Y. Chai, T. H. Cheng, Y. Ye and Q. Liu, "Inband Crosstalk Analysis of Optical Cross-Connect Architectures", *J. Lightw. Technol.*, vol. 23, no. 2, pp. 688-701, Feb. 2005.

[35] L. Cancela and J. Pires, "On the Accuracy of the Gaussian Approximation for Performance Estimation in Optical DPSK Systems with In-Band Crosstalk", in *Proc. IEEE ICC 2007*, Glasgow, U.K., pp. 2474-2479, Jun 2007.

[36] E. Goldstein, L. Eskildsen, C. Lin and Y. Silberberg, "Polarization statistics of Crosstalk-Induced Noise in Transparent Lightwave Networks", *IEEE Photon. Technol. Lett.*, vol. 7, no. 11, pp. 1345-1347, Nov. 1995.

[37] L. Cancela, "Aspectos do Desempenho de Comutadores Ópticos Espaciais", Masters Degree Dissertation, Instituto Superior Técnico, Apr. 1998.

[38] A. Papoulis, "Probability, Random Variables and Stochastic Processes", Mc Graw–Hill, Third edition, 1991, chapt. 6.